2000

Robustness analysis and controller design for static var compensators in power systems

Xuechun Yu
Iowa State University

INFORMATION TO USERS

This manuscript has been reproduced from the microfilm master. UMI films the text directly from the original or copy submitted. Thus, some thesis and dissertation copies are in typewriter face, while others may be from any type of computer printer.

The quality of this reproduction is dependent upon the quality of the copy submitted. Broken or indistinct print, colored or poor quality illustrations and photographs, print bleedthrough, substandard margins, and improper alignment can adversely affect reproduction.

In the unlikely event that the author did not send UMI a complete manuscript and there are missing pages, these will be noted. Also, if unauthorized copyright material had to be removed, a note will indicate the deletion.

Oversize materials (e.g., maps, drawings, charts) are reproduced by sectioning the original, beginning at the upper left-hand corner and continuing from left to right in equal sections with small overlaps.

Photographs included in the original manuscript have been reproduced xerographically in this copy. Higher quality 6" x 9" black and white photographic prints are available for any photographs or illustrations appearing in this copy for an additional charge. Contact UMI directly to order.

Bell & Howell Information and Learning
300 North Zeeb Road, Ann Arbor, MI 48106-1346 USA
800-521-0600

Robustness analysis and controller design for static var compensators in power systems

by

Xuechun Yu

A dissertation submitted to the graduate faculty

in partial fulfillment of the requirements for the degree of

DOCTOR OF PHILOSOPHY

Major: Electrical Engineering (Electric Power)

Major Professors: Mustafa Khammash and Vijay Vittal

Iowa State University

Ames, Iowa

2000

UMI Number: 9977373

UMI Microform9977373

Bell & Howell Information and Learning Company
300 North Zeeb Road
P.O. Box 1346
Ann Arbor, MI 48106-1346

Graduate College
Iowa State University

This is to certify that the Doctoral dissertation of

Xuechun Yu

has met the dissertation requirements of Iowa State University

Signature was redacted for privacy.

Co-major Professor

Signature was redacted for privacy.

Co-major Professor

Signature was redacted for privacy.

For the Major Program

Signature was redacted for privacy.

For the Graduate College

TABLE OF CONTENTS

LIST OF TABLES

LIST OF FIGURES

ACKNOWLEDGMENTS

I would like to thank my co-major advisors, Dr. Mustafa Khammash and Dr. Vijay Vittal, for their invaluable guidance and continual support throughout this research project. They have shown me what true professorship is all about.

I would also like to express my gratitude to graduate committee members, Drs. V. Ajjarapu, Wolfgang Kliemann, and James McCalley for their generous contributions of time and effort in the process of this research project. My thanks also go to Dr. M. Djukanovic for his helpful suggestions to my research.

In addition, I am grateful to all the professors and graduate students in the electric power program at Iowa State University. They have made my stay here both productive and enjoyable.

Finally, I wish to thank my wife, Mei, for her understanding, encouragement, and support, especially during times of difficulty.

This research project was sponsored by the Electric Power Research Center at Iowa State University, to whom grateful acknowledgement is due.

1 INTRODUCTION

1.1 Today's Interconnected Power System

In the North American electric power interconnection, control systems play a prominent role in the stabilization and reliable operation of the system. Currently, the complexity of power systems is continually increasing because of the growth in the interconnection and use of new technologies. At the same time, financial and regulatory constraints have forced utilities to operate the systems closer than ever to their stability limits. As a result, the proper analysis and design of controls in power systems become even more important. Adequate system performance will depend largely on the proper operation and performance of critical controls such as excitation systems, power system stabilizers (PSSs), static var compensators (SVCs), and a new breed of control devices often referred to as flexible AC transmission systems (FACTS). The heavy reliance on controls requires a systematic procedure to analyze and design controls which demonstrates good performance for a wide range of operating conditions.

Accompanying the above trends has been an increasing tendency of power systems to exhibit oscillatory instability. For example, several instances of low frequency oscillations, associated with some machines in one part of the system swinging against machines in another part of the system, have been observed in the North American interconnection in the past decade [1]. These phenomena are referred to as inter-area oscillations and have frequencies typically in the range of 0.1Hz to 0.7Hz. These oscillations are due to the dynamics of inter-area power transfer and often exhibit poor

damping where the aggregate power transfer over a corridor is high relative to the transmission strength [2]. With the growth of interconnections and the advent of open access and competition in the industry, inter-area oscillations are more likely to happen, even under nominal operating conditions.

Controls once again are the main tools used for the mitigation of inter-area oscillations. While power system stabilizers (PSSs) remain the main damping method, there is an increasing interest in using FACTS devices to aid the damping of these oscillations [3], especially when the damping effect from PSSs alone is not enough. The SVC is one of these FACTS devices whose potential for damping inter-area oscillations will be studied in this dissertation.

1.2 Static Var Compensator And its Applications

Static var compensators (SVCs) are shunt-connected var generators and/or absorbers whose output are varied so as to control specific parameters of the power system. The term "static" is used to indicate that SVCs, unlike synchronous condensers, have no moving or rotating main components. Figure 1.1 gives a typical structure of the SVC which consists of a thyristor-controller reactor (TCR), a three-unit thyristor-switched capacitor (TSC) and a harmonic filter (for filtering harmonics generated by TCR). The TCR and TSC are controlled in such a manner that the bus voltage is kept at or close to a constant level depending on the control scheme used.

Since its first application in the late 1970s, the use of SVC in transmission system has been increasing steadily. By virtue of the ability to provide continuous and rapid control of reactive power and voltage, the SVC can enhance several aspects of transmission system performances including:

- Control of temporary overvoltages
- Prevention of voltage collapse

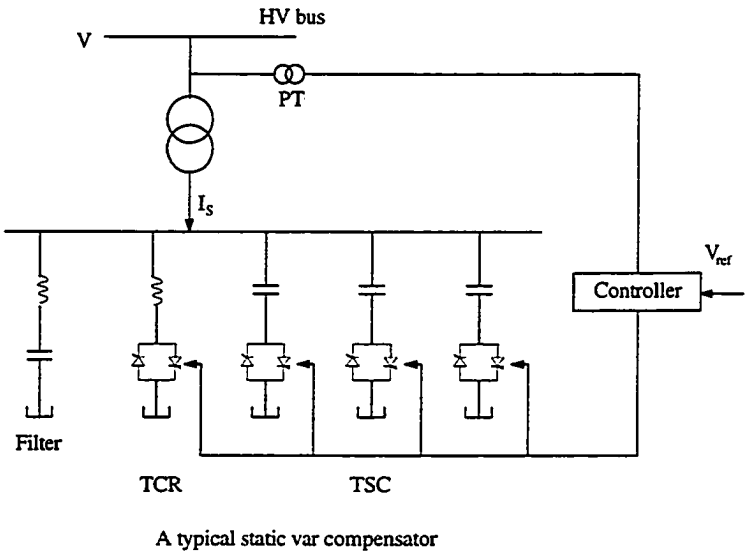

Figure 1.1 A typical SVC structure.

- Increase in power transmission capability
- Enhancement of transient stability

The fast response feature of the SVC also provides other opportunities to improve power system performances. By introducing a supplementary controller superimposed over its voltage control loop (see Figure 1.2), the SVC can be used to increase the system damping for undesirable inter-area oscillations. The careful design of the supplementary damping controller (SDC) is again necessary for the SVC to achieve effective damping.

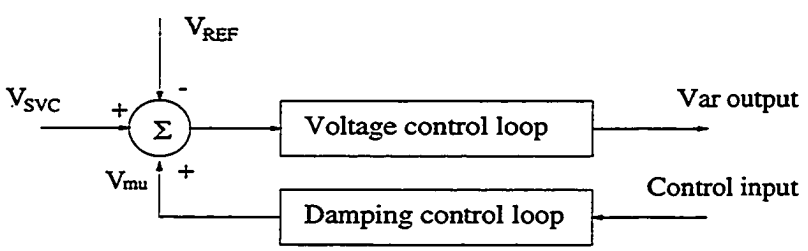

Figure 1.2 Supplementary damping scheme for SVC.

The current industry practice for the design and analysis of controls consists of conventional linear analysis tools coupled with detailed nonlinear simulations of the designed control settings. While this procedure is practical and has served the propose in the past, it lacks a systematic approach and does not guarantee robustness. Furthermore, it provides little insight and understanding of the parameters that have the most effect on robustness. Consequently, this approach offers little guidance for control design.

The past two decades have witnessed a significant development in control systems research mainly directed at understanding robustness properties of control systems. The purpose of these efforts is to obtain closed-loop systems that are stable and meet performance objectives despite the presence of plant uncertainties and parameter variations, i.e., provide robust stability and performance. The tools that have been developed for robustness analysis and synthesis have the potential to positively impact the way power systems controls are analyzed and designed.

1.3 Objectives and Scope of Research Work

The main objective of this research project is to apply the structured singular value (SSV or μ) analysis and synthesis technique to the robustness analysis and damping controller design of the SVC. This includes developing a good understanding of the way the system dynamic equations change with parameter variations and the way these variations can be incorporated into uncertainty models with minimum overbounding. A systematic procedure for analyzing robust stability and robust performance over a range of operating conditions will then be developed. This will be followed by the robust design of the supplementary damping controller for the SVC. The resulting controller should not only guarantee the system robust stability, but also damp the power system inter-area oscillations effectively over the whole operating range without compromising the voltage regulation function of the SVC.

The scope of this research work includes the following:

1. Formulate a general framework for the inclusion of the SVC model in order to apply the μ-based robustness approach. This consists of determining the changing elements of coefficient matrices of the linearized system dynamic equation and conducting a polynomial fit to obtain an expression for these changing elements in terms of the varying parameters in the power system. The system dynamic equations are then converted into a framework for robustness analysis by the application of linear fractional transformations (LFTs). The varying parameters include changes in generation setting and interface power flows.

2. Apply the μ-analysis technique to analyze the robustness of SVC over a range of operating conditions. Operating limits in terms of varying parameter values are obtained using the μ-based approach. These limits are then compared with those obtained by repeated eigenvalue analysis.

3. Investigate efficient ways to evaluate and refine μ bounds, which include formulating the state-space μ test and exploring the usage of μ lower bound in the μ frequency sweep test.

4. Develop criteria for the selection of SVC locations, the input signal to the SDC, and error signals and weighting functions used in the synthesis of the SDC.

5. Synthesize an SDC for the SVC using the μ-based approach. The resulting SDC usually has a high order, so appropriate model reduction techniques are carried out to reduce the controller to a reasonable low order for practical use while maintaining the essential characteristics of the original controller. The performance of the reduced-order SDC is also verified in both the frequency domain and the time domain.

Two test systems are extensively used in this research:

1. The IEEE 50-generator test system. In this system six generators are represented in the detail model and the remaining generators are represented in the classical model. This system exhibits complex dynamic behaviors and is often used to analyze the efficacy of the controls in damping inter-area oscillations.

2. The four-generator test system. This system has been specially designed by Ontario Hydro for fundamental studies of inter-area oscillations in power systems.

1.4 Thesis Outline

Following the introductory material in Chapter 1 and a concise literature review of the conventional and robust control design methods in Chapter 2, this dissertation presents the robustness methodology which will be used in Chapter 3. Chapter 4 gives a detailed description of the mathematical models of the power system components and the overall system dynamic equations. In Chapter 5, a systematic approach to characterize the parametric uncertainty and to construct the robustness analysis framework is given. The state-space μ-test to improve μ calculation is also included in Chapter 5. Chapter 6 considers the robust controller synthesis for the SVC based on the framework developed in Chapter 5. Finally, Chapter 7 presents the conclusions and provides suggestion for future work.

2 LITERATURE REVIEW

The interarea oscillations associated with groups of generators or plants in power systems are complex to study and control. Reference [4] provides a detailed account of a comprehensive study of the interarea oscillation problems, including the fundamental nature of the problem, methods of analysis, and control design procedures. Currently, power utilities mainly rely on the use of high-initial-response excitation systems supplemented with power system stabilizers (PSSs) to mitigate the interarea oscillations and enhance the over all system stability. Several research efforts pertaining to the design and coordination of PSSs have been reported in the literature [5, 6, 7, 8].

It has been known that SVC can extend the stability limit and improve the system damping when connected at the midpoint of long transmission lines [9]. While an SVC with pure voltage control may not adequately contribute to system damping, a significant enhancement can be achieved when the reactive power of the SVC is modulated in response to auxiliary control signals superimposed over its voltage control loop [9, 10]. Conventional linear methods were mainly used for the design of the supplementary damping controller in the previous research. Kundur (Chapter 17, [11]) described a design procedure with the classical pole-placement method. In [12] Padiyar and Varma used the damping torque analysis technique to design the damping controller, but the method is limited to the one-machine-infinite-bus system. In [13, 14], the linear quadratic Gaussian (LQG) control strategy was used on a reduced-order model of the power system to obtain a self-tuning adaptive damping controller. Taylor in [15] and Hauer in [16] discussed the applications of the SVC for the mitigation of interarea oscillations in the

WSCC system. The effectiveness of various supplementary signals as inputs to the controller are compared in a comprehensive study in [17].

Other effective means of stabilizing interarea oscillations include the modulation of HVDC converter controls [18, 19] and the use of thyristor-controlled series capacitors (TCSCs) [20]. The control coordination of these FACTS devices for system damping was studied in [21].

As mentioned before, the main drawback of the conventional design technique is that the robustness is not guaranteed. Almost all of the methods mentioned above consist of a single design at a nominal operating point which is selected from a wide range of operating conditions. However, the high degree of nonlinearity of power systems and presence of uncertainty, such as changes of operating conditions or unknown system parameters/models, make it very difficult to achieve a good controller design using only a single operating condition. The designed controller that is satisfactory under some operating conditions may become unacceptable under other operating conditions.

The analysis and design issues mentioned above lead themselves naturally to the tools of modern robust control, which have developed significantly within the control community in the past fifteen years. The purpose of these efforts is to obtain closed-loop systems that are stable and meet *a priori* specified performance objectives despite the presence of plant uncertainty and parameter variations. Recently, a number of studies in the literature have investigated the application of robust control techniques to power systems. Among them Kharitonov's theorem, interval analysis, L_1, H_∞, and structured singular value (SSV or μ) techniques have been used [22, 23, 24, 25, 26, 27, 28, 29, 30, 31, 32, 36, 37, 38]. The robust stability of power systems using Kharitonov's theorem was studied in [22]. In [23], the interval matrix analysis was used for the design of the PSS. In [24, 25] the robustness framework for multimachine power system using L_1 approach developed in [33, 34, 35] has been formulated. The main advantage of this approach is the simplicity of the derived conditions for robustness, which makes them suitable for large

scale power systems; on the other hand, this approach is conservative when the system variations are best characterized by uncertain parameters within fixed ranges. The H_∞ optimization method, used in [26, 27, 28, 29, 30] for the design of PSS and [31] for the design of SVC's damping controller, is capable of successfully dealing with modeling uncertainty, but is restricted to the multiplicative and/or additive uncertainty, again leading to conservative controller performances. Since the real parametric uncertainty, such as the tie-line power flow or the active power generation, is more meaningful with respect to robust stability in power systems, the SSV technique is more appropriate for analysis and controller design. This has been demonstrated in previous research on PSS design using the SSV method [36, 37, 38, 39] which provided robust stability (RS) and robust performance (RP) over a wide range of operating conditions.

3 ROBUSTNESS METHODOLOGY

A summary of uncertainty representation, linear fractional transformation (LFT), the definition of μ, and the μ-based robustness procedures, is presented in this chapter. The LFT machinery is very closely related to the uncertainty representation and SSV in robustness analysis. The complex SSV-μ, or equivalent stability measure k_m, was first introduced by Doyle [40] and Safonov [41] in 1982 as a systematic way of dealing with robust stability problems with respect to structured uncertainty to get less conservative conditions. It was subsequently extended to mixed real/complex cases by a number of researchers [42]. In this chapter, the framework of μ-based robust stability (RS) analysis, robust performance (RP) analysis, and robust synthesis will be established.

3.1 Uncertainty

No mathematical model can precisely describe the real physical systems, thus uncertainty is introduced into the mathematical model. The theory of robust control attempts to take into account these inherent inaccuracies in the modeling, and provides systematic analysis and design techniques in the presence of uncertainty. The various sources of model uncertainty may be grouped into two main classes:

1. Parametric uncertainty. Here the model structure is assumed to be known and only the values of certain real parameters in that model are uncertain.

2. Unmodeled dynamics. Here the model structure is not known exactly, or is approximated by a low order linear model.

Parametric uncertainty can be quantified by assuming that each uncertain parameter α is bounded within some region $[\alpha_{min}, \alpha_{max}]$. That is, we have the parameter set of the following form:

$$\alpha = \overline{\alpha}(1 + r\delta)$$

where $\overline{\alpha}$ is the mean parameter value, $r = (\alpha_{max} - \alpha_{min})/(\alpha_{max} + \alpha_{min})$ is the relative uncertainty in the parameter, and δ is any real scalar with $|\delta| \leq 1$.

Unmodeled dynamics are usually quantified in the frequency domain by the form of additive or multiplicative uncertainties [43]. This leads to the complex uncertainty which can be normalized such that $||\Delta(s)||_\infty \leq 1$ where $\Delta(s)$ is the transfer function representing the unmodeled dynamics.

In this dissertation, we will focus on the real parametric uncertainty in power systems. The wide range of operating conditions, including total generation in certain areas, power exchanges among areas, and unknown line parameters, can be viewed as parametric uncertainty. The unmodeled dynamics will only be used to represent the performance specification in the RP analysis of the power system and in the μ-synthesis of SVC's damping controller. It should be noted that the Structured Singular Value (SSV) technique, which will be detailed later, can be used for systems with both parametric uncertainty and unmodeled dynamics.

3.2 Linear Fractional Transformation

Consider a matrix $M \in \mathbf{C}^{n \times n}$ partitioned as

$$M = \begin{bmatrix} M_{11} & M_{12} \\ M_{21} & M_{22} \end{bmatrix} \tag{3.1}$$

with $M_{11} \in \mathbf{C}^{n_1 \times n_1}$, $M_{22} \in \mathbf{C}^{n_2 \times n_2}$ and $n_1 + n_2 = n$. Suppose we have block structures $X_{\mathcal{K}_1}$ and $X_{\mathcal{K}_2}$ defined as follows:

$$\begin{aligned} X_{\mathcal{K}_1} &= \{\Delta_1 : \Delta_1 \in \mathbf{C}^{n_1 \times n_1}\} \\ X_{\mathcal{K}_2} &= \{\Delta_2 : \Delta_2 \in \mathbf{C}^{n_2 \times n_2}\} \end{aligned}$$

then the block structure of $X_{\mathcal{K}}$ defined as

$$X_{\mathcal{K}} := \{\Delta = \text{block diag}(\Delta_1, \Delta_2) : \Delta_1 \in X_{\mathcal{K}_1}, \Delta_2 \in X_{\mathcal{K}_2}\} \tag{3.2}$$

is compatible with M. Now given any $\Delta_1 \in X_{\mathcal{K}_1}$, the LFT $F_u(M, \Delta_1)$ is said to be well-posed if and only if there exists a unique solution to the loop equations shown in Figure 3.1, namely

$$\begin{aligned} w &= M_{11} z + M_{12} d \\ e &= M_{21} z + M_{22} d \\ z &= \Delta_1 w \end{aligned}$$

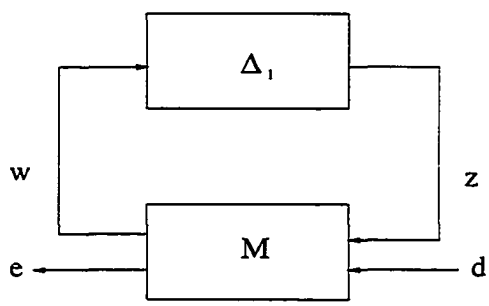

Figure 3.1 Upper and lower LFT

It is easy to see that $F_u(M, \Delta_1)$ is well posed if and only if $(I_{n_1} - M_{11}\Delta_1)$ is invertible. When the LFT is well-posed, it is defined to be an unique mapping from d to e, i.e., the vectors e and d satisfy $e = F_u(M, \Delta_1)d$ where

$$F_u(M, \Delta_1) := M_{22} + M_{21}\Delta_1(I_{n_1} - M_{11}\Delta_1)^{-1} M_{12} \tag{3.3}$$

Note that in the above derivation we always assume that the feedback is closed around the top inputs and outputs, and hence we obtain an upper LFT (denoted by F_u). We can analogously define lower LFT (denoted by F_l) as

$$F_l(M, \Delta_2) := M_{11} + M_{12}\Delta_2(I_{n_2} - M_{22}\Delta_2)^{-1}M_{21} \tag{3.4}$$

A fundamental property of the LFT is that the interconnections of LFTs are again LFTs. Therefore, the LFT is very flexible in representing both parametric uncertainty and unmodeled dynamics. An uncertain real parameter $\alpha = \overline{\alpha}(1 + r\delta)$ can be written in an upper LFT form

$$\alpha = F_u\left(\begin{bmatrix} 0 & r \\ \overline{\alpha} & \overline{\alpha} \end{bmatrix}, \delta\right) \tag{3.5}$$

For a system with parametric uncertainty, the coefficient matrices of the state space equation are typically uncertain. By representing each uncertain coefficient of these matrices in the LFT form, the whole system can also be represented in the LFT form in which case the uncertainty is represented in a structured manner (diagonal block with real numbers or repeated real numbers). Since problems involving additive and/or multiplicative uncertainty are special cases of linear fractional uncertainty descriptions, we may allow these uncertainties to enter the system in a linear fractional way and obtain the complex uncertainty block in a structured manner. Therefore, by using structured real and complex uncertainties, we can capture both parametric uncertainty and unmodeled dynamics and formulate the standard framework for robustness analysis as shown in Figure 3.2. This will become more clear in Chapter 5 when we model different operating conditions in power systems as parametric uncertainties.

3.3 Structured Singular Value μ

The definition of μ for a general complex matrix M comes from the task of finding the smallest structured uncertainty Δ (measured in terms of the maximal singular value

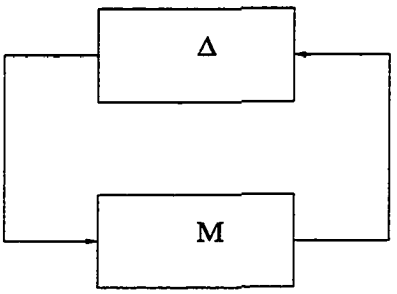

Figure 3.2 Robustness analysis framework.

of Δ, $\bar{\sigma}(\Delta)$), which makes $\det(I - M\Delta) = 0$, so μ is dependent on the underlying block structure of the uncertainty.

More precisely, suppose we have a complex matrix $M \in C^{n\times n}$ and three non-negative integers m_r, m_c, and m_C (with $m := m_r + m_c + m_C \leq n$), which specify the number of uncertainty blocks of repeated real scalars, repeated complex scalars, and full complex blocks, respectively. Then the block structure $K(m_r, m_c, m_C)$ is an m-tuple of positive integers:

$$\mathcal{K} = (k_1, ..., k_{m_r}, k_{m_r+1}, ..., k_{m_r+m_c}, k_{m_r+m_c+1}, ..., k_m) \tag{3.6}$$

This m-tuple specifies the dimensions of the perturbation blocks, and we require $\sum_{i=1}^{m} k_i = n$ in order that these dimensions are compatible with M. This determines the following set of allowable uncertainty:

$$\begin{aligned} X_{\mathcal{K}} := \{\Delta = \text{block diag}(&\delta_1^r I_{k_1}, ..., \delta_{m_r}^r I_{k_{m_r}}, \delta_1^c I_{k_{m_r+1}}, ..., \delta_{m_c}^c I_{k_{m_r+m_c}}, \\ &\Delta_1^C, ..., \Delta_{m_C}^C) : \delta_i^r \in \mathbf{R}, \delta_i^c \in \mathbf{C}, \Delta_i^C \in \mathbf{C}^{k_{m_r+m_c+i}\times k_{m_r+m_c+i}}\} \end{aligned} \tag{3.7}$$

Then $\mu_{\mathcal{K}}(M)$, the SSV of matrix M with respect to a block structure $\mathcal{K}(m_r, m_c, m_C)$, is defined as follows:

$$\mu_{\mathcal{K}}(M) := (\min_{\Delta\in X_{\mathcal{K}}} \{\bar{\sigma}(\Delta) : \det(I - M\Delta) = 0\})^{-1} \tag{3.8}$$

with $\mu_{\mathcal{K}}(M) = 0$ if $\det(I - M\Delta) \neq 0$ for all $\Delta \in X_{\mathcal{K}}$.

Note that the block structure of $X_{\mathcal{K}}$ in (3.7) is sufficiently general to allow (any combination of) repeated real scalars, repeated complex scalars, and full complex blocks. There are two special cases in which the definition of μ can be simplified:

1. Δ is a repeated real scalar block, i.e., $m_r = 1$ and $m_c = m_C = 0$, we have

$$\mu_{\mathcal{K}}(M) = \rho_R(M)$$

where $\rho_R(M) := max\{|\lambda| : \lambda \text{ is a real eigenvalue of } M\}$, with $\rho_R(M) = 0$ if M has no real eigenvalues. Thus μ is the real spectral radius of M.

2. Δ is a full complex block (unstructured uncertainty), i.e., $m_r = m_c = 0$ and $m_C = 1$, we have

$$\mu_{\mathcal{K}}(M) = \overline{\sigma}(M)$$

For a general type of uncertainty $\Delta \in X_{\mathcal{K}}$, the following holds:

$$\rho_R(M) \leq \mu_{\mathcal{K}}(M) \leq \overline{\sigma}(M) \tag{3.9}$$

so μ can be viewed as a generalization of both the real spectral radius and the maximal singular value.

From the definition of μ in (3.8), it is not obvious how the value of μ may be computed. In fact, the exact calculation of μ is generally very difficult [44]. Equation (3.9) provides the lower and upper bounds for μ, however, both bounds are too crude since the gap between them can be arbitrarily large in some cases. In order to reduce the gap, we define the following sets of scaling matrices $Q_{\mathcal{K}}$ and $D_{\mathcal{K}}$:

$$Q_{\mathcal{K}} := \{\Delta \in X_{\mathcal{K}} : \delta_i^r \in [-1, 1], \delta_i^{c*}\delta_i^c = 1, \Delta_i^{C*}\Delta_i^C = I_{k_{m_r+m_c+i}}\}$$

$$D_{\mathcal{K}} := \{\text{block diag}(D_1, ..., D_{m_r+m_c}, d_1 I_{k_{m_r+m_c+1}}, ..., d_{m_C} I_{k_m}) :$$
$$0 < D_i = D_i^* \in \mathbf{C}^{k_i \times k_i}, 0 < d_i \in \mathbf{R}\}$$

then the lower bound and upper bound can be refined as

$$\max_{Q \in Q_{\mathcal{K}}} \rho_R(QM) \leq \mu_{\mathcal{K}}(M) \leq \inf_{D \in D_{\mathcal{K}}} \overline{\sigma}(DMD^{-1}) \tag{3.10}$$

It has been proved in [40] that the first inequality in (3.10) is actually an equality. However, the function $\rho(QM)$ is not convex in $Q \in Q_{\mathcal{K}}$ and therefore it is not guaranteed to find the global maximum. The practical computation uses a power iteration algorithm to find a local maximum and thus obtains a lower bound for μ. On the other hand, the calculation of upper bound from (3.10) is a convex minimization problem for the maximal singular value, so all local minima are global and hence this bound is computationally attractive. In this research, we will use the commercially available MATLAB μ-toolbox to compute μ upper and lower bounds [46].

3.4 Robust Stability

The general definition of μ is now extended to the linear system case. Instead of being a constant complex matrix, M is now a transfer function matrix. Since we only consider the real parametric uncertainty in the RS analysis, the general uncertainty structure $X_{\mathcal{K}}$ in (3.7) can be simplified to a new set $\mathbf{\Delta}_S$ defined as:

$$\mathbf{\Delta}_S := \{\delta_1^r I_{k_1}, ..., \delta_S^r I_{k_S} : \delta_i^r \in \mathbf{R}\} \tag{3.11}$$

where $\sum_{i=1}^{S} k_i = n$.

The following theorem addresses the robust stability of linear systems and gives rise to the most common usage of μ as a frequency domain robustness test.

Theorem 3.1 (Robust Stability [44]) *Suppose $M(s)$ is a nominal stable system(otherwise the problem is trivial), then for all Δ in $\mathbf{\Delta}_S$ satisfying $\overline{\sigma}(\Delta) \leq \frac{1}{\beta}$, the perturbed closed-loop system shown in Figure 3.2 is well posed and internally stable if and only if*

$$\sup_{\omega \in R} \mu_{\mathbf{\Delta}_S}(M(j\omega)) < \beta \tag{3.12}$$

This expression means that we can evaluate the robustness properties of a closed-loop system by using a frequency evaluation of μ. For any given frequency point we have a constant matrix μ problem, and the peak value of the frequency μ-plot determines the maximal size of the uncertainty for which the close-loop system can maintain stability.

As mentioned above, the μ-Toolbox software does not compute μ exactly, but bounds it from above and below by several optimization steps. Hence the conclusion can be restated in terms of upper and lower bounds. Let β_u and β_l be upper and lower bounds of μ respectively, then

- For all uncertainty matrices Δ in $\mathbf{\Delta}_S$ satisfying $\overline{\sigma}(\Delta) < \frac{1}{\beta_u}$, the closed-loop system is stable;
- There is a particular uncertainty matrix Δ in $\mathbf{\Delta}_S$ satisfying $\overline{\sigma}(\Delta) = \frac{1}{\beta_l}$ that causes instability.

3.5 Robust Performance

The RS setup presented above also allows direct calculation of robust performance (RP). Typically, there are exogenous disturbances acting on the system which result in tracking or regulation errors. With uncertainty in the system, the effect that these disturbances have on the error signals can greatly increase. In most cases, long before the onset of instability, the closed-loop performance will degrade to unacceptable levels. Hence the RP test is necessary.

The framework for RP analysis in shown in Figure 3.3. $T = F_u(M, \Delta)$ is the transfer function matrix from the disturbance signal vector d to the error signal vector e. The

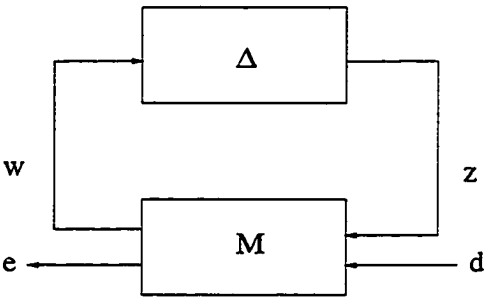

Figure 3.3 RP analysis framework.

performance of the system is characterized by the H_∞ norm of T defined as

$$\|T\|_\infty = \max_{\omega \in \mathbf{R}} \overline{\sigma}(T(j\omega))$$

It can be shown that an RP problem is equivalent to an RS problem with augmented uncertainty block $diag(\Delta, \Delta_p)$, as illustrated in Figure 3.4 (see [46]). Here Δ_p is an $n_d \times n_e$ full complex matrix, and n_d and n_e are dimensions of d and e, respectively. This is formally stated in the following theorem:

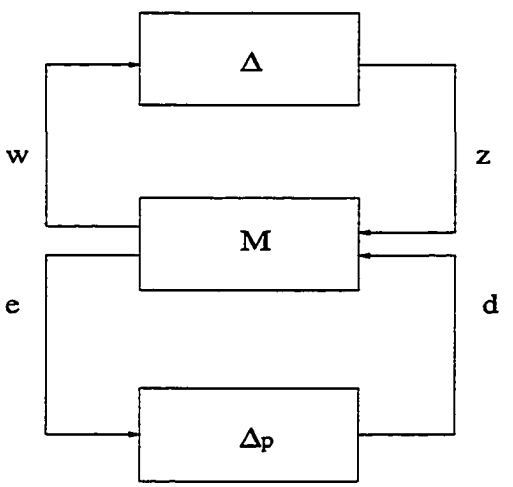

Figure 3.4 Equivalent RP analysis framework.

Theorem 3.2 (Robust Performance [44]) *Suppose $M(s)$ is a nominal stable system(otherwise the problem is trivial), then for all $\Delta \in \mathbf{\Delta}_S$ satisfying $\overline{\sigma}(\Delta) \leq \frac{1}{\beta}$, the perturbed closed-loop system shown in Figure 3.3 is well posed, internally stable, and $\|F_u(M,\Delta)\|_\infty < \beta$ if and only if*

$$\sup_{\omega \in R} \mu_{\mathbf{\Delta}_P}(M(j\omega)) < \beta \tag{3.13}$$

where

$$\mathbf{\Delta}_P := \left\{ \begin{bmatrix} \Delta & 0 \\ 0 & \Delta_p \end{bmatrix} : \Delta \in \mathbf{\Delta}_S, \Delta_p \in \mathbf{C}^{n_d \times n_e} \right\} \tag{3.14}$$

Specifically, for normalized Δ ($\beta = 1$), the closed-loop system is said to achieve RP if $\sup_{\omega \in R} \mu_{\mathbf{\Delta}_P}(M(j\omega)) < 1$.

3.6 μ Synthesis

The standard framework for μ-synthesis is given in Figure 3.5. The system labeled P is the open-loop interconnection and contains all of the the known elements including the nominal plant model and appropriate weighting functions, and Δ is the uncertainty block from the set $\mathbf{\Delta}_S$. The set of uncertain systems to be controlled is described by the LFT

$$\{F_u(P,\Delta) : \Delta \in \mathbf{\Delta}_S, \overline{\sigma}(\Delta) \leq 1\}$$

The design objective is to find a controller K that belongs to the class K_s of all rational proper controllers such that for all uncertainty $\Delta \in \mathbf{\Delta}_S$, $\overline{\sigma}(\Delta) \leq 1$, , the closed-loop system is stable and satisfies

$$\|F_l[F_u(P,\Delta), K]\|_\infty < 1 \tag{3.15}$$

It is clear from Figure 3.5 that

$$F_l[F_u(P,\Delta), K] = F_u[F_l(P,K), \Delta]$$

Therefore, the performance requirement in (3.15) becomes:

$$\|F_u[F_l(P,K),\Delta]\|_\infty < 1 \tag{3.16}$$

Since the robust performance problem can be treated as an "augmented" robust stability problem, and K achieves robust performance if and only if

$$\max_\omega \mu_{\Delta_P}(F_l(P,K)(j\omega)) < 1 \tag{3.17}$$

so the μ-synthesis is equivalent to minimizing the peak value of $\mu_{\Delta_P}(.)$ of the closed-loop transfer function $F_l(P,K)$ over all stabilizing controllers K, i.e.,

$$\min_K \max_\omega \mu_{\Delta_P}(F_l(P,K)(j\omega)) \tag{3.18}$$

While the exact solution to this problem is not known yet, the standard "D-K iteration" procedure works very well to obtain a satisfactory controller in many designs. The procedure involves two optimization problems: a standard H_∞ optimization problem and a standard convex optimization problem. Details about "D-K iteration" can be found in [46, 47].

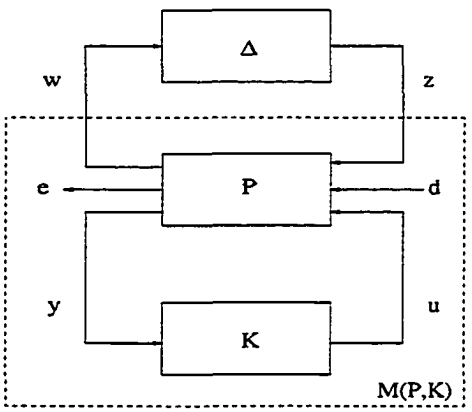

Figure 3.5 μ synthesis framework.

4 POWER SYSTEM MODELS

In order to apply the robust methodology to power systems, the nominal system model must be obtained first. The state space representation of the nominal system can be obtained from the linearized models of the power system components including generators, exciters, and SVCs. Since the power system is a nonlinear system and the models of these components are coupled implicitly with the network model, the system to be linearized has the following general form:

$$\begin{cases} \dot{X} = f(X, Y) \\ 0 = g(X, Y) \end{cases} \tag{4.1}$$

where X and Y are the vectors of state variables and non-state variables, respectively; f and g are nonlinear functions of X and Y. In this chapter, we will show how the equations for the power system can be formulated and linearized into the common state space representation.

4.1 Generator Model

In this dissertation, we use two kinds of generator models which are the two-axis model and the classical model [49]. We assume that in a power system with n generators, the first m generators are represented by the two-axis model and equipped with exciters and the remaining $n - m$ generators are represented using the classical model.

4.1.1 Classical Model

The classical model is the simplest model to represent generators without excitation control in a multi-machine system (see Chapter 2 of [49]). It is based on the following assumptions:

1. Mechanical power input is constant.
2. Damping or asynchronous power is negligible.
3. Constant-voltage-behind-transient-reactance model for the synchronous machines is valid.
4. The mechanical rotor angle of a machine coincides with the angle of the voltage behind the transient reactance.

With the loads represented by constant impedance, the load nodes and the terminal voltage nodes of the generators are eliminated. The resulting network contains only the internal generator nodes (numbered from 1 to n) and the SVC node (numbered $n+1$). The generator reactance and the constant impedance loads are included in the bus admittance matrix Y_{bus} of the reduced network.

The dynamic equations for the classical model are given by

$$M_i\dot{\omega}_i = P_i - P_{ei} \tag{4.2}$$

$$\dot{\delta}_i = \omega_i - \omega_S \qquad i = m+1, m+2, ..., n \tag{4.3}$$

where,

$$P_i = P_{mi} - E_i^2 G_{ii}$$

$$P_{ei} = \sum_{j=1, j\neq i}^{n} [E_i E_j B_{ij} \sin(\delta_i - \delta_j) + E_i E_j G_{ij} \cos(\delta_i - \delta_j)]$$
$$+ E_i V_{n+1} B_{i,n+1} \sin(\delta_i - \theta_{n+1}) + E_i V_{n+1} G_{i,n+1} \cos(\delta_i - \theta_{n+1})$$

and

E_i: internal bus voltage of generator i

M_i: inertia constant of generator i

P_{mi}: mechanical power input of generator i

G_{ii}: driving point conductance of node i

$G_{ij} + jB_{ij}$: the transfer admittance between node i and node j in the reduced network

ω_i: rotor speed of generator i (with respect to the synchronous frame)

ω_S: synchronous speed

V_{n+1}: voltage magnitude of the SVC bus

θ_{n+1}: voltage angle of the SVC bus

4.1.2 Two-axis Model

Generators with excitation control are described by the two-axis model (see chapter 4 of [49]) in this work. In the two-axis model the transient effects are accounted for and the following assumptions are required.

1. In the stator voltage equations the variation of flux linkages of d-q axes are negligible compared to the speed voltage terms.

2. $\omega \cong \omega_S = 1$ p.u.

The resultant dynamic equations are given by

$$\tau'_{d0i}\dot{E}'_{qi} = E_{FDi} - E'_{qi} + (x_{di} - x'_{di})I_{di} \tag{4.4}$$

$$\tau'_{q0i}\dot{E}'_{di} = -E'_{di} - (x_{qi} - x'_{qi})I_{qi} \tag{4.5}$$

$$M_i\dot{\omega}_i = P_{mi} - (I_{di}E'_{di} + I_{qi}E'_{qi}) + (x'_{qi} - x'_{di})I_{qi}I_{di} - D_i(\omega_i - \omega_S) \tag{4.6}$$

$$\dot{\delta}_i = \omega_i - \omega_S \qquad i = 1, 2, ..., m \tag{4.7}$$

where,

E'_d, E'_q: direct and quadrature axes stator EMFs corresponding to rotor transient flux components, respectively

I_d, I_q: the d and q axes stator currents

τ'_{d0}, τ'_{q0}: open-circuit direct and quadrature axes transient time constants

x_d, x'_d: direct axis synchronous and transient reactances

x_q, x'_q: quadrature axis synchronous and transient reactances

E_{FD}: stator EMF corresponding to the field voltage

D_i: damping coefficient of generator i

4.1.3 Angle Reference

In (4.3) and (4.7), we used the absolute rotor angles (δ_i, $i = 1, 2, \ldots, n$) as state variables. Since these n state variables are not independent, we can introduce the relative rotor angles as new state variables which are independent. Without loss of generality, δ_1 is chosen as reference, then the relative rotor angles are defined as:

$$\delta_{i1} = \delta_i - \delta_1, \qquad i = 2, 3, \ldots, n$$

The dynamic equations (4.2) — (4.7) remain unchanged with each δ_i replaced by δ_{i1} and ω_S replaced by ω_1. Therefore (4.3) and (4.7) becomes

$$\dot{\delta}_{i1} = \omega_i - \omega_1 \qquad i = 2, 3, \ldots, n \tag{4.8}$$

4.2 Excitation System Model

The type of excitation system used is ETMSP Type-30 [51] (same as IEEE AC-4, see [52]), as shown in Figure 4.1. The state variables are E_{FD}, X_{E1}, and X_{E2}, and the dynamic equations are given by

$$\dot{E}_{FDi} = \frac{K_{Ai}}{T_{Ai}} X_{E2i} - \frac{1}{T_{Ai}} E_{FDi} + \frac{aK_{Ai}}{T_{Ai}} (V_{REFi} - X_{E1i}) \tag{4.9}$$

$$\dot{X}_{E1i} = -\frac{1}{T_{Ri}} X_{E1i} + \frac{1}{T_{Ri}} V_{Ti} \tag{4.10}$$

$$\dot{X}_{E2i} = -\frac{1}{T_{Bi}} X_{E2i} + \frac{1-a}{T_{Bi}} (V_{REFi} - X_{E1i}) \tag{4.11}$$

$$V_T = V_{Tq} + jV_{Td}$$

$$= (E'_q + x'_d I_d) + j(E'_d - x'_q I_q) \qquad i = 1, 2, ..., m \tag{4.12}$$

where,

V_T: generator terminal voltage

V_{REF}: exciter reference voltage

$a = T_{Ci}/T_{Bi}$, T_{Bi} and T_{Ci} are time constants

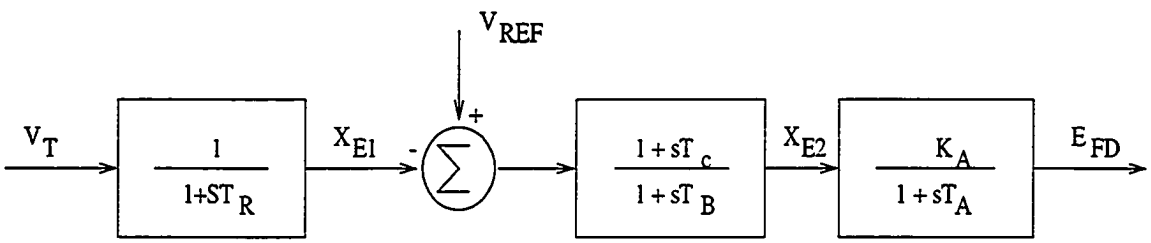

Figure 4.1 Excitation system model: ETMSP Type-30.

4.3 SVC model

The standard ETMSP Type-1 model is used for the SVC [51]. Its block diagram is shown in Figure 4.2. The state variables are X_{S1}, X_{S2}, and B_{SVC}, and the dynamic equations are given by:

$$\dot{X}_{S1} = -\frac{1}{T_3} X_{S1} + \frac{(1-a_1)K}{T_3} (V_{SVC} - V_{REF}) \tag{4.13}$$

$$\dot{X}_{S2} = \frac{1-a_2}{T_4} X_{S1} - \frac{1}{T_4} X_{S2} + \frac{(1-a_2)a_1 K}{T_4} (V_{SVC} - V_{REF}) \tag{4.14}$$

$$\dot{B}_{SVC} = \frac{a_2}{T_5}X_{S1} + \frac{1}{T_5}(X_{S2} - B_{SVC}) + \frac{a_1 a_2 K}{T_5}(V_{SVC} - V_{REF}) \qquad (4.15)$$

where,

B_{SVC}: equivalent admittance of the SVC

V_{SVC}: voltage magnitude of the SVC bus ($= V_{n+1}$)

V_{REF}: SVC reference voltage

$a_1 = T_1/T_3$

$a_2 = T_2/T_4$

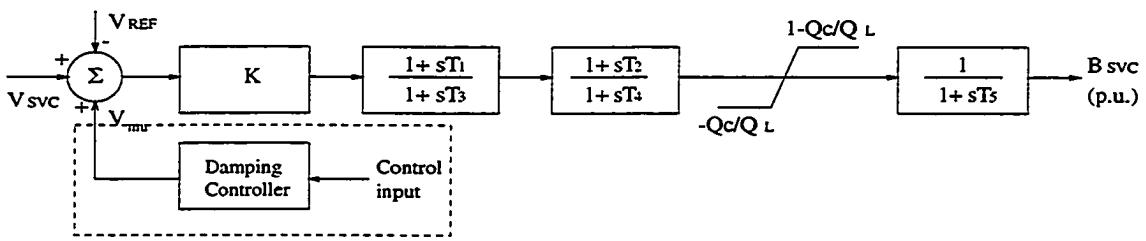

Figure 4.2 ETMSP standard SVC type-1 with SDC added.

Later in Chapter 6 of this thesis, a supplementary damping controller (SDC) will be designed and added to the SVC's voltage control loop to damp the interarea oscillations, as shown in Figure 4.2.

4.4 Network Modeling

As mentioned before, the network has been reduced to contain only the generator internal buses and the SVC bus. The bus admittance matrix Y_{bus} consists of $Y_{ij}\angle\gamma_{ij} = G_{ij} + jB_{ij}$. Therefore the general network equation is given by

$$\overline{I} = Y_{bus}\overline{V} \qquad (4.16)$$

where,

$\overline{I}$: the vector of bus current injections in the common reference frame

$\overline{V}$: the vector of bus voltages in the common reference frame

Since generators are reduced to their internal buses, the associated currents and voltages are usually in the $d-q$ axis reference frame, as shown in (4.2) — (4.6). Therefore, a procedure based on Chapter 9 of [49] for reference transformation needs to be carried out on (4.16). For generator buses (both the two-axis model and the classical model), this procedure yields the generator currents in the following form:

$$I_{qi} = \sum_{j=1}^{m}[F_{G+B}(\delta_{ij})E'_{qj} - F_{B-G}(\delta_{ij})E'_{dj}] + \sum_{k=m+1}^{n} F_{G+B}(\delta_{ik})E_k + F_{G+B}(\delta_{i,n+1})V_{n+1} \quad (4.17)$$

$$I_{di} = \sum_{j=1}^{m}[F_{B-G}(\delta_{ij})E'_{qj} + F_{G+B}(\delta_{ij})E'_{dj}] + \sum_{k=m+1}^{n} F_{B-G}(\delta_{ik})E_k + F_{B-G}(\delta_{i,n+1})V_{n+1} \quad (4.18)$$

$$I_k = \sum_{j=1}^{m}[F_{G+B}(\delta_{kj})E'_{qj} - F_{B-G}(\delta_{kj})E'_{dj}] + \sum_{l=m+1}^{n} F_{G+B}(\delta_{kl})E_l + F_{G+B}(\delta_{k,n+1})V_{n+1} \quad (4.19)$$

$$i = 1, 2, ..., m \qquad k, l = m+1, ..., n$$

where

$$F_{G+B}(\delta_{ij}) = G_{ij}\cos(\delta_{ij}) + B_{ij}\sin(\delta_{ij}) \quad (4.20)$$

$$F_{B-G}(\delta_{ij}) = B_{ij}\cos(\delta_{ij}) - G_{ij}\sin(\delta_{ij}) \quad (4.21)$$

$$\delta_{ij} = \delta_i - \delta_j \quad (4.22)$$

$$F_{G+B}(\delta_{i,n+1}) = G_{i,n+1}\cos(\delta_i - \theta_{n+1}) + B_{i,n+1}\sin(\delta_i - \theta_{n+1}) \quad (4.23)$$

$$F_{B-G}(\delta_{i,n+1}) = B_{i,n+1}\cos(\delta_i - \theta_{n+1}) - G_{i,n+1}\sin(\delta_i - \theta_{n+1}) \quad (4.24)$$

For the SVC bus, the above procedure yields expression of similar form for I_{SVC}. We further derive the injected power of the SVC bus in the following form:

$$P_{n+1} = V_{n+1}\sum_{i=1}^{m}[F_{G+B}(\delta_{n+1,i})E'_{qi} - F_{B-G}(\delta_{n+1,i})E'_{di}] + V_{n+1}\sum_{i=m+1}^{n}[F_{G+B}(\delta_{n+1,i})E_i] + G_{n+1,n+1}V_{n+1}^2 \quad (4.25)$$

$$\begin{aligned} Q_{n+1} &= -V_{n+1}\sum_{i=1}^{m}[F_{G+B}(\delta_{n+1,i})E'_{di} + F_{B-G}(\delta_{n+1,i})E'_{qi}] \\ &\quad -V_{n+1}\sum_{i=m+1}^{n}[F_{B-G}(\delta_{n+1,i})E_i] - B_{n+1,n+1}V_{n+1}^2 \end{aligned} \tag{4.26}$$

where

$$F_{G+B}(\delta_{n+1,i}) = G_{n+1,i}\cos(\theta_{n+1}-\delta_i) + B_{n+1,i}\sin(\theta_{n+1}-\delta_i) \tag{4.27}$$

$$F_{B-G}(\delta_{n+1,i}) = B_{n+1,i}\cos(\theta_{n+1}-\delta_i) - G_{n+1,i}\sin(\theta_{n+1}-\delta_i) \tag{4.28}$$

We also know that the injected power at the SVC bus is the (reactive) power output of the SVC, i.e.,

$$\begin{cases} P_{n+1} = 0 \\ Q_{n+1} = -B_{SVC}V_{n+1}^2 \end{cases} \tag{4.29}$$

Therefore, we have the following nonlinear algebraic equations:

$$\begin{aligned} g_1 &= 0 \\ &= \sum_{i=1}^{m}[F_{G+B}(\delta_{n+1,i})E'_{qi} - F_{B-G}(\delta_{n+1,i})E'_{di}] \\ &\quad + \sum_{i=m+1}^{n}[F_{G+B}(\delta_{n+1,i})E_i] + G_{n+1,n+1}V_{n+1} \end{aligned} \tag{4.30}$$

$$\begin{aligned} g_2 &= 0 \\ &= \sum_{i=1}^{m}[F_{G+B}(\delta_{n+1,i})E'_{di} + F_{B-G}(\delta_{n+1,i})E'_{qi}] \\ &\quad + \sum_{i=m+1}^{n}[F_{B-G}(\delta_{n+1,i})E_i] + (B_{n+1,n+1} - B_{SVC})V_{n+1} \end{aligned} \tag{4.31}$$

4.5 Overall System Equation

From the above discussions, the dynamic equations governing the generators, exciters, and the SVC have the following general form:

$$\dot{X} = f(X, Y, u) \tag{4.32}$$

where,

$X^T = [X_{SM}^T, X_{ES}^T, X_{SVC}^T]$, the vector of state variables

$$X_{SM} = [E'_{q1}, E'_{d1}, \omega_1, ..., E'_{qm}, E'_{dm}, \omega_m, \delta_{m1}, \omega_{m+1}, \delta_{(m+1)1}, ..., \omega_n, \delta_{n1}]^T$$

$$X_{ES} = [E_{FD1}, X_{E11}, X_{E21}, ..., E_{FDm}, X_{E1m}, X_{E2m}]^T$$

$$X_{SVC} = [X_{S1}, X_{S2}, B_{SVC}]^T$$

$Y = [V_{n+1}, \theta_{n+1}]^T$, the vector of non-state (network) variables

$u = [V_{REF1}, \ldots, V_{REFm}, V_{REF,SVC}]^T$, the vector of control inputs

and f is the vector of nonlinear functions summarized below:

$$\begin{aligned}
f_{1i} &= \dot{E}'_{qi} \\
&= \frac{1}{\tau'_{d0i}}[E_{FDi} - E'_{qi} + (x_{di} - x'_{di})I_{di}] \qquad i = 1, ..., m \qquad (4.33) \\
f_{2i} &= \dot{E}'_{di} \\
&= \frac{1}{\tau'_{q0i}}[-E'_{di} - (x_{qi} - x'_{qi})I_{qi}] \qquad i = 1, ..., m \qquad (4.34) \\
f_{3i} &= \dot{\omega}_i \qquad i = 1, ..., n \\
&= \frac{1}{M_i}[P_{mi} - (I_{di}E'_{di} + I_{qi}E'_{qi}) + (x'_{qi} - x'_{di})I_{qi}I_{di} - D_i(\omega_i - \omega_S)] \qquad (4.35) \\
f_{4i} &= \dot{\delta}_{i1} \\
&= \omega_i - \omega_1 \qquad i = 2, ..., n \qquad (4.36) \\
f_{5i} &= \dot{E}_{FDi} \\
&= \frac{K_{Ai}}{T_{Ai}}X_{E2i} - \frac{1}{T_{Ai}}E_{FDi} + \frac{aK_{Ai}}{T_{Ai}}(V_{REFi} - X_{E1i}) \qquad i = 1, ..., m \qquad (4.37) \\
f_{6i} &= \dot{X}_{E1i} \\
&= -\frac{1}{T_{Ri}}X_{E1i} + \frac{1}{T_{Ri}}V_{Ti} \qquad i = 1, ..., m \qquad (4.38) \\
f_{7i} &= \dot{X}_{E2i} \\
&= -\frac{1}{T_{Bi}}X_{E2i} + \frac{1-a}{T_{Bi}}(V_{REFi} - X_{E1i}) \qquad i = 1, ..., m \qquad (4.39) \\
f_8 &= \dot{X}_{S1} \\
&= -\frac{1}{T_3}X_{S1} + \frac{(1-a_1)K}{T_3}(V_{SVC} - V_{REF,SVC}) \qquad (4.40) \\
f_9 &= \dot{X}_{S2} \\
&= \frac{1-a_2}{T_4}X_{S1} - \frac{1}{T_4}X_{S2} + \frac{(1-a_2)a_1K}{T_4}(V_{SVC} - V_{REF,SVC}) \qquad (4.41)
\end{aligned}$$

$$
\begin{aligned}
f_{10} &= \dot{B}_{SVC} \\
&= \frac{a_2}{T_5} X_{S1} + \frac{1}{T_5}(X_{S2} - B_{SVC}) + \frac{a_1 a_2 K}{T_5}(V_{SVC} - V_{REF,SVC}) \qquad (4.42)
\end{aligned}
$$

Note that we use (4.35) to model generators in the two-axis model as well as in the classical model. This is true because the classical model can be viewed as a special case of the two-axis model with $E'_q = E$, $E'_d = 0$, $I_q = I$, and $I_d = 0$. I_{di}, I_{qi}, I_k in (4.17) — (4.19) are not included as non-state variables since they can be substituted into (4.33) — (4.42) directly.

Linearization of (4.32) leads to

$$\Delta\dot{X} = \frac{\partial f}{\partial X}\Delta X + \frac{\partial f}{\partial Y}\Delta Y + \frac{\partial f}{\partial u}\Delta u \qquad (4.43)$$

We also have the network algebraic equation

$$g(X, Y) = 0 \qquad (4.44)$$

from (4.30) and (4.31) where $g = [g_1, g_2]^T$. Linearization of (4.44) results in

$$\frac{\partial g}{\partial X}\Delta X + \frac{\partial g}{\partial Y}\Delta Y = 0 \qquad (4.45)$$

$$\Delta Y = -(\frac{\partial g}{\partial Y})^{-1}\frac{\partial g}{\partial X}\Delta X \qquad (4.46)$$

The details of the linearization in (4.43) and (4.45) can be found in Appendix A.

Substituting (4.46) into (4.43), we obtain the representation of the whole system in the state space form

$$\Delta\dot{X} = A\Delta X + B\Delta u \qquad (4.47)$$

where

$$A = \frac{\partial f}{\partial X} - \frac{\partial f}{\partial Y}(\frac{\partial g}{\partial Y})^{-1}\frac{\partial g}{\partial X} \qquad (4.48)$$

$$B = \frac{\partial f}{\partial u} \qquad (4.49)$$

The detailed expressions for the elements of A and B matrices are listed in Appendix A.

5 ROBUST STABILITY ANALYSIS

In this chapter, we analyze the robust stability of the power system under different operating conditions. These operating conditions are treated as parametric uncertainties and captured using a minimum overbounding approach. The general $M - \Delta$ framework for the robust stability analysis is then established. Two SSV-based methods will be used to analyze the robust stability. The frequency sweep method, presented in Section 5.2 and 5.3, has the advantage of finding the accurate μ upper bound, but usually involves a large amount of computation. The state space μ test in Section 5.4 and 5.5, can avoid the frequency sweep and save computation time. The combination of these two methods for robust stability analysis is discussed at the end of this chapter. Details of the state space test can be found in [44, 45, 48]

5.1 Uncertainty Characterization

In order to address the robust stability issue, we investigate the way in which the system dynamic equations change with the change in operating conditions. From the derivation in Chapter 4, the dynamic equation for the linearized power system model has the following form:

$$\Delta\dot{X} = A\Delta X + B\Delta u \tag{5.1}$$

Since the system stability is determined only by the A matrix in (5.1), we denote $x := \Delta X$ and consider a simplified form of (5.1) for the stability analysis:

$$\dot{x} = Ax \tag{5.2}$$

Routine analysis of the linearized model identifies that a few elements of the A matrix vary when the operating conditions change. For each machine the changing elements correspond to $\Delta E'_{qi}$, $\Delta E'_{di}$, $\Delta\omega_i$, ΔX_{E1i} rows and $\Delta E'_{qi}$, $\Delta E'_{di}$, $\Delta\delta_{1i}$ columns of the A matrix. For the SVC, the changing elements correspond to ΔX_{S1}, ΔX_{S2}, ΔB_{SVC} rows and ΔB_{SVC} column of the A matrix. Hence, for a n-machine system with all machines described by the detailed model, the dimension of the A matrix is $(7n+2) \times (7n+2)$, and a total of $(4n+3) \times (3n)$ entries of the A matrix will vary with the change of the operating conditions. The value of each varying element depends on a set of independent operating parameters $p_1, p_2, \ldots, p_m$, and can be expressed as

$$a_{ij} = f_{ij}(p_1, \ldots, p_m) \tag{5.3}$$

where p_k takes values in a known range $p_k^{min} \leq p_k \leq a_k^{max}$ for $k = 1, \ldots, m$.

Since the elements of the A matrix for a given operating condition are obtained only after the power flow equations are solved, the functions f_{ij} cannot be calculated explicitly in general. However, we can capture the dependence of a_{ij} on the parameters $p_1, p_2, \ldots, p_m$ by approximating f_{ij} with polynomials. The approximation procedure essentially consists of setting up an over determined system of linear equations for the coefficients at various points on a grid of varying operating conditions. These equations are then solved using a least square minimization approach. In most cases, a quadratic approximation can provide satisfactory precision.

Our objective is to determine whether or not the system will be stable for each value of the operating parameters in a given range $p_k^{min} \leq p_k \leq p_k^{max}$ for $k = 1, \ldots, m$. Another related objective is to determine the largest range of the operating parameters for which the system will remain stable. We will now describe how our problem can be cast as a robust stability problem in the $M - \Delta$ framework so that the SSV methods

can be applied. Without loss of generality, we assume that there are two operating parameters, p_1 and p_2, with possible values within known intervals. Each element of the A matrix which depends on these parameters is expressed by the following polynomial approximation:

$$a_{ij} = a'_{ij0} + a'_{ij1}p_1 + a'_{ij2}p_2 + a'_{ij11}p_1^2 + a'_{ij22}p_2^2 + a'_{ij12}p_1p_2 \tag{5.4}$$

where $p_k^{min} \leq p_k \leq a_k^{max}$ for $k = 1, 2$. It is desirable to normalize the range of the uncertain parameters such that the allowable range for each parameter is the interval $[-1, 1]$. This can be done by defining:

$$p_k = \frac{p_k^{max} + p_k^{min}}{2} + \frac{p_k^{max} - p_k^{min}}{2}\delta_k \tag{5.5}$$

where $-1 \leq \delta_k \leq 1$. Note that as δ_k varies within the interval $[-1, 1]$, p_k will vary within the interval $[p_k^{max}, p_k^{min}]$. Thus the variation in p_k is captured by the variation in δ_k. When substituting (5.5) into (5.4), we get a_{ij} as a polynomial of δ_1 and δ_2:

$$a_{ij} = a_{ij0} + a_{ij1}\delta_1 + a_{ij2}\delta_2 + a_{ij11}\delta_1^2 + a_{ij22}\delta_2^2 + a_{ij12}\delta_1\delta_2 \tag{5.6}$$

where the coefficients $a_{ij0}, a_{ij1}, ..., a_{ij12}$ depend on and $a'_{ij0}, a'_{ij1}, ..., a'_{ij12}$ and p_k^{min}, p_k^{max}.

Using the above equation, the dependence of the A matrix on the parameters δ_1 and δ_2 can be expressed. To do this efficiently, we define the matrix R consisting of 0's and 1's so that Rx gives the vector of those state variables whose corresponding columns in the A matrix change with the change of the operating conditions, as suggested in [36, 37]. For an n-machine system there are $3n$ such variables. Hence, R has $3n$ rows and as many columns as the total number of state variables $(7n + 2)$. Similarly we define L to be a matrix consisting of 0's and 1's so that Lx gives the vector of those state variables whose corresponding rows in the A matrix change with the change of the operating

conditions. There are $(4n+3)$ such elements. Now the dependence of the A matrix on the parameters δ_1 and δ_2 can be written as:

$$A = A_0 + L^T[A_1(\delta_1 I) + A_2(\delta_2 I) + A_{11}(\delta_1^2 I) + A_{22}(\delta_2^2 I) + A_{12}(\delta_1 \delta_2 I)]R \tag{5.7}$$

where:

$$A_0 = [a_{ij0}]_{(7n+2)\times(7n+2)},\ L^T A_p R = [a_{ijp}],\ L^T A_{pq} R = [a_{ijpq}]$$

With this representation of A, the differential equation $\dot{x} = Ax$ can be represented in an LFT form as shown in Figure 5.1.

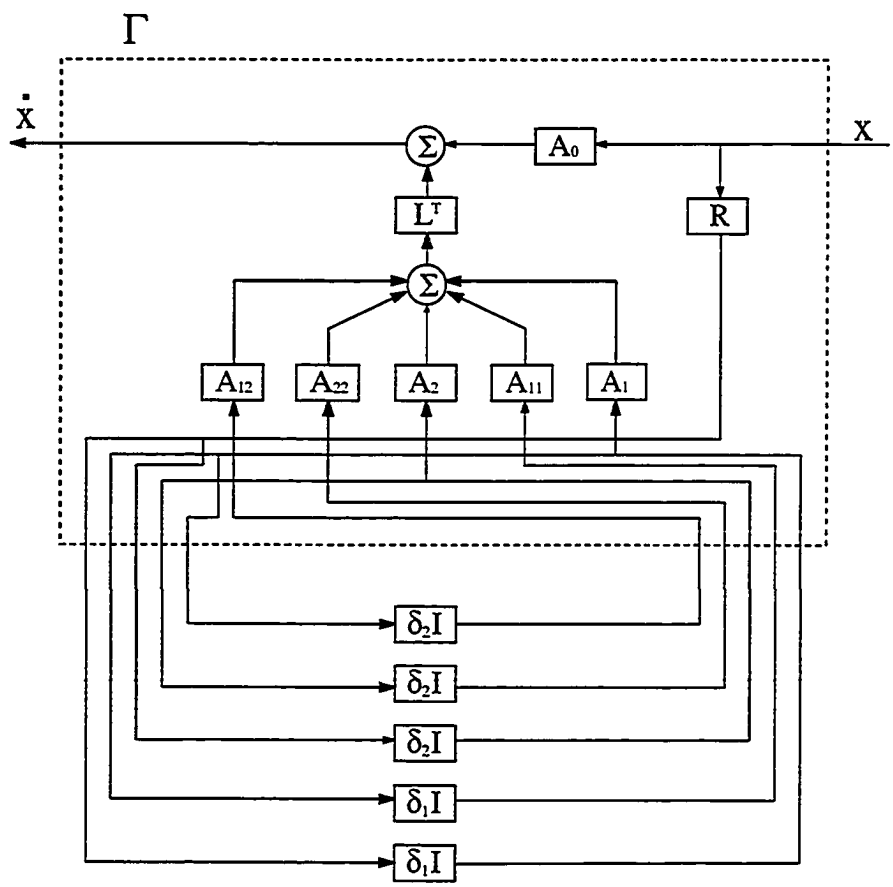

Figure 5.1 Robust stability framework in the case of two varying parameters.

In the sequel, we will be interested in the "transfer function seen by the δ's." To do this we define the matrix represented inside the dashed line in Figure 5.1 as Γ and define:

$$\Delta = \text{diag}[\delta_1 I_{6n}, \delta_2 I_{9n}]$$

Accordingly, Figure 5.1 is redrawn as Figure 5.2. From these two figures it is seen that the differential equation $\dot{x} = Ax$ can be expressed as:

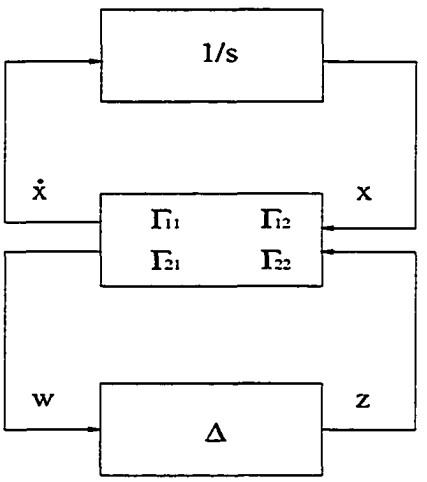

Figure 5.2 Representation of polynomial uncertainty for A-matrix.

$$\dot{x} = \Gamma_{11}x + \Gamma_{12}z \tag{5.8}$$

$$w = \Gamma_{21}x + \Gamma_{22}z \tag{5.9}$$

$$z = \Delta w \tag{5.10}$$

with:

$$\Gamma := \begin{bmatrix} \Gamma_{11} & \Gamma_{12} \\ \Gamma_{21} & \Gamma_{22} \end{bmatrix}$$

$$= \left[\begin{array}{c|ccccc} A_0 & L^T A_1 & L^T A_{11} & L^T A_2 & L^T A_{22} & L^T A_{12} \\ \hline R & 0 & 0 & 0 & 0 & 0 \\ 0 & I & 0 & 0 & 0 & 0 \\ R & 0 & 0 & 0 & 0 & 0 \\ 0 & 0 & 0 & I & 0 & 0 \\ 0 & I & 0 & 0 & 0 & 0 \end{array}\right] \tag{5.11}$$

where w and z are the vectors of perturbation inputs and outputs. $\Gamma_{11}, \Gamma_{12}, \Gamma_{21}$ and Γ_{22} are matrices with dimensions of $[(7n+2)\times(7n+2)]$, $[(7n+2)\times(15n)]$, $[(15n)\times(7n+2)]$ and $[(15n)\times(15n)]$, respectively. Δ is a diagonal $[(15n)\times(15n)]$ matrix of real repeated scalars representing the structured uncertainty of in the system.

The transfer function from w to z, $M(s)$, can then be computed using an upper LFT:

$$M = \Gamma_{22} + \Gamma_{21}\frac{1}{s}I(I - \frac{1}{s}\Gamma_{11})^{-1}\Gamma_{12} \tag{5.12}$$

It represents the transfer function seen by the uncertainty block Δ. In this way we obtain the general $M-\Delta$ framework for the robust stability analysis, as shown in Figure 3.2.

5.2 Robust Stability Assessment Approach

With the system in the $M-\Delta$ representation, we can use Theorem 3.1 to assess the robust stability of the power system. Namely, the peak value of the μ-plot of the frequency response of $M(j\omega)$ determines the size of uncertainty against which the system is robustly stable. Moreover, once the critical value of the uncertainty is obtained as a reciprocal of $\sup_{\omega\in R}\mu_\Delta[M(j\omega)]$, our set-up of the problem allows direct calculation of simultaneous maximum values of varying parameters which still guarantee the system stability by using (5.5). It should be noted that these indicators are essential to power system operators, providing them not only the indication of robust stability/instability

for a given operating range, but also an accurate estimation of the stability limits and consequently, an estimation of the stability margin measured from the current operating point. The proposed approach for robust stability analysis shown in Figure 5.3 is implemented using the following steps:

Step 1: For a defined range of parameter variations generate a reasonably dense grid of operating conditions.

Step 2: For each operating point run the power flow and create the corresponding A matrix.

Step 3: Determine coefficients of approximating polynomials for each varying element of A matrix using the least square minimization technique.

Step 4: Create matrices Γ_{11}, Γ_{12}, Γ_{21} and Γ_{22} which are defined by (5.11).

Step 5: Generate the $M - \Delta$ structure as defined by (5.12) .

Step 6: Determine the peak value of the μ-plot of the frequency response of $M(j\omega)$ using the MATLAB μ-toolbox.

Step 7: Using the reciprocal of the peak value of the μ upper bound, determine maximum values of varying parameters that still guarantee the system's stability.

To obtain the approximation in Step 3, numerical simulations are necessary in order to determine how elements in the A matrix depend on varying parameters. Accordingly, for a physically expected range of varying parameters (or equivalently in power system dispatching centers, during operation planning phase, for expected range of operating conditions), a reasonably dense grid of varying parameters should be created. Each point on the grid represents one steady-state operating regime characterized by the corresponding power flow and the A matrix. For the complete set of possible operating conditions we obtain a set of A matrices which correspond to discrete combinations of

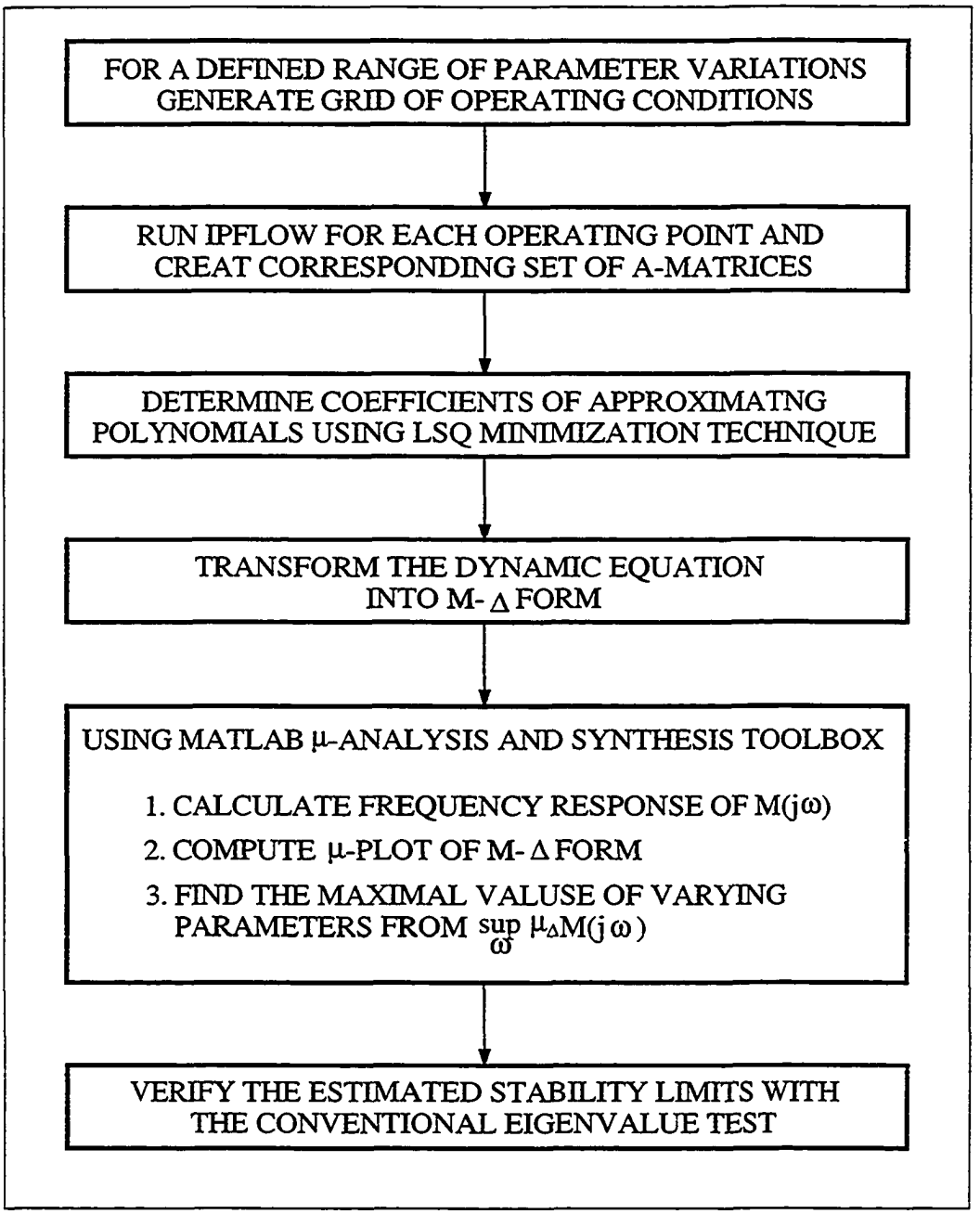

Figure 5.3 μ-Analysis procedure of multi-machine power system model.

uncertain parameters. Having in hand these data, each element of the A matrix in the presence of uncertainty can be approximated as a polynomial function of varying parameters, and the coefficients of the approximating polynomials can be obtained using the least square minimization technique.

This idea, based on LFTs for obtaining a standard linear uncertainty model, allows us to proceed with the SSV approach to formulate a complete stability robustness set-up. We note here that this formulation can be extended to any level of system modeling detail and can accommodate all types of uncertainties common in power systems, thus it is a generalized approach for the analysis of power system robust stability.

5.3 Numerical Simulations and Results

5.3.1 Four-machine System Results

The robust stability analysis approach presented above is now formulated for power systems. First, we consider a sample four-machine two-area system as shown in Figure 5.4. This system has been specifically designed by Ontario Hydro for fundamental studies of inter-area oscillations in power systems [2]. Although small, the system parameters and structure are realistic. The system has the complexity to verify the efficiency of the proposed procedure and it is characterized by the presence of both inter-area and local modes.

The test system consists of two identical areas, each including two generators with the same power output and a load. All generators are represented by the two-axis model equipped with ETMSP Type-30 Excitation system. The SVC is located at the center of the tie-line connecting Buses #5 and 6. This location provides ideal voltage regulation which is the primary function of the SVC. The ETMSP Type-1 model shown in Figure 4.2 is used to represent the SVC. The data for generators, exciters, and SVC are given as below.

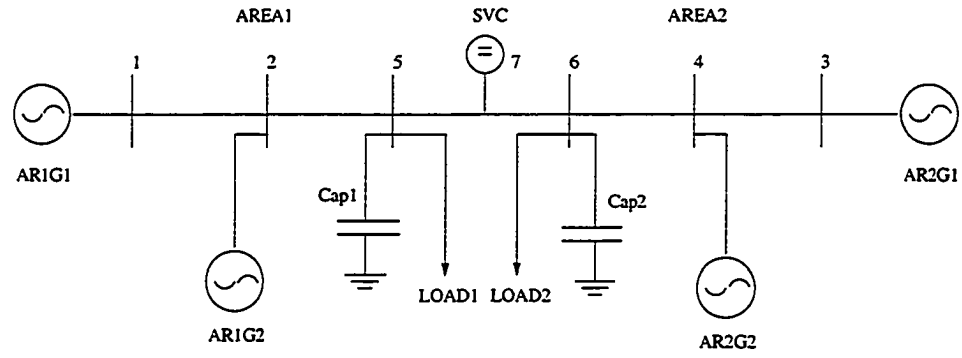

Figure 5.4 Four-machine two-area test system.

- Synchronous generator:

  Rating = 900 MVA, $H = 6.5$

  $r_a = 0.0025$, $x_d = 1.8$, $x_q = 1.7$

  $x'_d = 0.3$, $x'_q = 0.55$, $\tau'_{d0} = 8.0$ s, $\tau'_{q0} = 0.40$ s

  $D_1 = 9.0, D_2 = 10.0, D_3 = 11.0, D_4 = 12.0$

- Excitation system (see Figure 4.1):

  $K_A = 200$, $T_A = 0.01$ s, $T_B = 10.0$ s, $T_C = 1.0$ s, $T_R = 10.0$ s

- SVC (see Figure 4.2):

  Rating = 400 MVAR, $K = 10.0$

  $T_1 = 1.0$ s, $T_2 = 0.05$ s, $T_3 = 0.9$ s, $T_4 = 0.015$ s, $T_5 = 0.05$ s

The network and power flow data are given in [50].

5.3.1.1 CASE 1: One-parameter uncertainty

The exporting power from AREA1 to AREA2 is allowed to vary in the range [200—600 MW]. The varying coefficients in the A matrix are represented as:

$$a_{ij} = a_{ij0} + a_{ij1}\delta + a_{ij11}\delta^2$$

The dependence of the A-matrix on the parameter δ, shown in Figure 5.5, can be defined as:

$$A = A_0 + L^T[A_1(\delta_1 I) + A_{11}(\delta_1^2 I)]R \tag{5.13}$$

where:

$$A_0 = [a_{ij0}]_{30\times30},\ A_1 = [a_{ijp}]_{19\times12},\ A_{11} = [a_{ijpq}]_{19\times12},\ \Delta = diag[\delta I_{24}]$$

$$\Gamma = \left[\begin{array}{c|cc} A_0 & L^T A_1 & L^T A_{11} \\ \hline R & 0 & 0 \\ 0 & I & 0 \end{array}\right]$$

In this way we obtain $\Gamma_{11}, \Gamma_{12}, \Gamma_{21}$ and Γ_{22} which are in this case matrices of dimensions $[30\times30]$, $[30\times24]$, $[24\times30]$ and $[24\times24]$, respectively. In the $M-\Delta$ structure, M is a matrix of dimension $[24\times24]$, while the perturbation matrix Δ is $\{diag[\delta I_{24}] : \delta \in \mathbf{R}\}$.

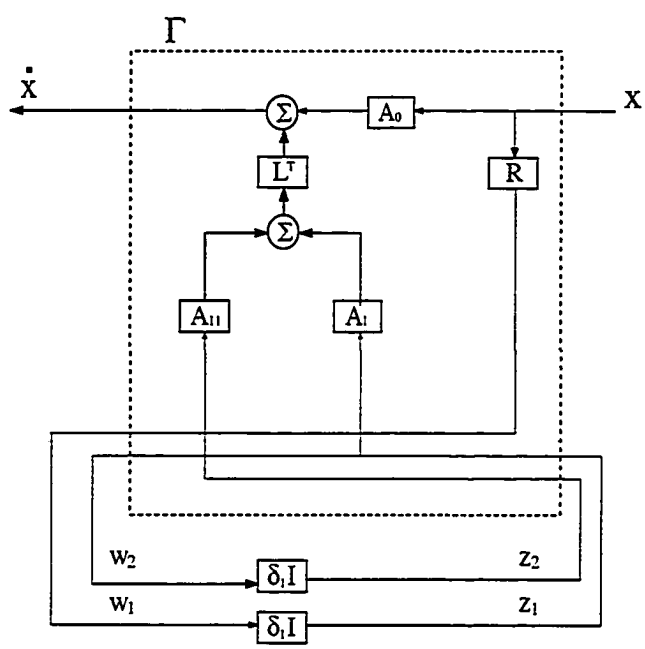

Figure 5.5 Robust stability framework in the case of one varying parameter.

Table 5.1 RS assessment — 4-machine system with one parametric uncertainty

Peak of μ upper bound	1.381
Frequency for this peak (rad/s)	2.79
Estimated power export (MW)	545
Exact power export (MW)	550
Error (%)	-0.91
Interarea mode	$-0.0003 \pm j2.793$

The numerical results for the one parametric uncertainty case are given in Table 5.1. The results are interpreted as follows. For the range of uncertainty considered, the value of the peak of μ upper bound given in row 2 indicates that the system is not robustly stable since $\mu > 1$. With this μ peak, (5.5) is then used to calculate the estimated maximal value of the varying parameter which still guarantee stability ($P_{exp} = 545$ MW in row 4). The estimated value is then compared with the exact value of the varying parameter (550 MW), which is determined by iteratively using the conventional eigenvalue test while increasing the varying parameters. The small error percentage (0.91%) means that μ gives an accurate estimation of the stability limit. The critical eigenvalues found by eigenvalue tests correspond to the interarea mode in row 7 since the system instability is caused by the interarea oscillation in our example.

The upper bound and lower bound μ-plots are shown in Figures 5.6. In this case, the lower bound is zero, which is possible for pure real uncertainties. On the other hand, the upper bound peaks to a value of 1.381 at the frequency of 2.92 rad/s (critical frequency), which means that for all uncertainties Δ with size $\overline{\sigma}(\Delta)$ smaller than 1/1.381, the system maintains stability. Note that the critical frequency is very close to the imaginary part of the interarea mode. The reason is that the μ-plot is obtained by calculating μ at each frequency point and the peak of μ frequency plot indicates the largest size of the allowable uncertainty for the whole frequency range, whereas the power system is most

prone to instability at the interarea frequency.

5.3.1.2 CASE 2: Two-parameter uncertainty

In this case, the exporting power from AREA1 to AREA2 varies in the range of [100-500 MW], and active power generated in AREA1 vary in the range of [1480 MW-1680 MW].

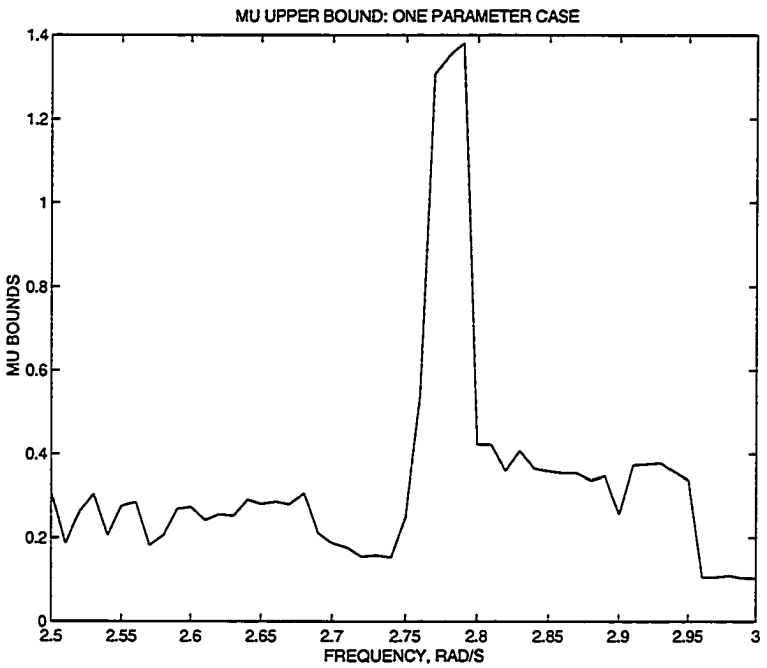

Figure 5.6 μ-bounds for Case 1 - one parameter variation.

The polynomial approximation, the dependence of the A matrix on the parameters δ_1 and δ_2, and the graphical illustration of the $M-\Delta$ form are all given in Section 5.1 . $\Gamma_{11}, \Gamma_{12}, \Gamma_{21}$ and Γ_{22} are in this case matrices of dimensions [30 × 30], [30 × 60], [60 × 30] and [60 × 60], respectively. M is a matrix of dimensions [60 × 60], while perturbation matrix Δ is:

$$\Delta := \{diag[\delta_1 I_{24},\ \delta_2 I_{36}] : \delta_1, \delta_2 \in \mathbf{R}\}$$

Table 5.2 RS assessment - 4-machine system with two parametric uncertainties.

Peak of μ upper bound	1.3551
Frequency for this peak	2.92 rad/s
Estimated power export	447.6 MW
Exact power export	457 MW
Error (%)	-2.06
Estimated power generation	1653.8 MW
Exact power generation	1663 MW
Error (%)	-0.55
Interarea mode	$-0.00021 \pm j2.90$

The numerical results are given in Tables 5.2. The system is not robustly stable for the given operating range since $\mu > 1$. (5.5) is then used to calculate the estimated stability limits. In case of two or more parameter variations, the reciprocal of the peak value of the μ-plot provides assessment of maximum allowable value of all varying parameters, which are simultaneously increased from their mid-point values. These estimated values agree with the exact values from the conventional eigenvalue test and the errors are within a small range of $[0.55\% - 2.06\%]$.

The upper and lower bounds of the μ-plot for the two-parameter variation case are given in Figure 5.7. In this case, the upper bound peaks to a value of 1.3551 at the frequency of 2.90 rad/s (critical frequency), which means that for all uncertainties Δ with size $\overline{\sigma}(\Delta)$ smaller than 1/1.3551, the system maintains stability. On the other hand, the lower bound has a peak of 1.209, which means that there is an uncertainty Δ with size $\overline{\sigma}(\Delta) = 1/1.209$ that destabilizes the system. This uncertainty provides physical insight to the types of variations for which the closed-loop system is most sensitive. The proximity of the upper bound peak and lower bound peak implies that the calculation of μ is very accurate in this case. The critical frequency from the μ bounds is again close to the interarea mode.

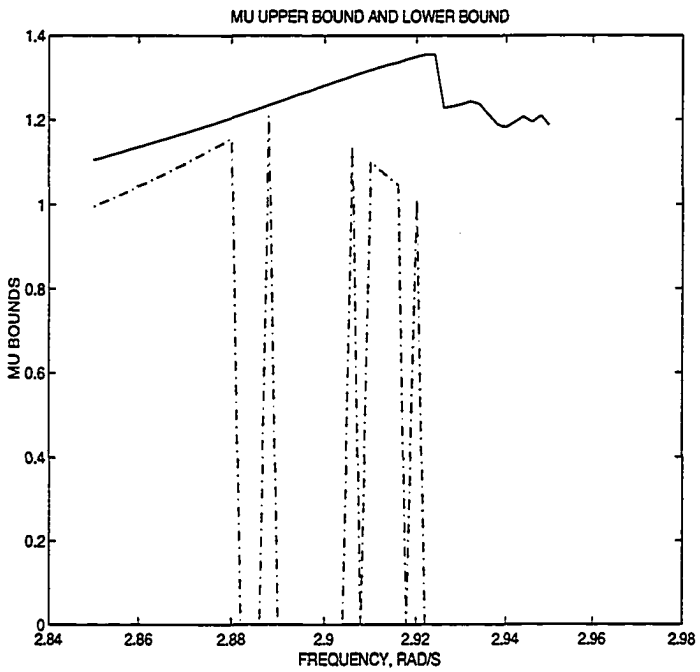

Figure 5.7 μ-bounds for Case 2 - two parameter variation.

5.3.2 IEEE 50-generator System Results

We now consider the 50-generator IEEE test system [56]. This test system demonstrates a wide range of dynamic characteristics at different generations at Bus #93 and 110 (Station A) and at Bus #104 and 111 (Station B). A one-line diagram of the area of interest is shown in Figure 5.8.

In this system, six generators are represented by the two-axis model and equipped with ETMSP Type-30 excitation system. The remaining 44 generators are represented by the classical model. The detailed data description for the IEEE 50-generator system can be found in [55, 56]. In our research, the system data have been have been slightly modified in order to avoid unrealistic instabilities introduced by big equivalent machines in the remote area from the study part of the system. Namely, active power loads at Buses #137 and 145 are changed from 12946 MW and 9173 MW to 11946 MW and 10173 MW, respectively. Reactive power load at Buses #119 is increased from 3774

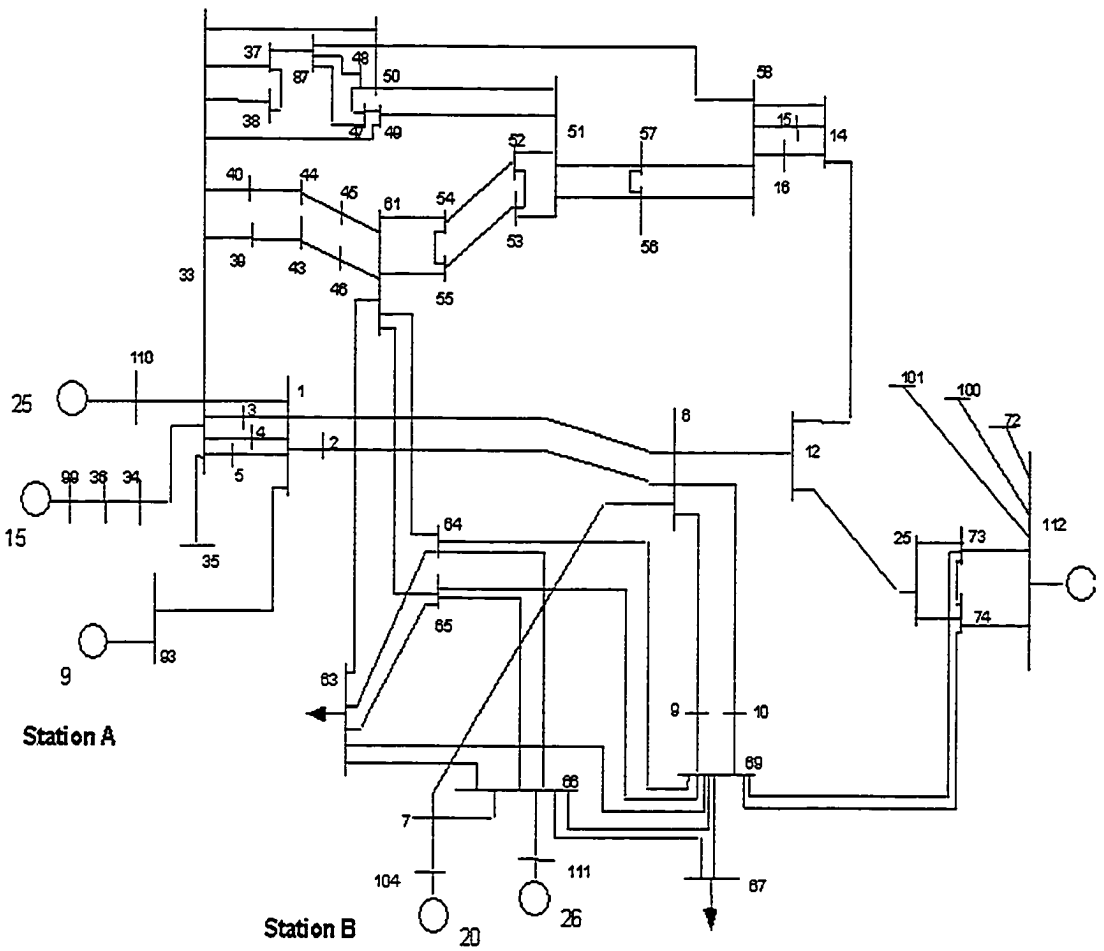

Figure 5.8 IEEE 50-generator system: a one-line diagram of the study area.

Table 5.3 Bus participation factors from VSTAB

$\lambda_1 = 2.234$		$\lambda_2 = 2.555$		$\lambda_3 = 3.4177$	
Bus #	Part. Factors	Bus #	Part. Factors	Bus #	Part. Factors
68	0.9935	107	0.95896	85	0.10238
107	0.00082	92	0.01124	84	0.09144
85	0.0003	19	0.0251	42	0.04892
				41	0.04890
				44	0.04867
				43	0.04864
				46	0.03936
				45	0.03936

MVAR to 5774 MVAR. All generators represented by the classical model have uniform damping $D_i/M_i = 0.1$ except that generators at Buses #137 and 140 have damping $D_i/M_i = 0.5$.

5.3.2.1 Selection of Location of SVC

The location of SVC should be chosen such that it strongly influences the mode of oscillation. Previous research [11, 17] has shown that SVC is generally effective for damping when it is located at the midpoint of transmission paths between two areas, where voltage swings are greatest without SVC. Therefore, the SVC location for the four-machine two-area system can be easily found by inspection (Bus #7 in Figure 5.4). For large systems such as the IEEE 50-generator system, however, the optimal location for SVC is not apparent. In such a situation, the bus participation factor computed by VSTAB program [54] serves as an useful sensitivity index for identifying SVC locations, as suggested in Chapter 17 of [11]. For the IEEE 50-generator system the bus participation factors are calculated at the nominal operating point for the three smallest eigenvalues evaluated by the VSTAB program. These participation factors are shown in Table 5.3.

From the analysis conducted, we observe from Table 5.3 that there are generally two

Table 5.4 Peak of RS μ-plot with SVC at different locations

Bus #	Peak of RS μ-plot
42	1.8315
41	1.8147
44	1.1397
43	1.1632
46	1.5238
45	1.4564

types of modes identified by the VSTAB data. The first type of mode has very few buses with large participation factors and all other buses in the mode have participation factors close to zero, indicating that the mode is very localized in terms of the voltage characteristic. Modes λ_1 and λ_2 in Table 5.3 belong to this category. The second type of mode has many buses with small but similar size of participation factors and the rest of the buses with close to zero participation indicating that the mode is seen at a number of buses. Mode λ_3 is such a mode. Thus the bus participation factors for λ_3 indicate that Buses # 85, 84, 42, 41, 44, 43, 46, and 45 are possible choices for the location of the SVC.

The topology and characteristics of the network data are further examined to narrow down the choice. Among the eight buses # 85 and 84 are terminal load buses and are hence eliminated. For the remaining buses, we want to decide one location for the SVC such that the system derives maximum benefit in terms of stability enhancement. Therefore, we conduct robust stability analysis with the SVC at each of the six buses for a given operating range. This procedure will be detailed in 5.3.2.2, and the peaks of μ-plots are given in Table 5.4.

From Table 5.4, the peak of the μ-plot is the lowest with the SVC located at Bus #44, which indicates the system is most stable. Therefore Bus #44 is chosen as a location

for the SVC.

The results of the robust stability analysis of the IEEE 50-generator system with the SVC located at bus # 44 are now presented.

5.3.2.2 CASE 1: One parameter uncertainty

The base case is characterized by setting the generation at Bus #93 and Bus #110 to be 1400 MW. This generation is treated as an uncertain parameter and allowed to vary in the range [2 × 1300 MW — 2 × 1500 MW]. The a-coefficients are represented as:

$$a_{ij} = a_{ij0} + a_{ij1}\delta + a_{ij11}\delta^2$$

The dependence of the A-matrix on the parameter δ, shown in Figure 5.5, can be defined as:

$$A = A_0 + L^T[A_1(\delta_1 I) + A_{11}(\delta_1^2 I)]R \tag{5.14}$$

where:

$$A_0 = [a_{ij0}]_{132\times132}; A_1 = [a_{ijp}]_{71\times62}; A_{11} = [a_{ijpq}]_{71\times62}; \Delta = diag[\delta I_{124}]$$

$$\Gamma = \left[\begin{array}{c|cc} A_0 & L^T A_1 & L^T A_{11} \\ \hline R & 0 & 0 \\ 0 & I & 0 \end{array}\right]$$

In this way we obtain $\Gamma_{11}, \Gamma_{12}, \Gamma_{21}$ and Γ_{22} which are matrices of dimensions [132 × 132], [132 × 124], [124 × 132] and [124 × 124], respectively. M is a matrix of dimensions [124 × 124], while the perturbation matrix $\Delta = \{diag[\delta I_{124}] : \delta \in \mathbf{R}\}$.

5.3.2.3 CASE 2: Two-parameter uncertainty

The generation at Buses #93 and 110 ("Station A") is treated as an uncertainty and allowed to vary in the range [2 × 1300 MW — 2 × 1500 MW], while generation at Bus

#104 and 111 ("Station B") is uncertain in the range [2 × 1800 MW — 2 × 2000 MW]. The power generation of the "Station A" and "Station B" takes the values in the above mentioned range in steps of 2 × 50 MW. This results in a 2-dimensional grid with 25 points.

The polynomial approximation, the dependence of the A matrix on the parameters δ_1 and δ_2, and the graphical illustration of the $M - \Delta$ form are all given in Section 5.1. $\Gamma_{11}, \Gamma_{12}, \Gamma_{21}$ and Γ_{22} are matrices of dimensions [132 × 132], [132 × 310], [310 × 132] and [310 × 310], respectively. M-is a matrix of dimensions [310 × 310], while perturbation matrix Δ is:

$$\Delta := \{diag[\delta_1 I_{124}\ \delta_2 I_{186}] : \delta_1, \delta_2 \in \mathbf{R}\}$$

The results of the analysis are given in Tables 5.5 and 5.6. For the range of uncertainty considered, the values of peak μ given in rows 2 of Tables 5.5 and 5.6 indicate that the system is not robustly stable for the uncertainty range and the control settings considered. This is because $\mu > 1$. With the peak of μ, the estimated stability limits are calculated using (5.5) and compared with the exact stability from the eigenvalue test. The errors are in the range [0.28% — 0.46%]. It can be concluded again that the proposed method provides an accurate tool for the estimation of power system stability.

Table 5.5 One parametric uncertainty — RS assessment of "Station A" power generation.

Peak of μ upper bound	1.1397
Frequency for this peak	1.796 rad/s
Estimated P_A (MW)	2× 1487.7
Exact P_A (MW)	2× 1492
Error (%)	-0.28
Interarea mode	$-0.00016 \pm j1.795$

Table 5.6 Two parametric uncertainties — RS assessment of "Station A" and "Station B" power generation.

Peak of μ upper bound	1.1348
Frequency for this peak (rad/s)	1.8031
Estimated P_A (MW)	2×1488
Exact P_A (MW)	2×1495
Error (%)	-0.46
Estimated P_B (MW)	2×1988
Exact P_B (MW)	2×1995
Error (%)	-0.35
Inter-area mode	$-0.00007 \pm j1.795$

The Upper Bound and Lower Bound m-plots for the two cases are given in Figures 5.9 and 5.10.

5.4 State Space Method for μ Calculation

So far, we have incorporated the parametric uncertainty in power systems into the $M - \Delta$ general framework, and analyzed the robust stability based on the frequency μ-plot of M that is obtained by calculating $\mu(M(j\omega))$ at each frequency ω. In practice, this frequency sweep method usually involves a large amount of computation. Moreover, the appropriate frequency range and the fineness of the frequency grid need to be decided. Since the rapid changes or "spikes" in the frequency μ-plot occur frequently for power system problems, there is the possibility of missing important points using the frequency sweep test. This is illustrated in the following example.

Figure 5.11 shows two frequency μ-plots of the IEEE 50-generator system with one parametric uncertainty (as discussed in Section 5.3.2). For the same uncertainty, the frequency range used is [0,10 rad/s] containing 50 equally-spaced points in figure (a), and a refined frequency range [1.793, 1.797 rad/s] with 50 points in figure (b), respectively.

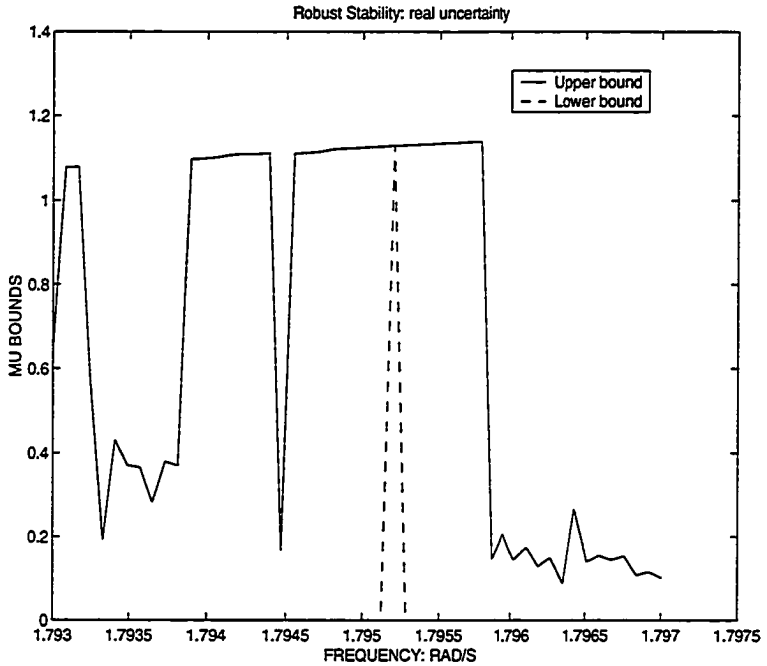

Figure 5.9 μ-bounds of one parametric uncertainty for 50-generator system.

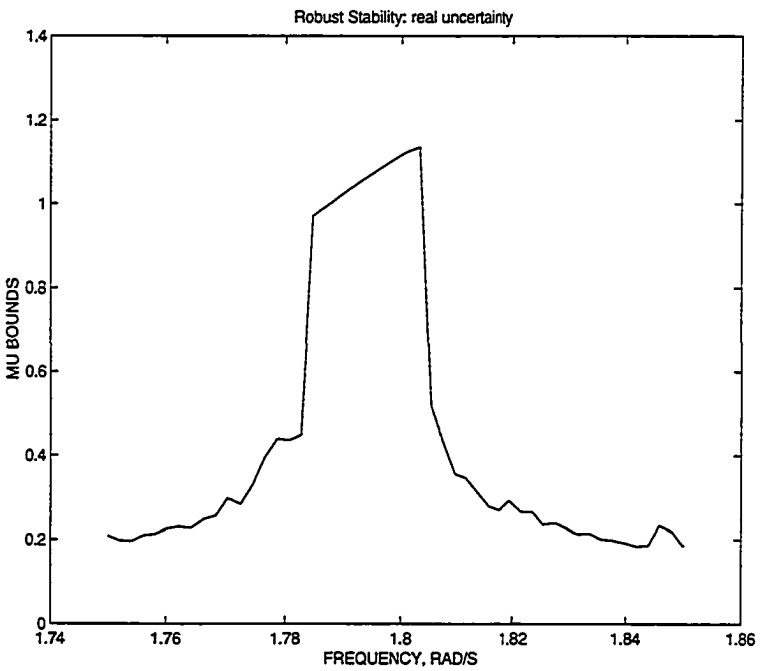

Figure 5.10 μ-bounds of two parametric uncertainties for 50-generator system .

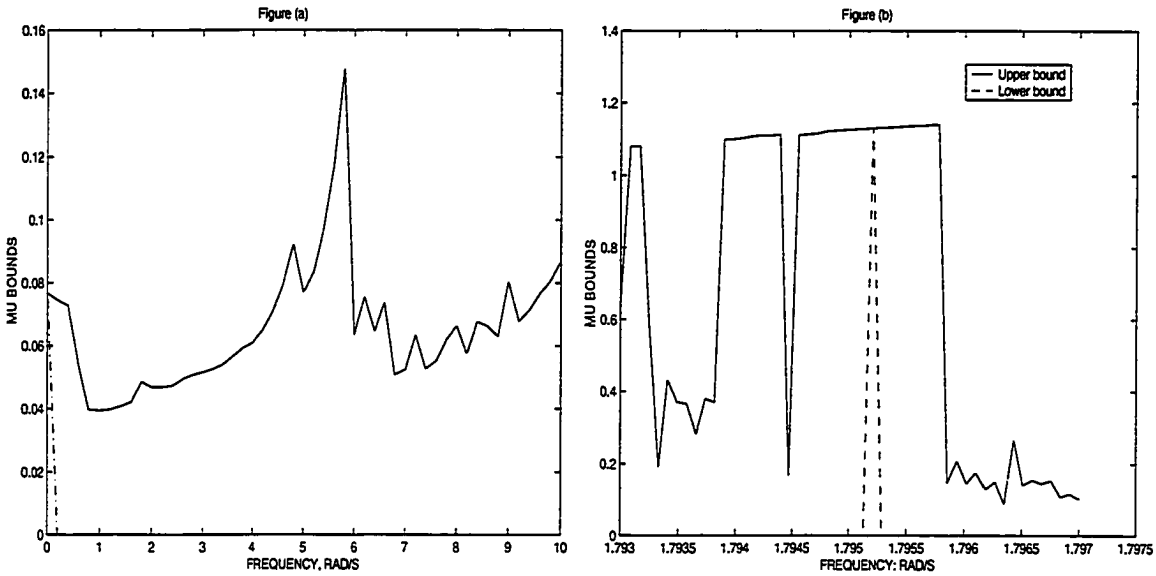

Figure 5.11 μ calculation on different frequency ranges. (a): a large frequency range, (b): a refined frequency range.

From figure (b), the peak value of the μ-plot is 1.1397 at the critical frequency $\omega_c = 1.796$, which agrees with the conventional eigenvalue test as we have seen in Section 5.3.2. However, the μ-plot in figure (a) missed that frequency point during the sweep and results in a misleading peak of 0.148 at $\omega = 5.82$ rad/s. Therefore, to obtain the exact peak of μ, one has to perform numerous frequency searches over all small peaks in figure (a), which causes a heavy computation burden.

In this section, we use the state space test method [48] for the analysis of robust stability which could avoid the frequency sweep. The main idea is that a transfer function can be expressed as an LFT of a constant matrix with respect to the frequency variable, and the frequency variable can then be treated as an uncertainty so that the SSV technique can be applied directly. Given a transfer function $M(s)$ in the $M - \Delta$ framework, we consider its dynamic representation and expand it using the state space formula:

$$M(s) = C(sI_p - A)^{-1}B + D = F_u(\begin{bmatrix} A & B \\ C & D \end{bmatrix}, \frac{1}{s}I_p) \tag{5.15}$$

where p is the dimension of the state space. We denote

$$M_f := \begin{bmatrix} A & B \\ C & D \end{bmatrix}$$

then the state equation for the robust stability problem of $M - \Delta$ can be written as

$$\dot{x} = F_l(M_f, \Delta)x \tag{5.16}$$

where $F_l(M_f, \Delta) = A + B\Delta(I - D\Delta)^{-1}C$. This is illustrated in Figure 5.12.

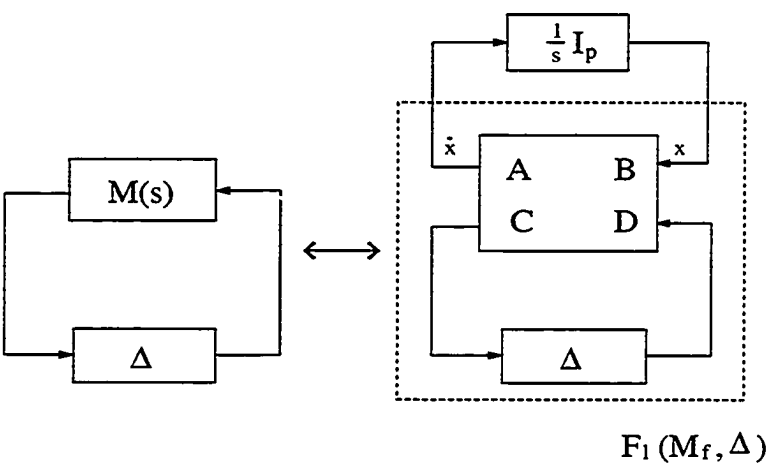

Figure 5.12 Transfer function in state space equation form with LFT.

Next we want to remove the frequency search and include $\frac{1}{s}I_p$ as one of the uncertainties. Since μ usually considers uncertainty insides the unit disk, while $\frac{1}{s}I_p$ covers the right half of the s-plane, we may apply a bilinear transformation to map the right half s-plane into the unit disk on the complex plane (see Figure 5.13). i.e.,

$$s = \frac{1-z}{1+z}, z \in \mathbf{C}, |z| \leq 1$$

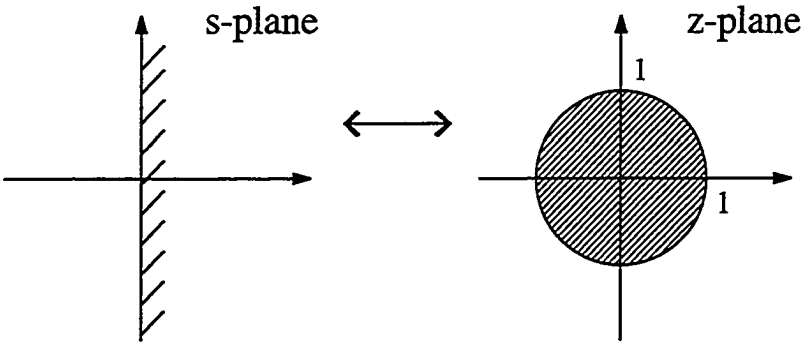

Figure 5.13 Bilinear transformation: the right half of s-plane to the unit disk in z-plane.

therefore,

$$\frac{1}{s}I_p = \frac{1+z}{1-z}I_p$$

This can be written in an LFT form again

$$\frac{1}{s}I_p = F_u(Q, zI_p) \text{ where } Q := \begin{bmatrix} I_p & 2I_p \\ I_p & I_p \end{bmatrix}$$

Now we can replace $\frac{1}{s}I_p$ with the LFT of this constant matrix Q with respect to the new frequency variable z, as shown in Figure 5.14. The interconnection of Q and M_f in lower and upper LFT can be simplified using Redhaffer's star product [43]. This results in a new connection shown in Figure 5.14.c with matrix T in the following form

$$T = \begin{bmatrix} I_p + 2A(I_p - A)^{-1} & 2(I_p - A)^{-1}B \\ C(I_p - A)^{-1} & D + C(I_p - A)^{-1}B \end{bmatrix}$$

From Figure 5.14, we removed the frequency sweep by including the frequency variable as one of the uncertainty parameter (a repeated complex scalar block). In this way, we obtain a one-shot μ test involving a constant matrix μ problem. This is formally stated in the following theorem:

Theorem 5.1 (Robust stability with state space test) [48]

$$\sup_{\omega \in \mathbf{R}} \mu_{\Delta}(M(j\omega)) \leq 1 \quad \textit{if and only if} \quad \mu_{\widetilde{\Delta}}(T) \leq 1$$

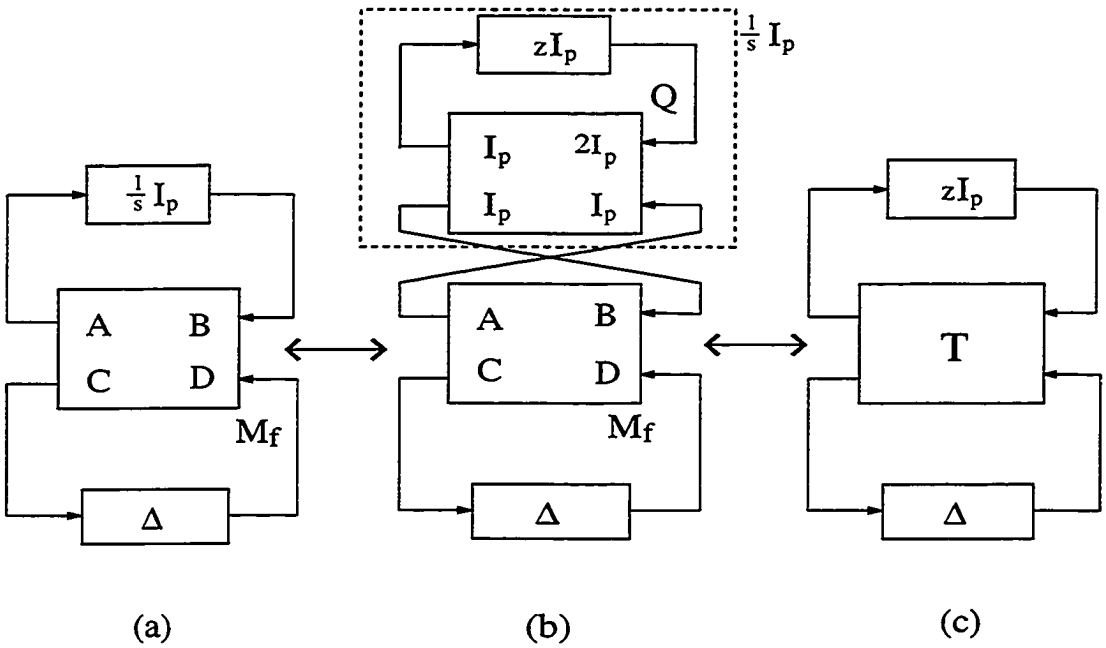

Figure 5.14 Frequency sweep transformed to state space test: a constant μ problem.

where $\tilde{\Delta} = \{diag(zI_p, \Delta), z \in \mathbf{C}, |z| \leq 1\}$.

Note that this theorem only tells us whether $\sup_\omega \mu_\Delta(M(j\omega))$ is less than or equal to 1, which is a direct test for robust stability/instability. In order to compute the value of $\sup_\omega \mu_\Delta(M(j\omega))$, we need to define:

$$T_\alpha = \begin{bmatrix} T_{11} & \frac{1}{\alpha}T_{12} \\ T_{21} & \frac{1}{\alpha}T_{22} \end{bmatrix} \tag{5.17}$$

$$\tilde{\mu}(T) = \inf_\alpha \left\{\alpha \geq 0 : \mu_{\tilde{\Delta}}(T_\alpha) \leq 1\right\} \tag{5.18}$$

Then Theorem 5.1 can be restated as:

$$\sup_{\omega \in \mathbf{R}} \mu_\Delta(M(j\omega)) = \tilde{\mu}(T) \tag{5.19}$$

Note that the right hand side of (5.18) involves a search over α, thus we haven't totally eliminated the need to search. But the search over α is simpler compared with

the frequency sweep. Since $\mu_{\tilde{\Delta}}(T_\alpha)$ is monotonically decreasing as α increases, so the binary search can be used for (5.18) which involves only several constant μ calculations.

As mentioned before, the μ-toolbox software computes the lower and upper bounds instead of the exact value of μ. Therefore, we also obtain lower and upper bounds for $\tilde{\mu}(T)$. Note that we now have a mixed uncertainty block $\tilde{\Delta}$ instead of a pure real uncertainty block as in frequency sweep, so the lower bound is better than that of frequency sweep (the lower bound in the pure real μ problem is always poor [44]). We shall also point out that the upper and lower bounds of $\mu_{\tilde{\Delta}}(T_\alpha)$ may not be always monotonic, so linear search over α is still needed.

5.5 Numerical Results for State Space Method

5.5.1 Four-machine System With One Parametric Uncertainty

The state space test is now applied to the four-machine two-area system with one parametric uncertainty, as discussed in Section 5.3.1. From the frequency sweep test results listed in Table 5.1, the peak of the μ-plot is 1.381 at $\omega_c = 2.79$rad/s. After forming the state space test framework, we carry out a linear search for (5.18) over α from $\alpha = 1$ to $\alpha = 10$. At each α, the upper bound β_u and lower bound β_l of $\mu_{\tilde{\Delta}}(T_\alpha)$ are calculated and listed in Table 5.7. The corresponding curves of upper and lower bounds are shown in Figure 5.15.

From Figure 5.15, the upper bounds are always larger than 1.0, which means the upper bound of $\tilde{\mu}(T)$ could be arbitrary large and leads to very conservative results. On the other hand, the lower bound plot crosses 1.0 within the interval of [1.0, 2.0], which means the lower bound of $\tilde{\mu}(T)$ is also in [1.0, 2.0] by (5.18). This value is close to the result from the frequency sweep test $\mu = 1.381$.

In order to achieve a better lower bound, we carry out a refined linear search from $\alpha = 0.1$ to $\alpha = 2$. The results are shown in Table 5.8 and in Figure 5.16.

Table 5.7 Linear search for α in [1, 10]

α	Upper bound β_u	Lower bound β_l
1.0	1.0905	1.0074
2.0	1.0400	0.9844
3.0	1.0309	0.9863
4.0	1.0285	0.9894
5.0	1.0223	0.9894
6.0	1.0207	0.9894
7.0	1.0229	0.9868
8.0	1.0222	0.9860
9.0	1.0209	0.9860
10.0	1.0170	0.9856

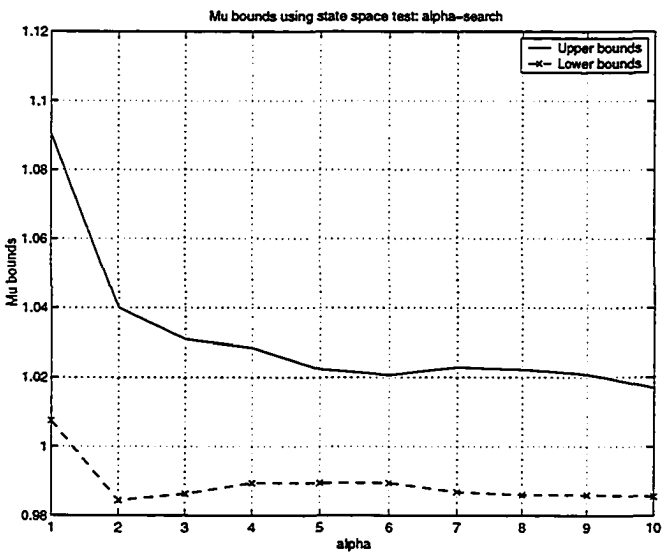

Figure 5.15 μ-bounds in state space test - one parametric uncertainty.

Table 5.8 Linear search for α in [0.1, 2.0]

α	Upper bound β_u	Lower bound β_l
0.1	2.9892	2.4904
0.2	1.7047	1.4877
0.3	1.3863	1.2097
0.4	1.2624	1.1036
0.5	1.1968	1.0654
0.6	1.1518	1.0285
0.7	1.1246	1.0204
0.8	1.1017	1.0181
0.9	1.0914	1.0108
1.0	1.0905	1.0074
1.1	1.0724	0.9814
1.2	1.0719	1.0019
1.3	1.0699	0.9892
1.4	1.0650	0.9895
1.5	1.0669	0.9894
1.6	1.0611	0.9895
1.7	1.0552	0.9889
1.8	1.0555	0.9957
1.9	1.0460	0.9951
2.0	1.0464	0.9893

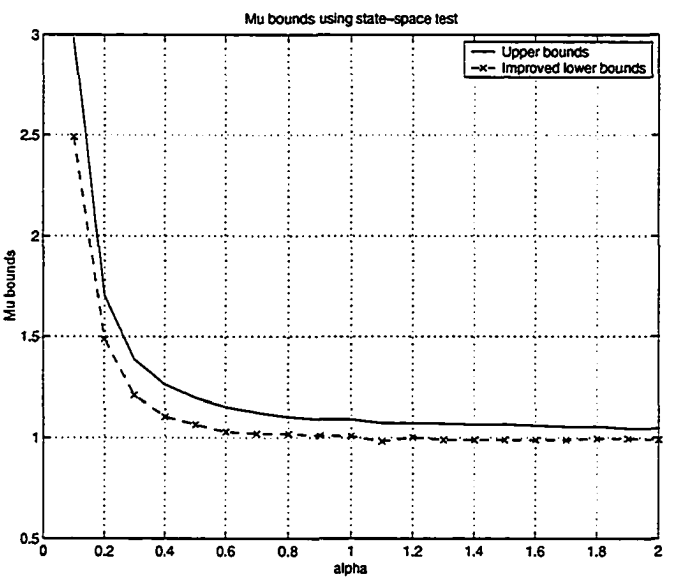

Figure 5.16 μ-bounds in state space test — 4-machine system with one parametric uncertainty.

From Figure 5.16, the lower bound for $\tilde{\mu}(T)$ is 1.2, which is very close to $\mu = 1.38$ from the frequency sweep test. Therefore, the lower bound from state space test provides good approximation to the exact μ.

As mentioned in Chapter 3, for the lower bound β_l in μ calculation, there is a particular uncertainty matrix Δ satisfying $\overline{\sigma}(\Delta) = \frac{1}{\beta_l}$ that causes system instability. Since we replace the frequency search $\frac{1}{s}I_p$ with the uncertainty block of repeated complex scalars, the state space now looks for the worst case frequency at the same time. Therefore, for the particular α which makes lower bound equal (or close) to 1.0, we may construct such an uncertainty block that contains the worst case frequency z in its complex block; then we can apply the bilinear transformation to obtain the worst frequency s. In this example, the uncertainty block Δ_p corresponding to $\beta_l = 1.0019$ at $\alpha = 1.2$ is

$$\Delta_p = \begin{bmatrix} diag_{30\times 30}(-0.7655 + j0.6405) & \\ & diag_{24\times 24}(0.9676) \end{bmatrix}$$

The first block corresponds to the repeated complex block in the state space test. Let $z = -0.7655 + j0.6405$, then the bilinear transformation gives

$$s = \frac{1-z}{1+z} = 0.0083 - j2.7534$$

This frequency $\omega_s = 2.7534$ is very close to the critical frequency $\omega_c = 2.79$ from the frequency sweep test.

We now compare the computation time of the state space test and the frequency sweep test. The computation is carried on Pentium III-500 with Matlab Version 5.3. In this example, the CPU time for μ calculation at each α is about 8s , so the total CPU time for the α search in Table 5.8 is 160s. On the other hand, the CPU time for one frequency sweep (50 points) is about 65s. However, as we pointed out earlier, it usually takes numerous frequency sweeps to obtain the exact μ peak, so the actually computation time for the frequency sweep test is much longer than 65s. In this sense, the state space test saves computation time compared with the frequency sweep test.

Table 5.9 Comparison of state space test and frequency sweep

	State space test	Frequency sweep
μ bound	1.20	1.38
critical frequency (rad/s)	2.75	2.79

The above comparisons of the state space test and the frequency sweep test are summarized in Table 5.9.

5.5.2 Four-machine System With Two Parametric Uncertainties

For the same uncertainties as discussed in Section 5.3.1, the search over α gives the lower bound of $\tilde{\mu}(T) = 1.20$. The bounds are listed in Table 5.10 and Figure 5.17.

The uncertainty Δ_p constructed at $\alpha = 1.2$ is:

$$\Delta_p = \begin{bmatrix} diag_{30\times30}(-0.7844 - j0.6186) & \\ & diag_{60\times60}(0.9924) \end{bmatrix}$$

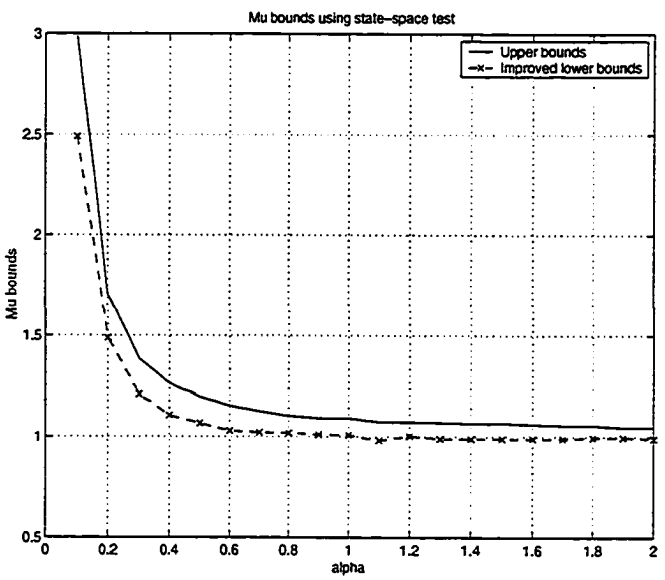

Figure 5.17 μ-bounds in state space test — 4-machine system with two parametric uncertainties.

Table 5.10 Linear search for α in [0.5, 2.0], 4-machine system with two parametric uncertainties

α	Upper bound β_u	Lower bound β_l
0.5	1.1725	1.0592
0.6	1.1403	1.0213
0.7	1.1103	1.0099
0.8	1.0885	1.0030
0.9	1.0947	1.0099
1.0	1.0774	1.0057
1.1	1.0685	0.9851
1.2	1.0698	1.0010
1.3	1.0677	0.9960
1.4	1.0628	0.9895
1.5	1.0560	0.9895
1.6	1.0540	0.9836
1.7	1.0498	0.9838
1.8	1.0435	0.9783
1.9	1.0412	0.9895
2.0	1.0400	0.9844

Table 5.11 Comparison of state space test and frequency sweep — 4-machine system with two parametric uncertainties.

	State space test	Frequency sweep
μ bound	1.20	1.3567
critical frequency (rad/s)	2.8827	2.92

The first block corresponds to the repeated complex block in the state space test. Let $z = -0.7844 - j0.6186$, then the bilinear transformation gives

$$s = \frac{1-z}{1+z} = 0.0047 - j2.8827$$

So the frequency $\omega_s = 2.8827$ is very close to the critical frequency $\omega_c = 2.92$ from the frequency sweep (see Table 5.2).

The comparisons of the state space test with the frequency sweep test in this case are given in Table 5.11.

5.5.3 IEEE 50-generator System With One Parametric Uncertainty

For the same uncertainties as discussed in Section 5.3.2, the search over α gives the lower bound of $\tilde{\mu}(T) = 1.0$. The bounds are listed in Table 5.12 and Figure 5.18.

Table 5.12 Linear search for α in [0.1, 2.0]— 50-generator system one parametric uncertainty

α	Upper bound β_u	Lower bound β_l
0.1	1.4037	1.3155
0.2	1.1776	1.1042
0.3	1.1322	1.0503
0.4	1.1179	1.0293
0.5	1.1137	1.0189
0.6	1.1158	1.0130
0.7	1.1122	1.0087
0.8	1.1041	1.0055
0.9	1.1070	1.0043
1.0	1.1081	1.0011
1.1	1.0978	0.9997
1.2	1.0973	0.9997
1.3	1.0986	0.9992
1.4	1.0976	0.9997
1.5	1.1024	0.9993
1.6	1.1113	0.9997
1.7	1.1092	0.9997
1.8	1.1072	0.9996
1.9	1.1074	0.9997
2.0	1.0968	0.9930

The uncertainty Δ_p constructed at $\alpha = 1.0$ is:

$$\Delta_p = \begin{bmatrix} diag_{132\times132}(-0.5176 + j0.8489) & \\ & diag_{124\times124}(0.9989) \end{bmatrix}$$

The first block corresponds to the repeated complex block in the state space test. Let $z = -0.5176 + j0.8489$, then by the bilinear transformation

$$s = \frac{1-z}{1+z} = 0.0120 - j1.7809$$

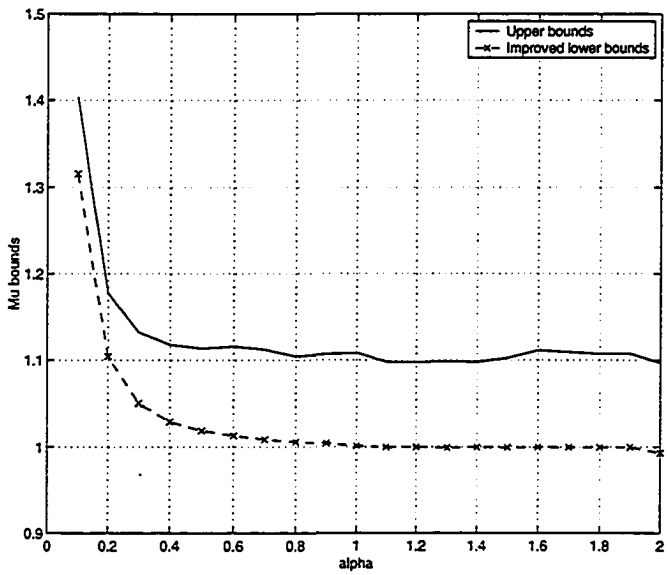

Figure 5.18 μ-bounds in state space test — 50-generator system with one parametric uncertainty.

Table 5.13 Comparison of state space test and frequency sweep — 50-generator system with one parametric uncertainty.

	State space test	Frequency sweep
μ bound	1.0	1.14
critical frequency (rad/s)	1.7809	1.796

So the frequency $\omega_s = 1.7809$ is very close to the critical frequency $\omega_c = 1.796$ from the frequency sweep.

The comparisons of the state space test with the frequency sweep in this case are given in Table 5.13.

5.5.4 IEEE 50-generator System With Two Parametric Uncertainties

For the same uncertainties as discussed in Section 5.3.2, the search over α gives the lower bound of $\tilde{\mu}(T) = 0.8$. The bounds are listed in Table 5.14 and Figure 5.19.

Table 5.14 Linear search for α in [0.1, 2.0] — 50-generator system with two parametric uncertainties

α	Upper bound β_u	Lower bound β_l
0.1	1.8956	1.7775
0.2	1.3630	1.2561
0.3	1.2176	1.1824
0.4	1.1694	1.1224
0.5	1.1302	1.0752
0.6	1.1250	1.0680
0.7	1.1195	1.0574
0.8	1.1206	1.0410
0.9	1.1221	0.9998
1.0	1.1182	0.9997
1.1	1.1138	0.9922
1.2	1.1112	0.9940
1.3	1.1083	0.9968
1.4	1.1076	0.9947
1.5	1.1020	0.9965
1.6	1.1019	0.9973
1.7	1.1016	0.9990
1.8	1.1028	0.9989
1.9	1.0965	0.9997
2.0	1.0944	0.9997

The uncertainty Δ_p constructed at $\alpha = 0.8$ is:

$$\Delta_p = \begin{bmatrix} diag_{132\times132}(-0.4713 + j0.8370) & \\ & diag_{310\times310}(0.9603) \end{bmatrix}$$

The first block corresponds to the repeated complex block in the state space test. Let $z = -0.4713 - j0.8370$, then the bilinear transformation gives

$$s = \frac{1-z}{1+z} = 0.0788 - j1.7081$$

So the frequency $\omega_s = 1.7081$ is close to the critical frequency $\omega_c = 1.803$ from the frequency sweep.

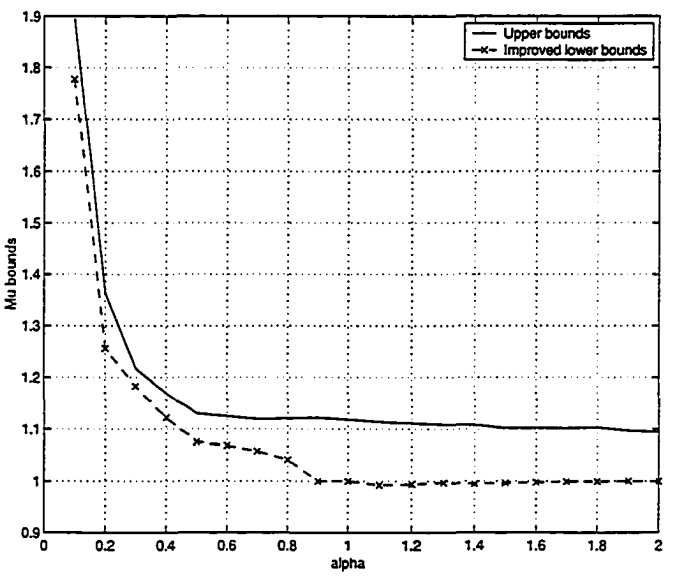

Figure 5.19 μ-bounds in state space test — 50-generator system with two parametric uncertainties.

The comparisons of the state space test with the frequency sweep in this case are given in Table 5.15.

Based on the numerical results presented in Section 5.5.1 — 5.5.4, we can draw the following conclusions about the state space test in the RS analysis of power systems:

1. The μ lower bound from state space test is a good approximation to the exact μ.

Table 5.15 Comparison of state space test and frequency sweep — 50-generator system two parametric uncertainties.

	State space test	Frequency sweep
μ bound	0.8	1.135
critical frequency (rad/s)	1.7081	1.803

2. The worst case frequency obtained from state space test gives a good estimate of the critical frequency.

3. The state space test saves computation time compared with the frequency sweep test.

5.5.5 Combination of State Space Test and Frequency Test

The advantage of the state space test is that it gives a quick estimate of the lower bound of μ, but the lower bound is less accurate than the frequency sweep test which, on the other hand, may suffer from the large computation burden and the choice of frequency range. Since the state space test also gives an estimate of the critical frequency, we can combine these two methods in the following way to implement an intelligent frequency sweep scheme:

1. Use state space test first to get a lower bound of μ and an estimate of the critical frequency;

2. Perform frequency sweeps near the critical frequency to find a better μ upper bound.

In this way, we obtain an efficient frequency sweep test and still guarantee the accuracy of the μ.

6 DAMPING CONTROLLER SYNTHESIS FOR the SVC

This chapter presents the robust synthesis of the supplementary damping controller (SDC) for the SVC to damp interarea oscillations in the power system. A simplified example with an SVC in a one-machine infinite-bus system is used in Section 6.1 to explain the concepts of using SVC for damping the interarea oscillation. The SVC's capability for providing damping control depends on its location, the signal used as the input to the damping controller, and the design of the damping controller. The location issue has been addressed in Chapter 5 where the bus participation factors and robust stability μ calculation are mainly used to choose the SVC location. The choice of the input signal is determined by the residues and observability factors from the MASS program [53], as detailed in Section 6.2. Based on the RS analysis framework developed in Chapter 5, the robust synthesis framework is formed in Section 6.3, and therefore the D-K iteration can be carried out to synthesize a robust controller. The robust synthesis procedures are then applied to two test systems in Section 6.4 and 6.5. The resulting SDC for the SVC not only guarantees the robust stability of the power system, but also damps the interarea oscillation within the whole range of operating conditions.

6.1 Concepts in Using SVC for Damping

The control requirement for the SVC, which defines the variation of the output of the SVC to stabilize specific parameters of the power system, can be derived from the functional compensation needs of a particular power system. These needs usually fall

into one of the following two main categories:

1. Direct voltage support (to prevent voltage instability)

2. Transient and dynamic stability improvement (to increase the first swing stability margin and provide damping for power oscillations)

As mentioned before, interarea oscillations in power systems are closely related to the power transfer and the network characteristics. Since SVCs can control the voltage at a given terminal of the transmission system, and thereby alter its power transmission characteristics, it is expected that with approprite controls they can provide damping for the interarea oscillation.

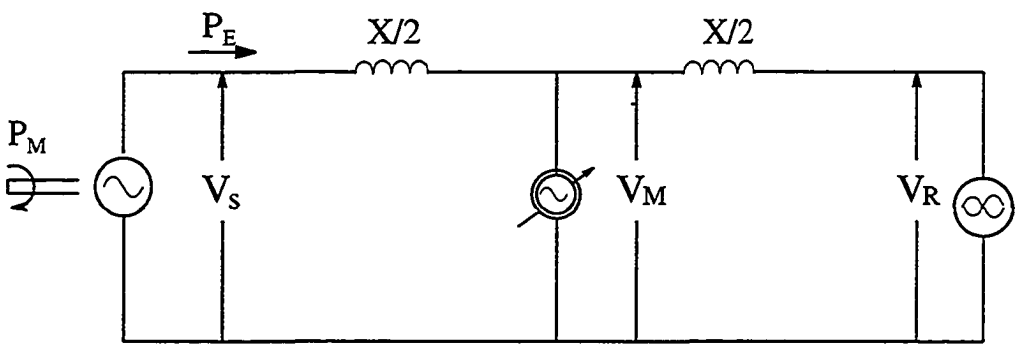

Figure 6.1 SVC in a OMIB system.

A greatly simplified example is used here to illustrate the basic concepts and help establish the damping control requirements for the SVC. Consider a one-machine-infinite-bus system where a generator is linked to an infinite bus by a reactive line. The voltage magnitudes at the sending end and the infinite bus are V and V_0, respectively. The SVC is located at the middle of the line to control the magnitude of the midpoint voltage V_m, as shown in Figure 6.1. Therefore, the voltages at the sending end, middle point, and the infinite bus are given by:

$$V_S = V\sin(\omega t + \delta)$$

$$V_M = V_m \sin(\omega t + \delta/2)$$
$$V_R = V_0 \sin \omega t$$

where δ is the power angle between the sending end (generator internal bus) and the infinite bus voltage. Let X be the total reactance of the transmission line, then the electric power P_E from the generator to the transmission line is given by the following well-known equation:

$$P_E = \frac{VV_m}{X/2} \sin \frac{\delta}{2} \tag{6.1}$$

The swing equation of the generator is given as follows:

$$M \frac{d^2\delta}{dt^2} = P_M - P_E \tag{6.2}$$

where M is the inertia constant of the generator, and P_M is the mechanical power applied to the generator.

For small signal stability, we linearize (6.2) as:

$$M \frac{d^2(\Delta\delta)}{dt^2} = \Delta P_M - \Delta P_E \tag{6.3}$$

Since the mechanical power P_M is constant, so $\Delta P_M = 0$. From (6.1), the change in the electrical power can be expressed as:

$$\Delta P_E = \frac{\partial P_E}{\partial V}\Delta V + \frac{\partial P_E}{\partial V_m}\Delta V_m + \frac{\partial P_E}{\partial \delta}\Delta\delta \tag{6.4}$$

In (6.4) $\Delta V = 0$, since the magnitude of the sending end voltage is constant. Therefore, the substitution of $\Delta P_M = 0$ and (6.4) with $\Delta V = 0$ into (6.3) results in the following expression:

$$M \frac{d^2(\Delta\delta)}{dt^2} + \frac{\partial P_E}{\partial V_m}\Delta V_m + \frac{\partial P_E}{\partial \delta}\Delta\delta = 0 \tag{6.5}$$

In (6.5), the middle term $\frac{\partial P_E}{\partial V_m}\Delta V_m$ represents the effect of the midpoint SVC on the dynamic behavior of the system. Recall that the function of the SVC is to control the midpoint voltage (by supplying appropriate amount of VArs). Consider first that the

magnitude of the midpoint voltage is kept constant, i.e., the SVC is operated as a voltage regulator. Then, with V_m=constant and $\Delta V_m = 0$, (6.5) becomes:

$$M\frac{d^2(\Delta\delta)}{dt^2} + \frac{\partial P_E}{\partial \delta}\Delta\delta = 0 \tag{6.6}$$

The corresponding characteristic equation

$$s^2 + \frac{1}{M}\frac{\partial P_E}{\partial \delta}\,|_0 = 0$$

indicates an undamped oscillation of rotor angle δ (the roots being on the imaginary axis of the s-plane) with an angular frequency of

$$\omega_0 = \sqrt{\frac{1}{M}\frac{\partial P_E}{\partial \delta}\,|_0} \tag{6.7}$$

This means that, in general, an SVC maintaining constant (midpoint) terminal voltage is not effective in damping power oscillations.

In order to damp the power oscillation in the above example, the midpoint voltage in Figure 6.1 must be varied as a function of $d(\Delta\delta)/dt$, that is,

$$\Delta V_m = K\frac{d(\Delta\delta)}{dt} \tag{6.8}$$

where K is a constant.

With (6.8), (6.5) becomes

$$M\frac{d^2(\Delta\delta)}{dt^2} + \frac{\partial P_E}{\partial V_m}\,|_0\, K\frac{d(\Delta\delta)}{dt} + \frac{\partial P_E}{\partial \delta}\Delta\delta = 0 \tag{6.9}$$

which yields the following characteristic equation

$$s^2 + 2\zeta s + \omega_0^2 = 0 \tag{6.10}$$

where

$$2\zeta = \frac{K}{M}\frac{\partial P_E}{\partial V_m}\,|_0$$

and ω_0 is given by (6.7).

The characteristic equation (6.10) clearly represents a positively damped system (the roots being on the left hand side of the s-plane) meaning that the oscillation of angle δ decays with time.

The conclusion therefore can be made that, in order to obtain oscillation damping, the VAr output of the SVC must be controlled so as to vary the terminal voltage in proportion to the rate of change of the rotor angle, $\frac{d(\Delta\delta)}{dt}$. This can be implemented by introducing a supplementary damping controller (SDC) superimposed over SVC's voltage control loop, as shown in Figure 6.2.

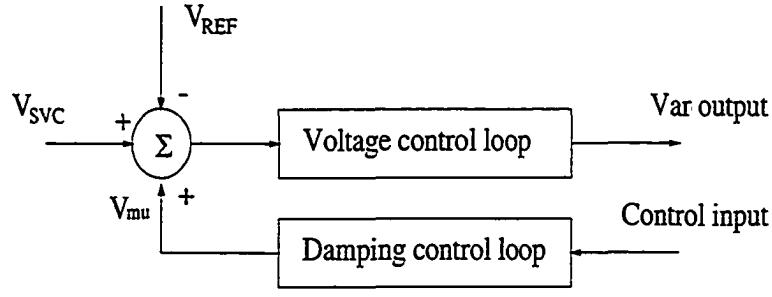

Figure 6.2 Supplementary damping controller to the SVC.

6.2 Selection of Control Input Signal

We now consider the selection of the input signal to the SDC to achieve satisfactory damping performance. The input signal should be readily available and responsive to the mode of oscillation to be damped. For the example of one-machine infinite-bus system with local oscillation in Section 6.1, an apparent choice of the input signal is the shaft speed of the generator $\Delta\omega$. For a multimachine system with interarea oscillations, there are better choices for input signals. A comprehensive research about various input signals to the SVC was studied in [17], with the conclusion that the use of current magnitude as the input signal to the SDC enables substantial damping to be attained, with a positive contribution for all operating conditions.

In this research, we determine the input signal by calculating residues and observability factors using the MASS program [53]. The frequency responses of the transfer function between the SDC input signal and the SVC voltage reference signal are also calculated to ensure that the input signal has a large gain at the interarea frequency range. In both the test systems considered later in this dissertation, the magnitude of line current is chosen as the SDC input signal.

We now derive the general form of representing the current magnitude in terms of the state variables so that the state space description can be established. We assume that for the same power system model described in Chapter 4, the current magnitude of line $p-q$ is chosen as the input signal, where p and q are load buses in the system with voltages $V_p\angle\theta_p$ and $V_q\angle\theta_q$, respectively. Let $g+jb$ be the admittance of line $p-q$, then the current of line $p-q$ is:

$$\begin{aligned} I_{pq} &= (g+jb)(V_p\angle\theta_p - V_q\angle\theta_q) \\ &= (g+jb)[(V_p\cos\theta_p - V_q\cos\theta_q) + j(V_p\sin\theta_p - V_q\sin\theta_q)] \\ &= I_R + jI_I \end{aligned} \tag{6.11}$$

where:

$$I_R = g(V_p\cos\theta_p - V_q\cos\theta_q) - b(V_p\sin\theta_p - V_q\sin\theta_q) \tag{6.12}$$

$$I_I = b(V_p\cos\theta_p - V_q\cos\theta_q) + g(V_p\sin\theta_p - V_q\sin\theta_q) \tag{6.13}$$

From (6.11), we have

$$|I_{pq}|^2 = I_R^2 + I_I^2 \tag{6.14}$$

Linearizing (6.14), we obtain:

$$2|I_{pq}|\Delta I_{pq} = 2I_R\Delta I_R + 2I_I\Delta I_I \tag{6.15}$$

Therefore,

$$\Delta I_{pq} = \alpha\Delta I_R + \beta\Delta I_I \tag{6.16}$$

where

$$\alpha = \frac{I_R}{|I_{pq}|}, \beta = \frac{I_I}{|I_{pq}|}$$

Linearizing (6.12), we have

$$\begin{aligned}
\Delta I_R &= \Delta[g(V_p\cos\theta_p - V_q\cos\theta_q) - b(V_p\sin\theta_p - V_q\sin\theta_q)] \\
&= g(\Delta V_p\cos\theta_p - V_p\sin\theta_p\Delta\theta_p) - g(\Delta V_q\cos\theta_q - V_q\sin\theta_q\Delta\theta_q) \\
&\quad -b(\Delta V_p\sin\theta_p + V_p\cos\theta_p\Delta\theta_p) + b(\Delta V_q\sin\theta_q + V_q\cos\theta_q\Delta\theta_q) \\
&= \begin{bmatrix} g\cos\theta_p - b\sin\theta_p \\ -gV_p\sin\theta_p - bV_p\cos\theta_p \\ -g\cos\theta_q + b\sin\theta_q \\ gV_q\sin\theta_q + bV_q\cos\theta_q \end{bmatrix}^T \begin{bmatrix} \Delta V_p \\ \Delta\theta_p \\ \Delta V_q \\ \Delta\theta_q \end{bmatrix} := c_1^T \begin{bmatrix} \Delta V_p \\ \Delta\theta_p \\ \Delta V_q \\ \Delta\theta_q \end{bmatrix}
\end{aligned} \tag{6.17}$$

Similarly for ΔI_I from (6.13):

$$\Delta I_I = \begin{bmatrix} g\sin\theta_p + b\cos\theta_p \\ gV_p\cos\theta_p - bV_p\sin\theta_p \\ -g\sin\theta_q - b\cos\theta_q \\ -gV_q\cos\theta_q + bV_q\sin\theta_q \end{bmatrix}^T \begin{bmatrix} \Delta V_p \\ \Delta\theta_p \\ \Delta V_q \\ \Delta\theta_q \end{bmatrix} := c_2^T \begin{bmatrix} \Delta V_p \\ \Delta\theta_p \\ \Delta V_q \\ \Delta\theta_q \end{bmatrix} \tag{6.18}$$

Substituting (6.17) and (6.18) into (6.16), we have

$$\Delta I_{pq} = (\alpha c_1^T + \beta c_2^T) \begin{bmatrix} \Delta V_p \\ \Delta\theta_p \\ \Delta V_q \\ \Delta\theta_q \end{bmatrix} \tag{6.19}$$

where α, β, c_1, and c_2 all depend on the linearization point.

Next, we represent $[\Delta V_p\ \Delta\theta_p\ \Delta V_q\ \Delta\theta_q]^T$ in terms of the state variables and therefore the state space representation of ΔI_{pq} is obtained. To do this, we reduce the system to the generator internal buses while retaining the SVC bus and buses p and q, and reorder the bus numbers of the reduced system as follows:

No. 1 — m: internal buses of generators with detailed model

No. $m+1$ — n: internal buses of generators with classical model

No. $n+1$: the SVC bus with voltage $V_{n+1}\angle\theta_{n+1}$

No. $n+2$: Bus p with voltage $V_{n+2}\angle\theta_{n+2}$

No. $n+3$: Bus q with voltage $V_{n+3}\angle\theta_{n+3}$

Since loads in the system are represented by constant impedances and absorbed into the reduced network during the reduction procedure, the injected currents at buses p and q are zero, i.e.,

$$I_{Q\,n+2} + jI_{D\,n+2} = 0,\ I_{Q\,n+3} + jI_{D\,n+3} = 0$$

where the subscripts Q and D indicate that these currents are in the synchronous reference frame.

By following the same procedure as in Section 4.4, we have

$$\begin{aligned} I_{Q\,n+2} &= 0 = f_1 \\ &= \sum_{i=1}^{m}[(G_{n+2,i}\cos\delta_i - B_{n+2,i}\sin\delta_i)E'_{qi} \\ &\quad -(G_{n+2,i}\sin\delta_i + B_{n+2,i}\cos\delta_i)E'_{di}] \\ &\quad + \sum_{i=m+1}^{n}(G_{n+2,i}\cos\delta_i - B_{n+2,i}\sin\delta_i)E_i \\ &\quad + \sum_{k=1}^{3}(G_{n+2,n+k}\cos\theta_{n+k} - B_{n+2,n+k}\sin\theta_{n+k})V_{n+k} \end{aligned} \tag{6.20}$$

$$\begin{aligned} I_{D\,n+2} &= 0 = f_2 \\ &= \sum_{i=1}^{m}[(G_{n+2,i}\cos\delta_i - B_{n+2,i}\sin\delta_i)E'_{di} \\ &\quad +(G_{n+2,i}\sin\delta_i + B_{n+2,i}\cos\delta_i)E'_{qi}] \\ &\quad + \sum_{i=m+1}^{n}(G_{n+2,i}\sin\delta_i + B_{n+2,i}\cos\delta_i)E_i \\ &\quad + \sum_{k=1}^{3}(G_{n+2,n+k}\sin\theta_{n+k} + B_{n+2,n+k}\cos\theta_{n+k})V_{n+k} \end{aligned} \tag{6.21}$$

$$
\begin{aligned}
I_{Q\,n+3} &= 0 = f_3 \\
&= \sum_{i=1}^{m}[(G_{n+3,i}\cos\delta_i - B_{n+3,i}\sin\delta_i)E'_{qi} \\
&\quad -(G_{n+3,i}\sin\delta_i + B_{n+3,i}\cos\delta_i)E'_{di}] \\
&\quad + \sum_{i=m+1}^{n}(G_{n+3,i}\cos\delta_i - B_{n+3,i}\sin\delta_i)E_i \\
&\quad + \sum_{k=1}^{3}(G_{n+3,n+k}\cos\theta_{n+k} - B_{n+3,n+k}\sin\theta_{n+k})V_{n+k}
\end{aligned} \tag{6.22}
$$

$$
\begin{aligned}
I_{D\,n+3} &= 0 = f_4 \\
&= \sum_{i=1}^{m}[(G_{n+3,i}\cos\delta_i - B_{n+3,i}\sin\delta_i)E'_{di} \\
&\quad +(G_{n+3,i}\sin\delta_i + B_{n+3,i}\cos\delta_i)E'_{qi}] \\
&\quad + \sum_{i=m+1}^{n}(G_{n+3,i}\sin\delta_i + B_{n+3,i}\cos\delta_i)E_i \\
&\quad + \sum_{k=1}^{3}(G_{n+3,n+k}\sin\theta_{n+k} + B_{n+3,n+k}\cos\theta_{n+k})V_{n+k}
\end{aligned} \tag{6.23}
$$

Linearizing (6.20)—(6.23), we obtain:

$$
\begin{aligned}
0 = \sum_{i=1}^{m}(\frac{\partial f_1}{\partial E'_{qi}}\Delta E'_{qi} + \frac{\partial f_1}{\partial E'_{di}}\Delta E'_{di}) + \sum_{k=2}^{n}\frac{\partial f_1}{\partial \delta_{k1}}\Delta\delta_{k1} \\
+ \sum_{k=1}^{3}(\frac{\partial f_1}{\partial V_{n+k}}\Delta V_{n+k} + \frac{\partial f_1}{\partial \theta_{n+k}}\Delta\theta_{n+k})
\end{aligned} \tag{6.24}
$$

$$
\begin{aligned}
0 = \sum_{i=1}^{m}(\frac{\partial f_2}{\partial E'_{qi}}\Delta E'_{qi} + \frac{\partial f_2}{\partial E'_{di}}\Delta E'_{di}) + \sum_{k=2}^{n}\frac{\partial f_2}{\partial \delta_{k1}}\Delta\delta_{k1} \\
+ \sum_{k=1}^{3}(\frac{\partial f_2}{\partial V_{n+k}}\Delta V_{n+k} + \frac{\partial f_2}{\partial \theta_{n+k}}\Delta\theta_{n+k})
\end{aligned} \tag{6.25}
$$

$$
\begin{aligned}
0 = \sum_{i=1}^{m}(\frac{\partial f_3}{\partial E'_{qi}}\Delta E'_{qi} + \frac{\partial f_3}{\partial E'_{di}}\Delta E'_{di}) + \sum_{k=2}^{n}\frac{\partial f_3}{\partial \delta_{k1}}\Delta\delta_{k1} \\
+ \sum_{k=1}^{3}(\frac{\partial f_3}{\partial V_{n+k}}\Delta V_{n+k} + \frac{\partial f_3}{\partial \theta_{n+k}}\Delta\theta_{n+k})
\end{aligned} \tag{6.26}
$$

$$
0 = \sum_{i=1}^{m}(\frac{\partial f_4}{\partial E'_{qi}}\Delta E'_{qi} + \frac{\partial f_4}{\partial E'_{di}}\Delta E'_{di}) + \sum_{k=2}^{n}\frac{\partial f_4}{\partial \delta_{k1}}\Delta\delta_{k1}
$$

$$+\sum_{k=1}^{3}\left(\frac{\partial f_4}{\partial V_{n+k}}\Delta V_{n+k}+\frac{\partial f_4}{\partial \theta_{n+k}}\Delta\theta_{n+k}\right) \tag{6.27}$$

All the partial derivatives in (6.24)—(6.27) can be found in Appendix B.

We then rewrite (6.24)—(6.27) in the following matrix form:

$$\begin{bmatrix} \frac{\partial f_1}{\partial V_{n+2}} & \frac{\partial f_1}{\partial \theta_{n+2}} & \frac{\partial f_1}{\partial V_{n+3}} & \frac{\partial f_1}{\partial \theta_{n+3}} \\ \frac{\partial f_2}{\partial V_{n+2}} & \frac{\partial f_2}{\partial \theta_{n+2}} & \frac{\partial f_2}{\partial V_{n+3}} & \frac{\partial f_2}{\partial \theta_{n+3}} \\ \frac{\partial f_3}{\partial V_{n+2}} & \frac{\partial f_3}{\partial \theta_{n+2}} & \frac{\partial f_3}{\partial V_{n+3}} & \frac{\partial f_3}{\partial \theta_{n+3}} \\ \frac{\partial f_4}{\partial V_{n+2}} & \frac{\partial f_4}{\partial \theta_{n+2}} & \frac{\partial f_4}{\partial V_{n+3}} & \frac{\partial f_4}{\partial \theta_{n+3}} \end{bmatrix} \begin{bmatrix} \Delta V_{n+2} \\ \Delta\theta_{n+2} \\ \Delta V_{n+3} \\ \Delta\theta_{n+3} \end{bmatrix}$$

$$+\begin{bmatrix} \frac{\partial f_1}{\partial V_{n+1}} & \frac{\partial f_1}{\partial \theta_{n+1}} \\ \frac{\partial f_2}{\partial V_{n+1}} & \frac{\partial f_2}{\partial \theta_{n+1}} \\ \frac{\partial f_3}{\partial V_{n+1}} & \frac{\partial f_3}{\partial \theta_{n+1}} \\ \frac{\partial f_4}{\partial V_{n+1}} & \frac{\partial f_4}{\partial \theta_{n+1}} \end{bmatrix} \begin{bmatrix} \Delta V_{n+1} \\ \Delta\theta_{n+1} \end{bmatrix} + \begin{bmatrix} \frac{\partial f_1}{\partial E'_{q1}} & \frac{\partial f_1}{\partial E'_{d1}} & \cdots \\ \frac{\partial f_2}{\partial E'_{q1}} & \frac{\partial f_2}{\partial E'_{d1}} & \cdots \\ \frac{\partial f_3}{\partial E'_{q1}} & \frac{\partial f_3}{\partial E'_{d1}} & \cdots \\ \frac{\partial f_4}{\partial E'_{q1}} & \frac{\partial f_4}{\partial E'_{d1}} & \cdots \end{bmatrix} [x] = 0 \tag{6.28}$$

where x are state variables described in Chapter 4. We simply denote (6.28) as

$$E_2 \begin{bmatrix} \Delta V_{n+2} \\ \Delta\theta_{n+2} \\ \Delta V_{n+3} \\ \Delta\theta_{n+3} \end{bmatrix} + E_1 \begin{bmatrix} \Delta V_{n+1} \\ \Delta\theta_{n+1} \end{bmatrix} + E_0\, x = 0 \tag{6.29}$$

where E_2, E_1, and E_0 are corresponding matrices from (6.28).

In Chapter 4, we derived the representation of non-state variables $\Delta Y = [\Delta V_{n+1}\ \ \Delta\theta_{n+1}]^T$ with state variables x (see (4.46)):

$$\begin{bmatrix} \Delta V_{n+1} \\ \Delta\theta_{n+1} \end{bmatrix} = -\left(\frac{\partial g}{\partial Y}\right)^{-1}\frac{\partial g}{\partial X}x = Gx \tag{6.30}$$

Substituting (6.30) into (6.29), we obtain

$$\begin{bmatrix} \Delta V_{n+2} \\ \Delta\theta_{n+2} \\ \Delta V_{n+3} \\ \Delta\theta_{n+3} \end{bmatrix} = -E_2^{-1}(E_1G + E_0)x \tag{6.31}$$

Therefore, from (6.19) and (6.31), we get the representation of the current magnitude with the state variables

$$\Delta I_{pq} = cx \tag{6.32}$$

where the row vector $c = -(\alpha c_1^T + \beta c_2^T)E_2^{-1}(E_1 G + E_0)$.

6.3 μ Synthesis Framework

In order to design a robust controller, we need to take uncertainty into account. In Chapter 5, we considered a simple form of the state space equation of the plant:

$$\dot{x} = Ax \tag{6.33}$$

for RS analysis. The characterization of uncertainty in the A-matrix essentially included approximating each changing element a_{ij} with a quadratic polynomial and representing it as a linear fractional transformation (LFT) form; then the whole A-matrix could be written in an LFT form and the standard framework for RS analysis was obtained. We now consider the input and output signals of the plant to form the robust synthesis framework as shown in Figure 6.3.

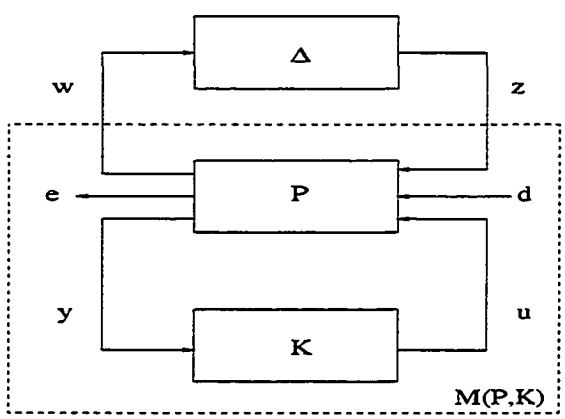

Figure 6.3 μ-synthesis framework.

From Chapter 4, by adding the disturbance input d (the reference voltage of the SVC, $\Delta V_{REF,SVC}$) and the control input u (the output from the damping controller K to be designed, ΔV_{mu}), (6.33) becomes:

$$\dot{x} = Ax + B \begin{bmatrix} d \\ u \end{bmatrix} \tag{6.34}$$

where B is a constant coefficient matrix.

For the given operating range (parametric uncertainty) characterized by δ, we obtain (6.35) by using the quadratic approximation for the A matrix:

$$\dot{x} = A_0 x + L^T[A_1(\delta I) + A_{11}(\delta^2 I)]Rx + B \begin{bmatrix} d \\ u \end{bmatrix} \tag{6.35}$$

From the derivation in Section 6.2, the output signal y from the plant P (also the input signal to the controller K) can be expressed as

$$y = \Delta I_{pq} = cx \tag{6.36}$$

The vector c depends on the linearization point, and hence varies when the operating conditions change. Moreover, the changing elements in c have the same column structure as in the A matrix, therefore, the quadratic approximation for c yields:

$$y = cx = \{c_0 + [c_1(\delta I) + c_{11}(\delta^2 I)]R\}\, x \tag{6.37}$$

(6.35) and (6.37) can be represented in Figure 6.4.

In this way, we capture the uncertainty in the vector c while keeping the size of the uncertainty block the same as RS analysis. Therefore, from Figure 6.4, we have

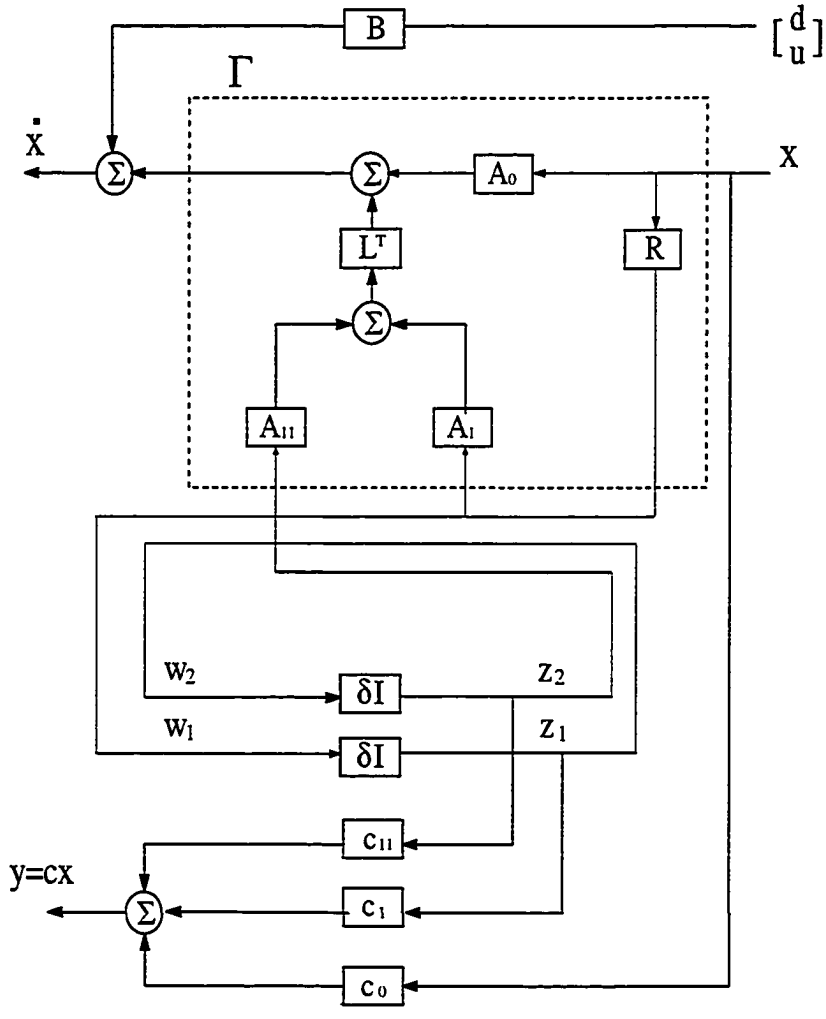

Figure 6.4 Uncertainty in the plant and the input signal to the SDC.

$$\begin{bmatrix} \dot{x} \\ w_1 \\ w_2 \\ y \end{bmatrix} = \begin{bmatrix} A_0 & L^T A_1 & L^T A_{11} & B \\ R & 0 & 0 & 0 \\ 0 & I & 0 & 0 \\ c_0 & c_1 & c_{11} & 0 \end{bmatrix} \begin{bmatrix} x \\ z_1 \\ z_2 \\ \begin{bmatrix} d \\ u \end{bmatrix} \end{bmatrix} \tag{6.38}$$

To specify the performance for the damping controller K, we introduce the error signals $\tilde{e}_1$, $\tilde{e}_2$ and their weighting functions W_{e1}, W_{e2}, as shown in Figure 6.5.

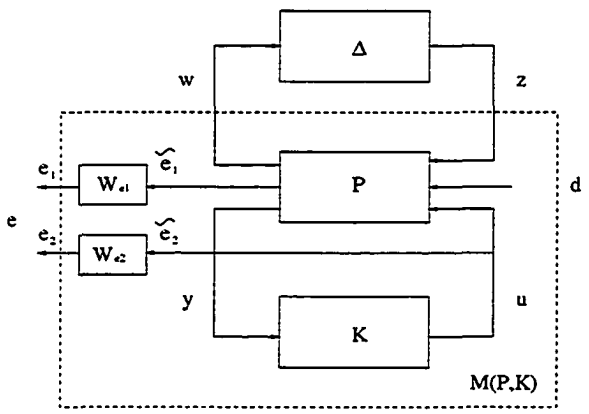

Figure 6.5 μ-synthesis framework with weighting functions.

The choice of error signals and their weighting functions play an important role in controller synthesis. In small systems, $\tilde{e}_1$ is chosen to be the inertia weighted average of the machine angular speeds. This choice is clear because essentially each machine participates in the interarea mode. However, for large systems this choice may be misleading. There are some machines with large inertia whose participation in the interarea mode are small. The following procedure is carried out to identify appropriate machine angular speeds to be included in the error signal $\tilde{e}_1$:

1. At the nominal operating point the dominant interarea mode is determined.

2. For the interarea mode, the mode shape [11] is determined and the machines are then grouped based on the real values of the mode shape. This process identifies the machines that oscillate against each other in the chosen interarea mode.

3. Participation factors are then calculated for the selected interarea mode and the group of machines that participate strongly in the interarea mode are retained in the group obtained in Step 2. The error signal $\tilde{e}_1$ is then chosen to be the inertia weighted average of the speeds of the retained machines in the group.

Therefore, $\tilde{e}_1$ can be represented in terms of the state variables as given below:

$$\tilde{e}_1 = \tilde{c}\,x$$

where $\tilde{c}$ corresponds to the inertia weighted coefficients of the angular speeds.

The weighting function W_{e1} is chosen such that at the low frequency range the closed-loop system rejects disturbance at the output by a significant ratio, thus the low frequency interarea oscillation will be effectively damped. $\tilde{e}_2$ is obtained directly from u and its weighting function W_{e2} is chosen to be small to satisfy the necessary "rank conditions" for the H_∞ synthesis [46].

By augmenting (6.38), the state space equation describing the plant in Figure 6.5 can be written as

$$\begin{bmatrix} \dot{x} \\ w_1 \\ w_2 \\ \tilde{e}_1 \\ \tilde{e}_2 \\ y \end{bmatrix} = \begin{bmatrix} A_0 & L^T A_1 & L^T A_1 1 & B \\ R & 0 & 0 & 0 \\ 0 & I & 0 & 0 \\ \tilde{c} & 0 & 0 & 0 \\ 0 & 0 & 0 & [0\ \ 1] \\ c_0 & c_1 & c_{11} & 0 \end{bmatrix} \begin{bmatrix} \begin{matrix} x \\ z_1 \\ z_2 \end{matrix} \\ \begin{bmatrix} d \\ u \end{bmatrix} \end{bmatrix} \tag{6.39}$$

The weighting functions, W_{e1} and W_{e2}, can be further absorbed into the plant to form the general framework of μ-synthesis as shown in Figure 3.5 which admits the following

state space representation:

$$\begin{aligned} \dot{x} &= \Gamma_{11}x + \Gamma_{12}z + B_1 d + B_2 u \\ w &= \Gamma_{21}x + \Gamma_{22}z \\ e &= C_{11}x + C_{12}z + D_{11}d + D_{12}u \\ y &= C_{21}x + C_{22}z + D_{21}d + D_{22}u \\ z &= \Delta w \end{aligned} \tag{6.40}$$

After forming the synthesis framework, the "D-K" iteration described in Chapter 3 will be carried out to synthesize a robust damping controller K. The resulting controller order will be typically much higher because of the frequency scalings, so appropriate model reduction techniques should be used to reduce the controller to a reasonably low order while maintaining the essential characteristics of the original controller. First, a balanced realization is performed which entails balancing the observability and controllability Grammians. Then the Hankel singular values are used to indicate the acceptable order of model reduction. Finally, the optimal Hankel norm approximation of a given order k is computed.

Note that the SDC should only work in the transient state and not interfere with the voltage regulation of SVC, therefore a washout filter with time constant $T_W = 10s$ will be added to the designed controller to ensure that the steady state output from the SDC is zero, as shown in Figure 6.6.

Finally, the performance of the designed SDC should be examined both in the frequency domain and in the time domain to guarantee that the SDC will not only achieve the system robust stability, but also damp the interarea oscillations effectively over the whole operation range.

In summary, the proposed approach for robust damping controller synthesis with μ-technique is implemented in the following steps:

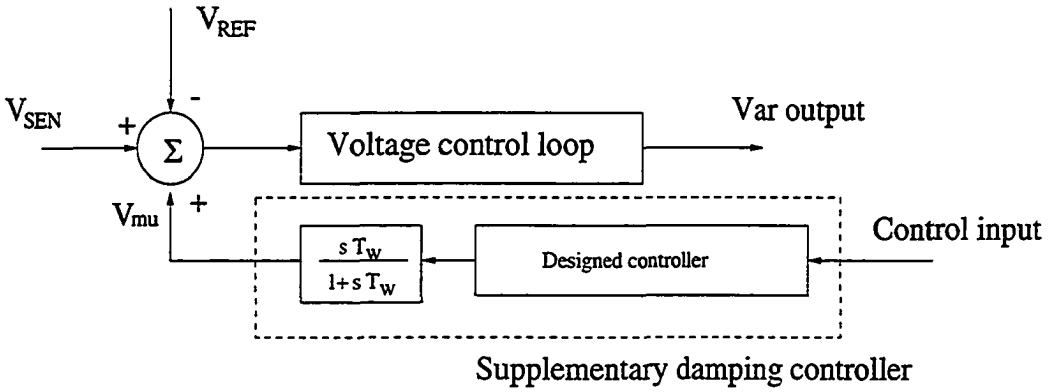

Figure 6.6 Supplementary damping controller.

Step 1: Identify the structured uncertainty using the expected range of operating conditions and associated power flow data and dynamic data, as explained in Section 5.1.

Step 2: Identify the best location for the SVC.

Step 3: Formulate the robust stability set-up within which the impact of changing operating conditions is expressed as a polynomial function of operating parameters and expressed in the form of matrix of real repeated scalars using the SSV theory.

Step 4: Choose the input signal to the SDC.

Step 5: Choose the error signals and their weighting functions.

Step 6: Form the μ-synthesis framework.

Step 7: Perform μ synthesis to obtain a controller and reduce it to lower order.

Step 8: Check the performance of the resulting SDC, both in frequency domain and in time domain.

6.4 Design and Simulation Results on Four-machine System

6.4.1 Preliminary Design Steps

The control design approach presented above is now applied to the four-machine two-area system described in Section 5.3.1. According to Table 5.1, when active power is exported from Area 1 to Area 2, a poorly damped interarea mode is observed. Therefore we focus on this case on power export from Area 1 to Area 2 (P_{5-7}) as a parameter uncertainty within the range of [200—600 MW] with the nominal operating condition 400 MW. The following points that specifically relate to the μ-synthesis set-up for the four-machine system are noted:

1. The SVC supplementary damping controller is generally effectively when SVC is located at the mid-point of long transmission line with heavy power transfer, thus the mid-point of tie-line 5-6 (Bus #7) is chosen as the SVC location.

2. The input signal y to the SDC is chose to be the line 5-7 current magnitude. This is a local signal and will effectively reflect the interarea oscillations excited by the disturbances. Table 6.1 lists the results of observability and residue calculation for the nominal operating condition by the MASS program, which indicates that line 5-7 current magnitude is a good choice for the input signal.

3. The error signal e_1 is chosen to be the system angular speed in the center of inertia (COI) frame of reference. This provides a weighted measure of the response of the system to the external disturbance.

4. Weighting functions:

$$W_{e1} = \frac{0.05s + 400}{s + 40}, \; W_{e2} = 0.001$$

The choice of W_{e1} implies that at low frequency the closed-loop system rejects disturbance at the output by a factor of 10:1.

Table 6.1 Residues and observability factors from MASS for the 4-machine system

Signal	Residues	Observability
$\Delta\omega$ of G1	-0.3849+j0.5349	0.5262
$\Delta\omega$ of G2	-0.3307+j0.4866	0.4671
$\Delta\omega$ of G3	1.1776+j0.1317	1.4140
$\Delta\omega$ of G4	1.6890+j0.1399	1.3460
ΔP, line 2-5	0.9657+j0.4953	0.8617
ΔP, line 5-7	0.5579+j2.1350	1.7520
ΔP, line 7-6	0.5108+j1.9100	1.5701
ΔP, line 6-4	-0.1229-j2.0300	1.4082
ΔQ, line 2-5	0.4686+j1.5330	1.2731
ΔQ, line 5-7	0.3211+j0.8092	0.6192
ΔQ, line 7-6	-0.0957+j0.5204	0.4058
ΔQ, line 6-4	0.2197+j0.7413	0.6139
ΔI, line 2-5	0.6617+j1.5133	1.3110
ΔI, line 5-7	0.5255+j2.5261	2.0497
ΔI, line 7-6	0.5135+j2.1932	1.7884
ΔI, line 6-4	-0.2762-j2.5650	1.8691

6.4.2 Controller and Reduction

After four steps of the D-K iteration procedure, a 102-order supplementary controller is obtained. For practical implementation, the order is reduced using the Hankel norm reduction procedure. This results in a reduced-order SDC of order 6 whose transfer function is given as below:

$$G_k(s) = \frac{-0.1085s^6 - 14.44s^5 - 27.94s^4 - 6.118s^3 + 263.5s^2 - 4.556s + 52.64}{s^6 + 53.47s^5 + 337s^4 + 773.6s^3 + 1450s^2 + 734.8s + 285.9} \quad (6.41)$$

The accuracy of the model reduction procedure is verified by the following procedure:

1. Compare the Bode plots: the Bode plots of the full-order controller and the reduced-order controller are shown in Figure 6.7.

2. Compare the closed-loop robust stability/robust performance: Form the closed-loop system with the full-order SDC and reduced-order SDC, and calculate μ_{RS} and μ_{RP} using the procedure described in Chapter 5 and Chapter 3. The comparison

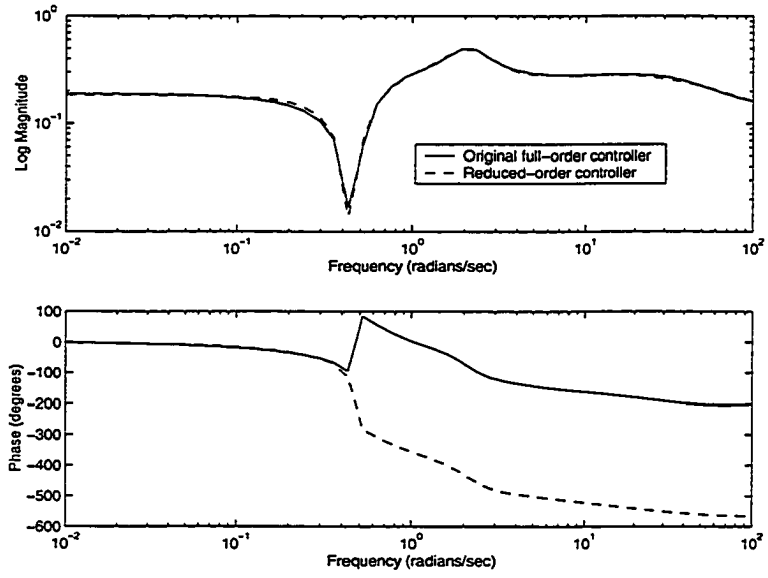

Figure 6.7 Bode plots comparison of full-order SDC and reduced-order SDC.

Table 6.2 Comparison of RS and RP

Index	Full-order SDC	Reduced-order SDC
μ_{RS}^{max}	0.689	0.707
μ_{RP}^{max}	0.915	0.940

of μ peak of RS and RP for the full-order SDC and the reduced-order SDC is given in Table 6.2.

It can be concluded from Figure 6.7 and Table 6.2 that the reduced-order controller retains the essential characteristics of the full-order controller; also the closed-loop system with reduced-order controller achieves RS and RP. This follows from the peak value 0.940 of RP μ-plot, which implies that for all perturbation matrices Δ satisfying $\overline{\sigma}(\Delta) \leq 1/0.940$ the perturbed system is stable and the H_∞ norm of the transfer function between disturbance input d and disturbance output e is less than 0.940.

The reduced-order SDC is then implemented in EPRI's MASS and ETMSP using the user-defined model (UDM) provided by EPRI and a number of tests have been conducted to verify SDC's damping performance.

6.4.3 Interarea Mode and Damping Ratio from MASS

At different operating conditions within the whole operating range, the eigenvalues of the linearized system are computed using MASS. The eigenvalue corresponding to the interarea mode and its damping ratio are given in Table 6.3. It can be seen from the table that SDC effectively damped the interarea mode by a large damping ratio over the whole range.

Table 6.3 Interarea mode and damping ratio

Operating condition		Interarea mode	Damping ratio
$P_{5-7} = 200$ MW	Without SDC	$-0.0799 \pm j3.000$	0.0266
	With SDC	$-0.7869 \pm j2.040$	0.3598
$P_{5-7} = 400$ MW	Without SDC	$-0.0424 \pm j2.838$	0.015
	With SDC	$-0.9005 \pm j1.871$	0.434
$P_{5-7} = 575$ MW	Without SDC	$0.0354 \pm j2.566$	-0.013
	With SDC	$-1.030 \pm j1.799$	0.4967

6.4.4 Damping Characteristics of the SDC Subjected to a Small Fault at Power Sending End.

The exported tie-line power is varied from 200 MW to 575 MW and a three phase fault is applied at Bus #5 for a period of 10ms and subsequently removed without changing the system topology. Three typical operating conditions within the whole range are considered here:

1. Low operating condition: The tie-line power flow $P_{5-7} = 200$ MW

2. Nominal operating condition: The tie-line power flow $P_{5-7} = 400$ MW

3. High operating condition: The tie-line power flow $P_{5-7} = 575$ MW

The responses of the system with and without the supplementary controller at these different operating conditions are shown in Figures 6.8—6.10.

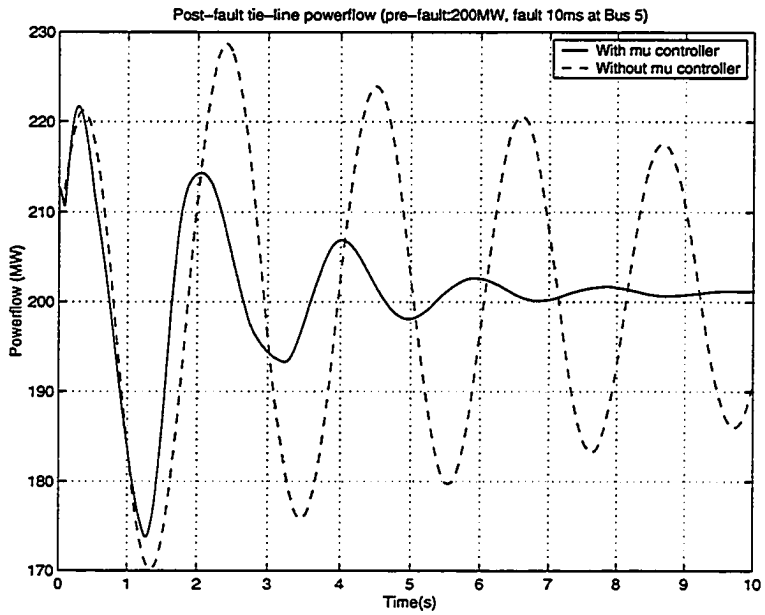

Figure 6.8 The time response of tie-line power (200 MW) with and without damping controller in the case of a 10ms three phase ground short circuit at Bus #5.

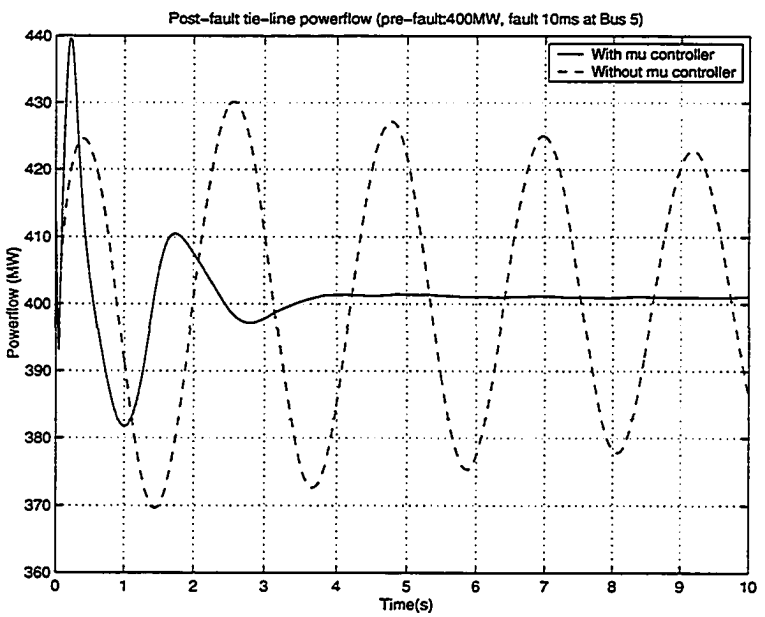

Figure 6.9 The time response of tie-line power (400 MW) with and without damping controller in the case of a 10ms three phase ground short circuit at Bus #5.

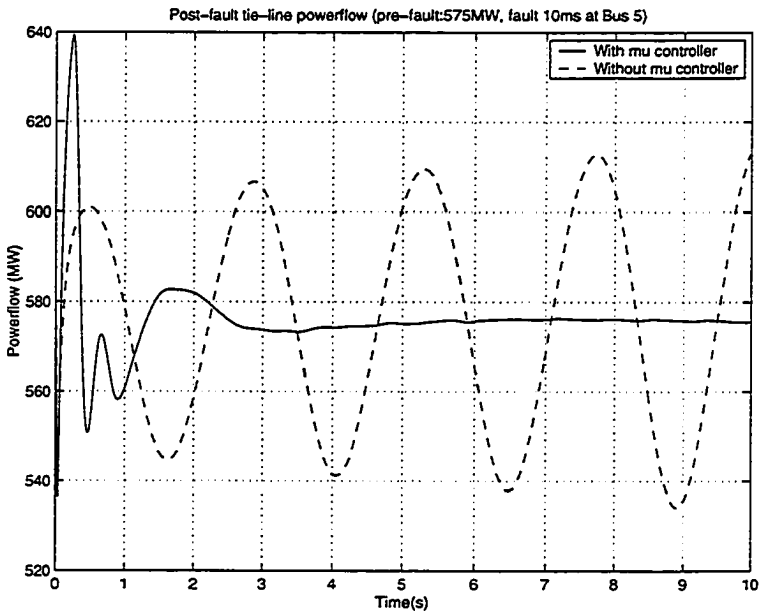

Figure 6.10 The time response of tie-line power (575 MW) with and without damping controller in the case of a 10ms three phase ground short circuit at Bus #5.

Figures 6.8—6.10 provide clear evidence that the supplementary controller obtained using μ-synthesis provides excellent damping. An interesting feature is seen in Figure 6.10 where the system is unstable without the supplementary controller. In this case the supplementary controller stabilizes the system and provides excellent damping.

The voltage magnitude of the SVC bus during the oscillation is plotted in Figure 6.11, compared with the case without SDC for the nominal operating condition. It can be seen from Figure 6.11 that the addition of the supplementary damping controller will not compromise the voltage regulation of SVC which is SVC's main application.

6.4.5 Damping Characteristics of the SDC Subjected to a Small Fault at Power Receiving End.

The exported tie-line power is varied from 200 MW to 575 MW and a three phase fault is applied at Bus #6 (power receiving end) for a period of 10ms and subsequently

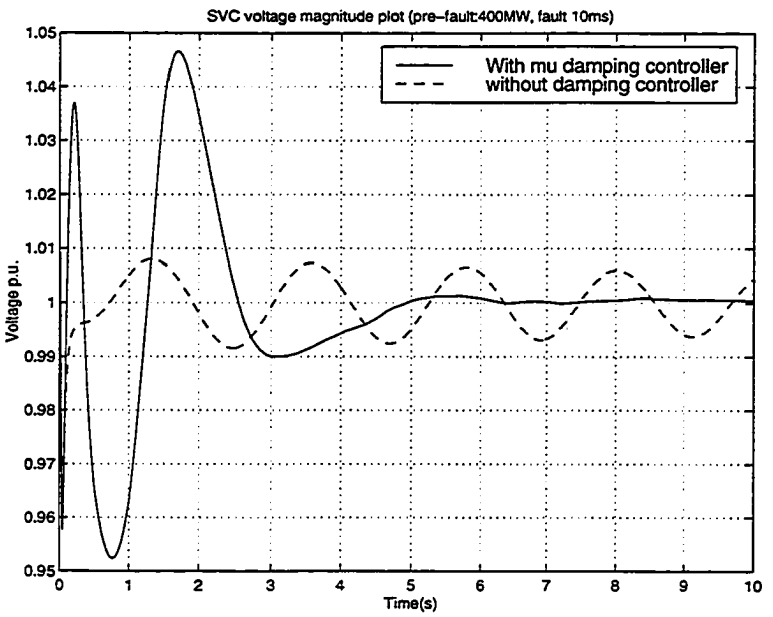

Figure 6.11 The voltage plot of SVC bus during oscillation.

removed without changing the system topology. The response of the system with and without the supplementary controller for the three typical operating conditions are shown in Figures 6.12—6.14.

Figures 6.12—6.14 provide clear evidence that the supplementary controller obtained using μ-synthesis provides excellent damping.

6.4.6 Damping Characteristics of the SDC Subjected to a Large Fault

A three-phase ground is applied at Bus #5, and cleared in 30ms without changing system topology. The pre-fault power flow on the tie-line is 400 MW. The time response of tie line power flow is shown in Figure 6.15.

Figure 6.15 again shows the efficacy of the supplementary controller in mitigating the effects of large disturbances.

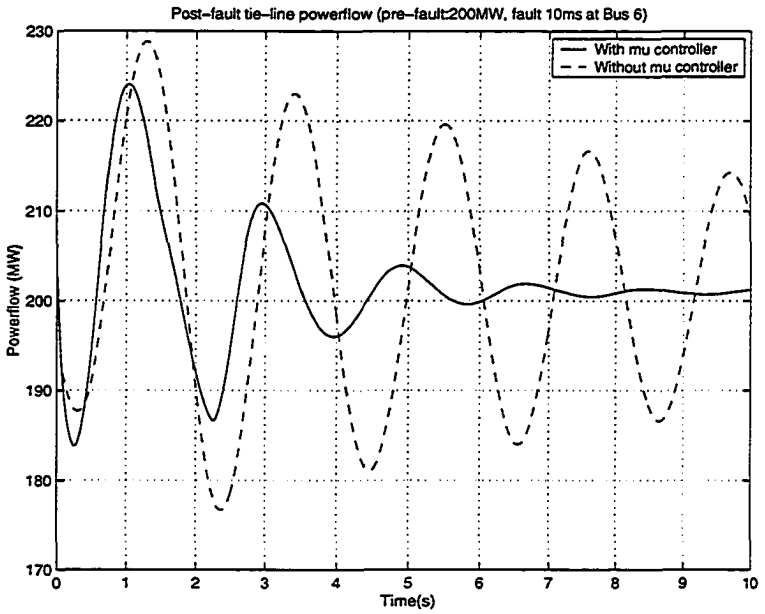

Figure 6.12 The time response of tie-line power (200 MW) with and without damping controller in the case of a 10ms three phase ground short circuit at Bus #6.

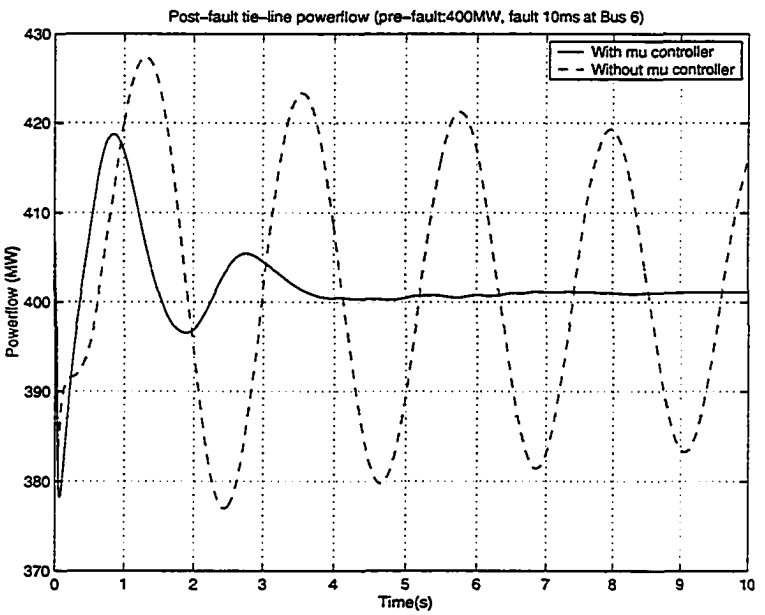

Figure 6.13 The time response of tie-line power (400 MW) with and without damping controller in the case of a 10ms three phase ground short circuit at Bus #6.

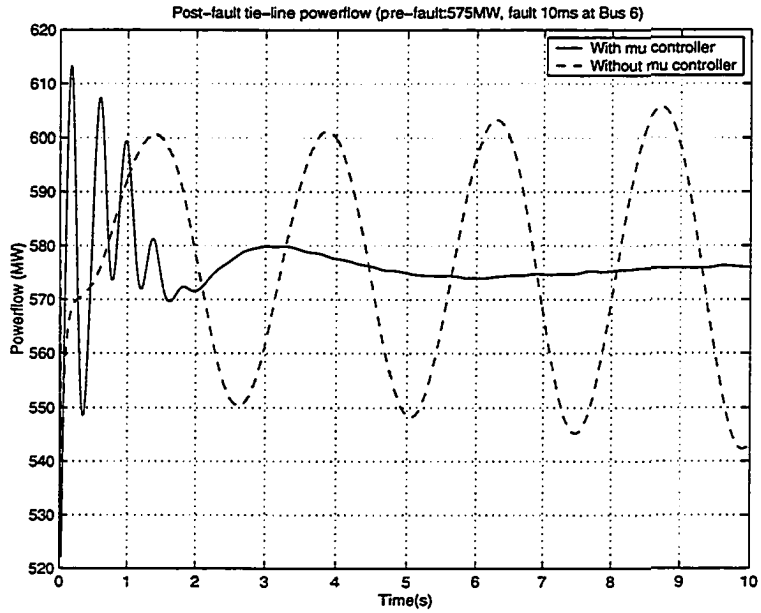

Figure 6.14 The time response of tie-line power (575 MW) with and without damping controller in the case of a 10ms three phase ground short circuit at Bus #6.

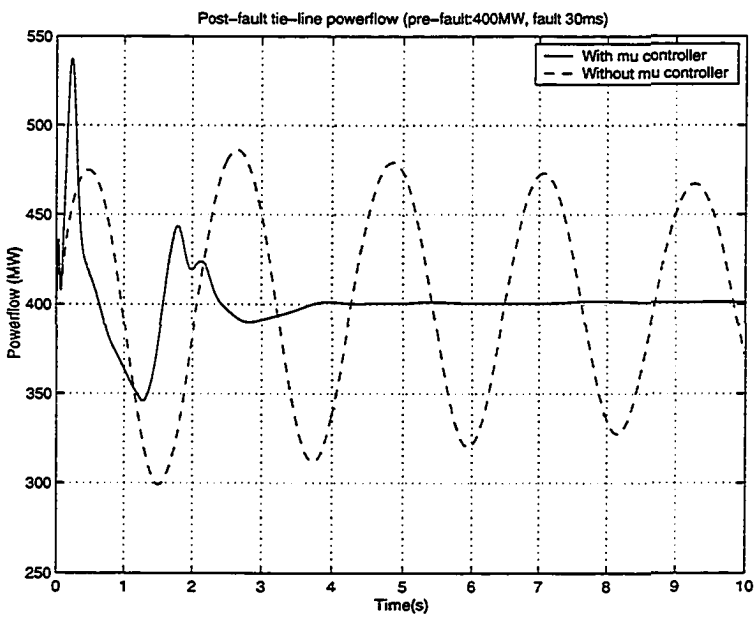

Figure 6.15 The time response of tie-line power (400 MW) with and without damping controller for a large three-phase to ground fault at Bus #5.

6.4.7 Transient Stability Test

The effect of the supplementary controller in enhancing transient stability performance is also verified by evaluating the critical clearing times (CCT) at three different operating conditions for the three-phase to ground fault at Bus #5. The results of this comparison are shown in Table 6.4.

Table 6.4 Transient stability test by measuring CCT

Operating conditions	CCT Without SDC	CCT With designed SDC
$P_{5-7} = 200$ MW	205 ms	235 ms
$P_{5-7} = 400$ MW	112 ms	145 ms
$P_{5-7} = 575$ MW	0 (unstable)	56 ms

The results shown in Table 6.4 again demonstrate the effective role played by the supplementary controller in enhancing the transient stability performance. It should be noted that structured singular value theory is developed for small signal stability problems, so the improvement of transient stability performance should be regarded as an additional benefit of the controller.

6.4.8 Damping characteristics comparison with a conventionally designed SDC

A supplementary controller was designed using conventional pole placement techniques presented in [11]. The design was performed at the nominal operating point where the tie-line flow is 400 MW. The resulting controller was then tested when the system was in the nominal operating condition and subjected to a three-phase fault at Bus #6 cleared in 40 ms . The comparison of the power generation at Bus #1 in the case of the conventionally designed supplementary controller and the supplementary controller designed using μ-synthesis is shown in Figure 6.16. These plots again illustrate the superior performance of the supplementary controller using μ-synthesis. This is especially true when the whole operating range is considered. Figure 6.17 gives

the damping characteristics of the robust SDC and the conventionally designed SDC when the system is at high operating condition (P_{5-7} = 575 MW) and subjected to a three-phase fault at Bus #6 for 10ms. In this case, the robust SDC still provides good damping, while the performance of the conventionally designed SDC becomes poor.

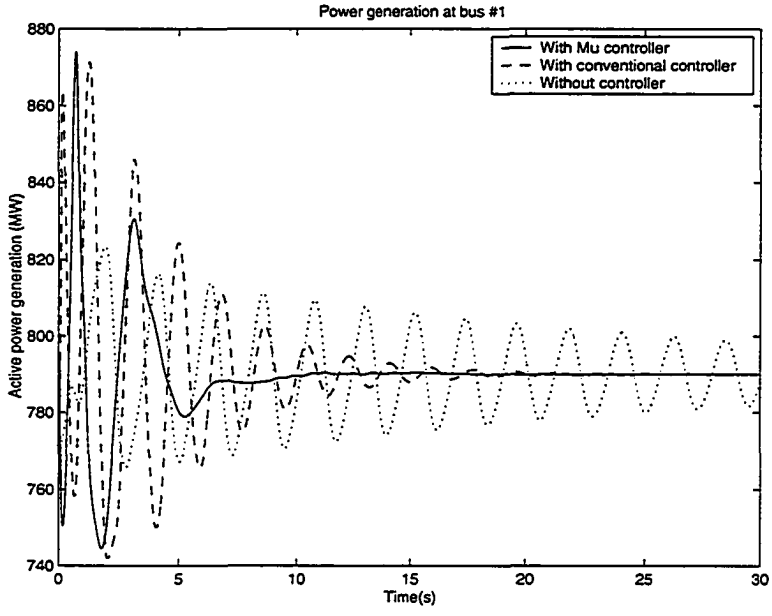

Figure 6.16 The time response of power generation at Bus #1 for fault at Bus #6.

6.5 Design and Simulation Results on IEEE 50-generator System

The base case power flow is characterized by setting the generation at Station A to be 2x1400MW. This generation is treated as an uncertainty and allowed to vary in the range of [2x1300MW — 2x1500MW].

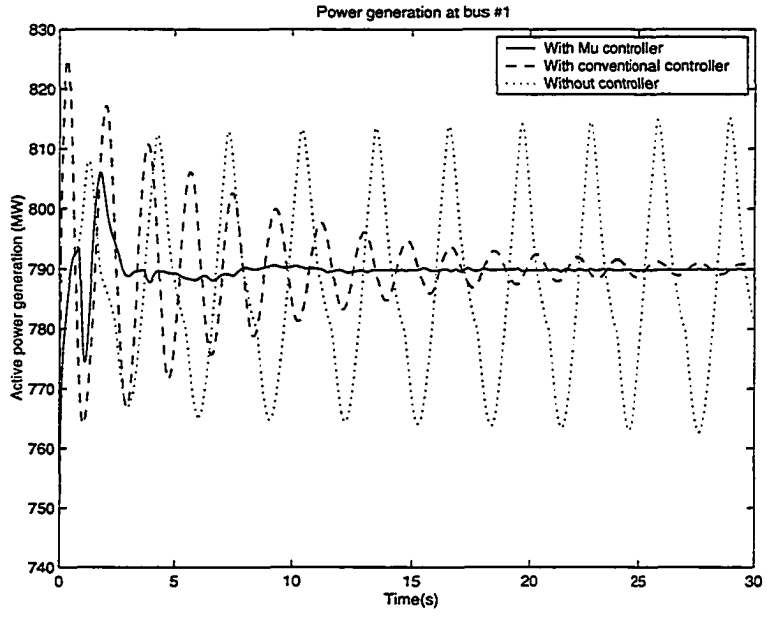

Figure 6.17 The time response of power generation at Bus #1 for fault at Bus #6.

6.5.1 Choice of SVC Location

For multimachine systems the choice of location of the SVC is an important consideration for the purpose of providing both the voltage support function and the damping function. The procedures to select the location and the final choice of the location are detailed in Section 5.3.2.1. Bus #44 is chosen as the location of the SVC for the IEEE 50-generator system.

6.5.2 Choice of the input signal to the SDC

As mentioned before, the magnitude of line current is chosen as the input signal to the SDC since it is readily available and enables substantial damping for all operating conditions [17]. Table 6.5 lists some input signals with large values of the residues and observability factors calculated by the MASS program.

The frequency response of the transfer function between these signals and the SVC voltage reference signal are also calculated. Table 6.6 lists the peak magnitude of these

Table 6.5 Residues and observability factors from MASS

Signal	Residues	Observability
ΔI, line 33-40	-0.1483+j0.2297	0.5273
ΔI, line 40-44	-0.1615+j0.2416	0.5605
ΔI, line 44-45	-0.1755+j0.2638	0.6110
ΔI, line 43-46	-0.1511+j0.2315	0.5331
ΔI, line 1-6	-0.2946+j0.4611	1.0551
ΔI, line 2-6	-0.2878+j0.4515	1.0334
ΔI, line 61-63	-0.5211+j0.8180	1.8073
ΔI, line 63-66	-0.6045+j0.9447	2.6130

Table 6.6 Peak magnitude of transfer function between control input and reference signal

Line	Magnitude (p.u.)	Phase (degree)
33-40	20.27	79.76
40-44	21.48	79.16
44-45	22.25	79.75
43-46	19.72	82.07
1-6	42.47	83.70
2-6	41.70	83.70
61-63	69.88	80.51
63-66	81.28	80.44

responses at the frequency of the interarea mode (0.296Hz).

The line 63-66 current magnitude is then chosen as the input signal to the controller since it has the largest residue and observability factor from Table 6.5. The choice is also verified from the frequency response in Table 6.6, where the peak magnitude of the transfer function at interarea mode implies that this signal detects the interarea oscillation.

6.5.3 Error Signals and Weighting functions

The following procedure is followed to identify appropriate machine speeds to include in the error signal.

1. At the nominal operating point the dominant interarea modes are determined.

2. For the interarea modes, the mode shapes are determined. The machines are then grouped based on the real values of the mode shape. This process identifies the machines that oscillate against each other in the chosen interarea mode.

3. Participation factors are then determined for the selected interarea mode and the group of machines that participate strongly in the interarea mode are retained in the group obtained in Step 2. This results in a critical machine group consisting of the machines at Buses # 137, 139, 140, 145, 67, 93, 110, 89, 121, 98, 99, 124, 104, 111, 105, and 106. The error signal is then chosen to be the inertia weighted average of the speeds of these critical machines

4. The weighting functions used for the synthesis are

$$W_{e1} = \frac{0.2s + 20}{s + 2}, \; W_{e2} = 0.001$$

6.5.4 Controller Design and Reduction

After four steps of D-K iteration, a 274-order robust controller is obtained. The controller is then reduced using the Hankel norm reduction to a controller of order 14. The Bode plots of the full-order controller and the reduced-order controller are shown in Figure 6.18, which clearly indicates that the reduced-order controller retains the essential characteristics of the full-order controller.

Table 6.7 gives the comparison of RS and RP indicators for the full-order and reduced-order SDC. We can conclude that the closed-loop system with the reduced-order controller achieves both RS and RP.

The reduced-order SDC is then implemented in EPRI's MASS and ETMSP using the user-defined model (UDM) by two cascading blocks G_1 (8-order) and G_2 (6-order), as shown in Figure 6.19.

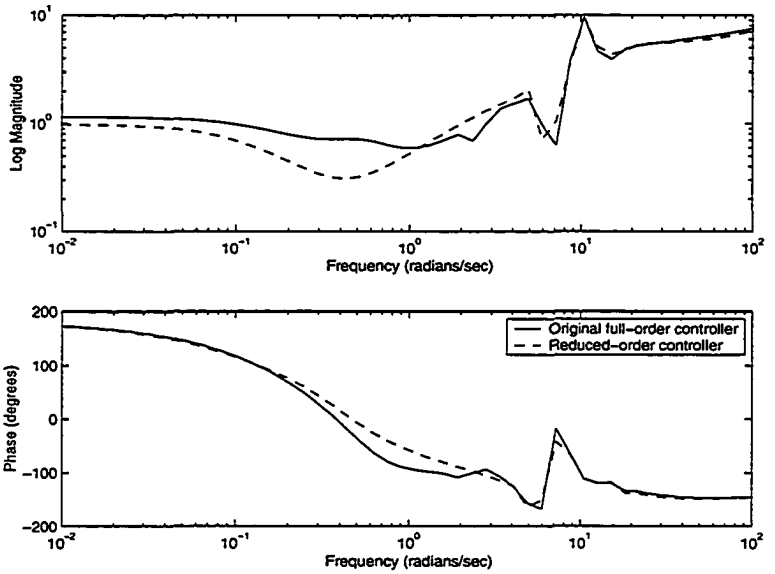

Figure 6.18 Bode plots comparison of full-order SDC and reduced-order SDC.

Table 6.7 Comparison of RS and RP

	Full-order SDC	Reduced-order SDC
μ_{RS}^{max}	0.354	0.436
μ_{RP}^{max}	0.877	0.892

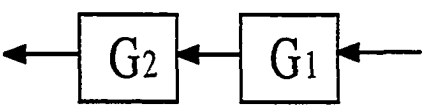

Figure 6.19 The cascading model for the reduced-order controller.

The state space representations of G_1 and G2 are as follows:

$$G_1 = \begin{bmatrix} A_1 & B_1 \\ C_1 & D_1 \end{bmatrix}$$

$$A_1 = \begin{bmatrix} -0.5441 & -12.9374 & 0.0000 & 0.0000 & 0.0000 & 0.0000 & 0.0000 & 0.0000 \\ 12.9374 & 0.0000 & 0.0000 & 0.0000 & 0.0000 & 0.0000 & 0.0000 & 0.0000 \\ 1.0369 & -7.2696 & -0.3097 & -10.1802 & 0.0000 & 0.0000 & 0.0000 & 0.0000 \\ 0.0000 & 0.0000 & 10.1802 & 0.0000 & 0.0000 & 0.0000 & 0.0000 & 0.0000 \\ 1.0369 & -7.2696 & 0.4986 & 6.3605 & -0.1230 & -11.1938 & 0.0000 & 0.0000 \\ 0.0000 & 0.0000 & 0.0000 & 0.0000 & 11.1938 & 0.0000 & 0.0000 & 0.0000 \\ 1.0369 & -7.2696 & 0.4986 & 6.3605 & -0.6998 & -7.7587 & -32.2674 & -0.3142 \\ 0.0000 & 0.0000 & 0.0000 & 0.0000 & 0.0000 & 0.0000 & 0.3142 & 0.0000 \end{bmatrix}$$

$$B_1 = [\ 1.0000 \quad 0.0000 \quad 1.0000 \quad 0.0000 \quad 1.0000 \quad 0.0000 \quad 1.0000 \quad 0.0000\ ]^T$$

$$C_1 = [\ -8.0740 \quad 56.6063 \quad -3.8826 \quad -49.5276 \quad 5.4494 \quad 60.4156 \quad 238.2364 \quad 1.7973\ ]$$

$$D_1 = -7.7868$$

$$G_2 = \begin{bmatrix} A_2 & B_2 \\ C_2 & D_2 \end{bmatrix}$$

$$A_2 = \begin{bmatrix} -0.4881 & -6.1728 & 0.0000 & 0.0000 & 0.0000 & 0.0000 \\ 6.1728 & 0.0000 & 0.0000 & 0.0000 & 0.0000 & 0.0000 \\ 0.0149 & 8.7026 & -0.4742 & -8.8568 & 0.0000 & 0.0000 \\ 0.0000 & 0.0000 & 8.8568 & 0.0000 & 0.0000 & 0.0000 \\ 0.0149 & 8.7026 & -0.3895 & 5.3409 & -0.0539 & -9.9787 \\ 0.0000 & 0.0000 & 0.0000 & 0.0000 & 9.9787 & 0.0000 \end{bmatrix}$$

$$B_1 = [\ 1.0000 \quad 0.0000 \quad 1.0000 \quad 0.0000 \quad 1.0000 \quad 0.0000\ ]^T$$

$$C_1 = [\ 0.0149 \quad 8.7026 \quad -0.3895 \quad 5.3408 \quad -0.0271 \quad 0.0058\ ]$$

$$D_1 = 1.0000$$

The performance of the SDC is then tested using MASS (frequency domain) and ETMSP (time domain, nonlinear simulation). The results are described as follows.

6.5.5 Interarea mode and Damping Ratio from MASS

At different operating conditions within the whole operating range, the eigenvalues of the linearized system are computed using MASS. The eigenvalue corresponding to the interarea mode and its damping ratio are given in Table 6.8. It can be seen from the table that SDC effectively damped the interarea mode by a large damping ratio over the whole range.

Table 6.8 Interarea mode and damping ratio for IEEE 50-generator system

Operating condition		Interarea mode	Damping ratio
$P_{G,93} = 1300$ MW	Without SDC	$-0.03145 \pm j1.883$	0.0167
	With SDC	$-0.2238 \pm j1.951$	0.1139
$P_{G,93} = 1400$ MW	Without SDC	$-0.01004 \pm j1.850$	0.0054
	With SDC	$-0.2320 \pm j1.917$	0.1202
$P_{G,93} = 1500$ MW	Without SDC	$0.0165 \pm j1.813$	-0.0091 (unstable)
	With SDC	$-0.2396 \pm j1.870$	0.1271

6.5.6 Damping characteristics of the supplementary controller subject to small faults

The system is subjected to a small disturbance which is a three-phase fault at Bus #33 lasting 10ms. At the end of the faulted period, the fault is removed without any change in topology. In order to verify the robustness of the controller, the disturbance is applied for three different operating conditions. These conditions are characterized by the output of the generators at Buses #93 and 110. The three different operating conditions are given below:

1. Low Operating Point: Generation at Buses #93 and 110 is 2600 MW

2. Nominal Operating Point: Generation at Buses #93 and 110 is 2800 MW

3. High Operating Point: Generation at Buses #93 and 110 is 3000 MW

The response of the system with the supplementary controller to the disturbance at these three operating conditions is shown in Figures 6.20—6.22.

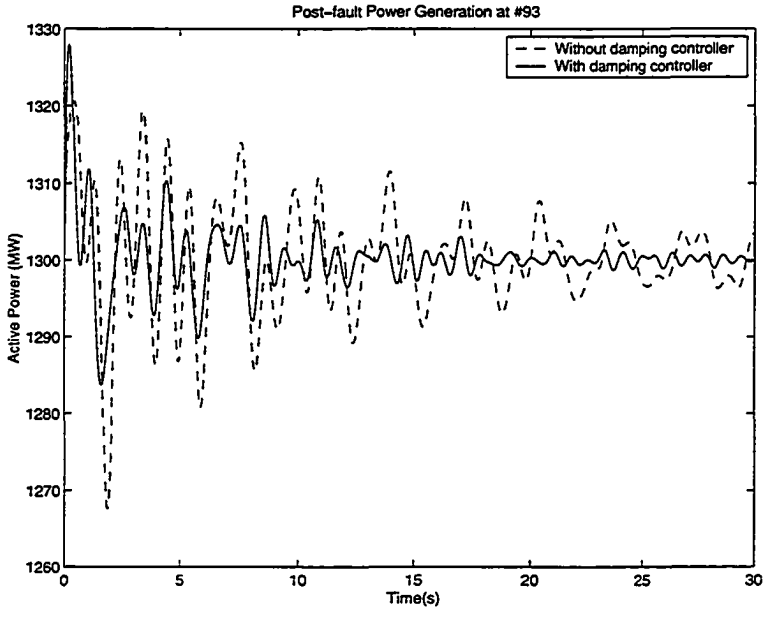

Figure 6.20 The time response of the active power generation at bus #93 (1300 MW) with and without SDC in the case of a large three phase ground fault at Bus #33.

The responses in Figures 6.20—6.22 indicate that the supplementary controller effectively damps the system oscillations. It should be noted from Figure 6.22 that the system would be unstable without the supplementary controller.

6.5.7 Damping Characteristics of the SDC subject to Large Faults

With the power generation of 2x1400MW at Buses #93 and #110 a three-phase ground fault is applied at Bus #2 at T=1s and then cleared in 6 cycles (0.1s) without changing system topology. The comparison of damping characteristics for this fault is given in Figure 6.23. Figure 6.23 again shows the efficacy of the SDC in mitigating the effects of large disturbances.

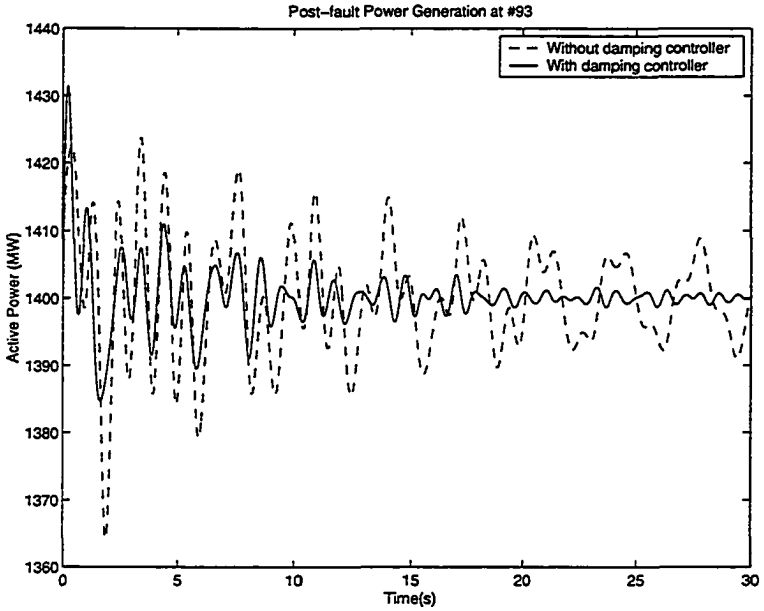

Figure 6.21 The time response of the active power generation at bus #93 (1400 MW) with and without SDC in the case of a large three phase ground fault at Bus #33.

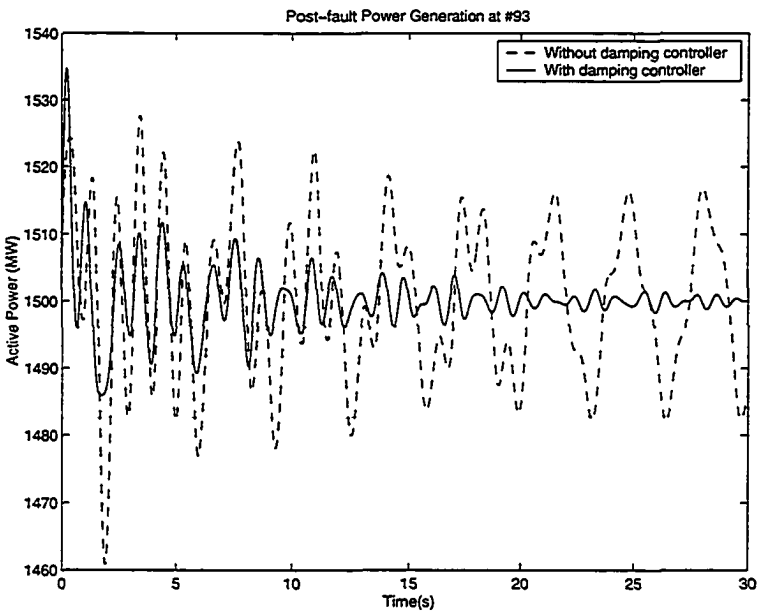

Figure 6.22 The time response of the active power generation at bus #93 (1500 MW) with and without SDC in the case of a large three phase ground fault at Bus #33.

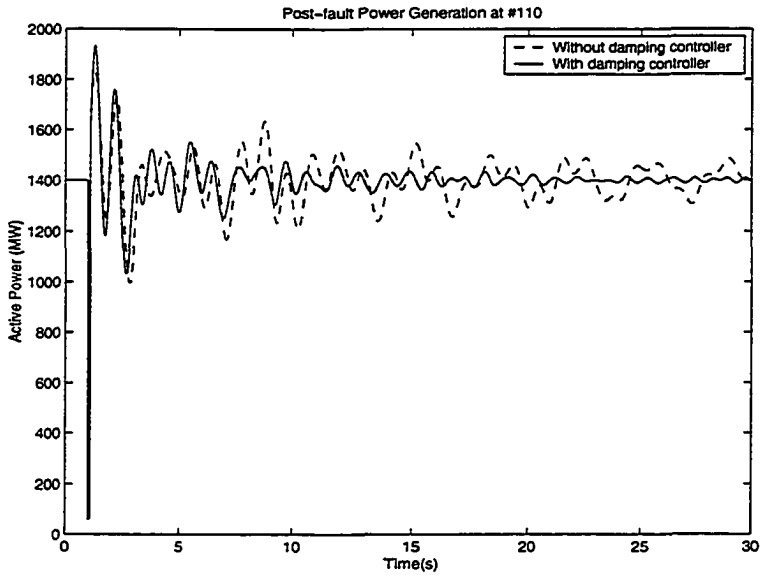

Figure 6.23 The time response of the active power generation at bus #110 with and without SDC in the case of a large three phase ground fault at Bus #2.

6.5.8 Transient Stability Test

A three-phase fault with fixed clearing time of 6 cycles is applied to different buses to verify the performance of the designed robust controller under transient conditions. The results are shown in Table 6.9. With the designed SDC, the system transient stability is enhanced in terms of the maximal power generation at Buses # 93 and #104 to keep the system stable after the fault.

Table 6.9 Comparison of critical power generation

Generator	Fault Location	Maximal Generation without SDC	Maximal Generation with SDC
#93	Bus #2	1475	1549
	Bus #7	1442	1493
	Bus #33	1481	1563
#104	Bus #2	2036	2105
	Bus #7	2025	2071
	Bus #33	2052	2119

7 CONCLUSIONS AND SUGGESTIONS FOR FUTURE WORK

7.1 General Summary

This research project investigates the application of the structured singular value (SSV or μ) to the robustness analysis and controller synthesis of static var compensators in power systems. The main work completed in this research includes:

1. Develop the linearized model of the power system with SVC included.

2. Model various operating conditions as parametric uncertainties, and capture these uncertainties by the polynomial approximation.

3. Formulate the general framework for the robust stability analysis with the tool of linear fractional transformation (LFT).

4. Apply the μ technique to analyze the robust stability of the power system under different operating conditions. Both the frequency sweep method and the state space μ test are used.

5. Establish the general criteria for the selection of SVC location, the input signal to the supplementary damping controller (SDC) of the SVC, and the error signals associated with the synthesis of the SDC.

6. Synthesize the SDC for the damping of interarea oscillation with the SVC. The performance of the SDC is tested in both the frequency domain and the time domain.

7.2 General Findings

The results in Chapter 5 and 6 lead to the following general findings:

1. The robustness analysis formulation used in this research can precisely characterize the parametric uncertainties in the power system and reduce the conservatism of the results. It can also be extended to any level of system modeling detail and can accommodate all types of uncertainties common in power systems.

2. The peak of the μ-plot from the frequency sweep test determines the robust stability of the power system. It also allows the direct calculation of simultaneous maximum values of varying parameters which still guarantee the system stability.

3. The state space μ test avoids the computationally expensive frequency sweep; The μ lower bound from the state space test provides good estimation of the exact μ peak and the critical frequency.

4. The frequency sweep test and the state space μ test can be combined to implement an intelligent frequency sweep, thereby saving computation time and still guaranteeing the accuracy of the μ.

5. The ideal location for the SVC should take into account the voltage support function of the SVC and the oscillation damping function of the supplementary controller. It can be determined by the bus participation factors and RS μ calculation.

6. The choice of the input signal can determined by the residues and observability factors from MASS program.

7. The error signals associated with the synthesis can be decided by the mode shape analysis and engineering judgement.

8. The resulting SDC from the μ-synthesis not only guarantees the robust stability of the power system, but also damps the interarea oscillations for a wide range of operating conditions.

7.3 Benefits to Electric Power Industry

The primary results from this research clearly demonstrate the efficacy of the structured singular value approach in analyzing and designing SVC controls for multimachine power systems. The research work provides the following benifits to the power industry:

1. A precise and effective tool to analyze the robust stability of the power system under different operating conditions.

2. A systematic approach to design the robust damping controller for the SVC to damp out the interarea oscillation while maintaining stability and performance requirement.

3. A general method to obtain effective designs for other FACTS based controls in power systems.

7.4 Suggested Future Work

In the future, the following issues should be addressed:

1. Efficient selection of the uncertain parameters. In large power systems with changing operating conditions, there is a potential to have a large number of independent uncertain variable. This would impose a severe computational burden on

the robustness analysis. Techniques need to be developed to make the selection tractable.

2. Development of more efficient techniques for the robustness calculations for large scale power systems. This would include reducing the size of the uncertainty block and refining the μ bounds with Branch and Bound technique in the state space μ test.

3. Control coordination with other control devices. Since SVC is normally used as an additional method to increase the damping of the interarea oscillation, its control should be coordinated with the power system stabilizers (PSSs) which are the main damping devices for the interarea oscillation.

4. Control designs of other FACTS devices to damp the interarea oscillations, for example, the thyristor-controlled series-capacitors (TSCSs).

5. Load modeling. It has been known that loads could affect the system damping due to the power-frequency characteristics of each specific load. The constant impedance model used in this research is not a true representation of the dynamic behavior of the loads, hence the control designs taking account of the load characteristics should be developed.

APPENDIX A DETAILS OF SYSTEM LINEARIZATION

We now derive the linearization of (4.32) and (4.44)

$$\dot{X} = f(X, Y, u) \tag{A.1}$$

$$0 = g(X, Y) \tag{A.2}$$

to form the state space representation of the system, as shown in (4.47).

For function f_{1i} from (4.33):

$$\begin{aligned} f_{1i} &= \dot{E}'_{qi} \\ &= \frac{1}{\tau'_{d0i}}[E_{FDi} - E'_{qi} + (x_{di} - x'_{di})I_{di}] \qquad i = 1, ..., m \end{aligned}$$

The partial derivatives of f_{i1} with respect to state variables and non-state variables are:

$$\frac{\partial f_{1i}}{\partial E'_{qj}} = \frac{1}{\tau'_{d0i}}[(x_{di} - x'_{di})\frac{\partial I_{di}}{\partial E'_{qj}} - \frac{\partial E'_{qi}}{\partial E'_{qj}}] \tag{A.3}$$

$$\frac{\partial f_{1i}}{\partial E'_{dj}} = \frac{1}{\tau'_{d0i}}(x_{di} - x'_{di})\frac{\partial I_{di}}{\partial E'_{dj}} \tag{A.4}$$

$$\frac{\partial f_{1i}}{\partial \delta_{k1}} = \frac{1}{\tau'_{d0i}}(x_{di} - x'_{di})\frac{\partial I_{di}}{\partial \delta_{k1}} \tag{A.5}$$

$$\frac{\partial f_{1i}}{\partial E_{FDi}} = \frac{1}{\tau'_{d0i}} \tag{A.6}$$

$$\frac{\partial f_{1i}}{\partial V_{n+1}} = \frac{1}{\tau'_{d0i}}(x_{di} - x'_{di})\frac{\partial I_{di}}{\partial V_{n+1}} \tag{A.7}$$

$$\frac{\partial f_{1i}}{\partial \theta_{n+1}} = \frac{1}{\tau'_{d0i}}(x_{di} - x'_{di})\frac{\partial I_{di}}{\partial \theta_{n+1}} \tag{A.8}$$

$$i,\ j = 1, ..., m \qquad k = 2, ..., n$$

where

$$\frac{\partial E'_{qi}}{\partial E'_{qj}} = \begin{cases} 1 & \text{for } i = j \\ 0 & \text{otherwise} \end{cases} \tag{A.9}$$

For function f_{2i} from (4.34):

$$\begin{aligned} f_{2i} &= \dot{E}'_{di} \\ &= \frac{1}{\tau'_{q0i}}[-E'_{di} - (x_{qi} - x'_{qi})I_{qi}] \qquad i = 1, ..., m \end{aligned}$$

The partial derivatives are:

$$\frac{\partial f_{2i}}{\partial E'_{qj}} = \frac{-1}{\tau'_{q0i}}(x_{qi} - x'_{qi})\frac{\partial I_{qi}}{\partial E'_{qj}} \tag{A.10}$$

$$\frac{\partial f_{2i}}{\partial E'_{dj}} = \frac{-1}{\tau'_{q0i}}[(x_{qi} - x'_{qi})\frac{\partial I_{qi}}{\partial E'_{dj}} + \frac{\partial E'_{di}}{\partial E'_{dj}}] \tag{A.11}$$

$$\frac{\partial f_{2i}}{\partial \delta_{k1}} = \frac{-1}{\tau'_{q0i}}(x_{qi} - x'_{qi})\frac{\partial I_{qi}}{\partial \delta_{k1}} \tag{A.12}$$

$$\frac{\partial f_{2i}}{\partial V_{n+1}} = \frac{-1}{\tau'_{q0i}}(x_{qi} - x'_{qi})\frac{\partial I_{qi}}{\partial V_{n+1}} \tag{A.13}$$

$$\frac{\partial f_{2i}}{\partial \theta_{n+1}} = \frac{-1}{\tau'_{q0i}}(x_{qi} - x'_{qi})\frac{\partial I_{qi}}{\partial \theta_{n+1}} \tag{A.14}$$

$$i,\ j = 1, ..., m \qquad k = 2, ..., n$$

where

$$\frac{\partial E'_{di}}{\partial E'_{dj}} = \begin{cases} 1 & \text{for } i = j \\ 0 & \text{otherwise} \end{cases} \tag{A.15}$$

For function f_{3i} from (4.35):

$$\begin{aligned} f_{3i} &= \dot{\omega}_i \qquad i = 1, ..., n \\ &= \frac{1}{M_i}[P_{mi} - (I_{di}E'_{di} + I_{qi}E'_{qi}) + (x'_{qi} - x'_{di})I_{qi}I_{di} - D_i(\omega_i - \omega_S)] \end{aligned}$$

The partial derivatives are:

$$\begin{aligned} \frac{\partial f_{3i}}{\partial E'_{qj}} &= -\frac{1}{M_i}(\frac{\partial I_{di}}{\partial E'_{qj}}E'_{di} + \frac{\partial I_{qi}}{\partial E'_{qj}}E'_{qi} + \frac{\partial E'_{qi}}{\partial E'_{qj}}I_{qi}) \\ &\quad + \frac{1}{M_i}(\frac{\partial I_{di}}{\partial E'_{qj}}I_{qi} + \frac{\partial I_{qi}}{\partial E'_{qj}}I_{di})(x'_{qi} - x'_{di}) \end{aligned} \tag{A.16}$$

$$\frac{\partial f_{3i}}{\partial E'_{dj}} = -\frac{1}{M_i}\left(\frac{\partial I_{di}}{\partial E'_{dj}}E'_{di} + \frac{\partial E'_{di}}{\partial E'_{dj}}I_{di} + \frac{\partial I_{qi}}{\partial E'_{dj}}E'_{qi}\right) + \frac{1}{M}\left(\frac{\partial I_{di}}{\partial E'_{dj}}I_{qi} + \frac{\partial I_{qi}}{\partial E'_{dj}}I_{di}\right)(x'_{qi} - x'_{di}) \tag{A.17}$$

$$\frac{\partial f_{3i}}{\partial \delta_{k1}} = -\frac{1}{M_i}\left(\frac{\partial I_{di}}{\partial \delta_{k1}}E'_{di} + \frac{\partial I_{qi}}{\partial \delta_{k1}}E'_{qi}\right) + \frac{1}{M_i}\left(\frac{\partial I_{di}}{\partial \delta_{k1}}I_{qi} + \frac{\partial I_{qi}}{\partial \delta_{k1}}I_{di}\right)(x'_{qi} - x'_{di}) \tag{A.18}$$

$$\frac{\partial f_{3i}}{\omega_i} = -\frac{D_i}{M_i} \tag{A.19}$$

$$\frac{\partial f_{3i}}{\partial V_{n+1}} = -\frac{1}{M_i}\left(\frac{\partial I_{di}}{\partial V_{n+1}}E'_{di} + \frac{\partial I_{qi}}{\partial V_{n+1}}E'_{qi}\right) + \frac{1}{M_i}\left(\frac{\partial I_{di}}{\partial V_{n+1}}I_{qi} + \frac{\partial I_{qi}}{\partial V'_{n+1}}I_{di}\right)(x'_{qi} - x'_{di}) \tag{A.20}$$

$$\frac{\partial f_{3i}}{\partial \theta_{n+1}} = -\frac{1}{M_i}\left(\frac{\partial I_{di}}{\partial \theta_{n+1}}E'_{di} + \frac{\partial I_{qi}}{\partial \theta_{n+1}}E'_{qi}\right) + \frac{1}{M_i}\left(\frac{\partial I_{di}}{\partial \theta_{n+1}}I_{qi} + \frac{\partial I_{qi}}{\partial \theta'_{n+1}}I_{di}\right)(x'_{qi} - x'_{di}) \tag{A.21}$$

$$i = 1, ..., n \qquad j = 1, ..., m \qquad k = 2, ..., n$$

For function f_{4i} from (4.36):

$$f_{4i} = \dot{\delta}_{i1} = \omega_i - \omega_1 \qquad i = 2, ..., n$$

The partial derivatives are:

$$\frac{\partial f_{4i}}{\partial \omega_j} = \begin{cases} -1 & \text{for } j = 1 \\ 1 & \text{for } j = i, j \neq 1 \\ 0 & \text{otherwise} \end{cases} \tag{A.22}$$

$$i = 2, ..., n \qquad j = 1, ..., n$$

For function f_{5i} from (4.37):

$$f_{5i} = \dot{E}_{FDi} = \frac{K_{Ai}}{T_{Ai}}X_{E2i} - \frac{1}{T_{Ai}}E_{FDi} + \frac{aK_{Ai}}{T_{Ai}}(V_{REFi} - X_{E1i}) \qquad i = 1, ..., m$$

The partial derivatives are:

$$\frac{\partial f_{5i}}{\partial E_{FDi}} = -\frac{1}{T_{Ai}} \tag{A.23}$$

$$\frac{\partial f_{5i}}{\partial X_{E1i}} = -\frac{aK_{Ai}}{T_{Ai}} \tag{A.24}$$

$$\frac{\partial f_{5i}}{\partial X_{E2i}} = \frac{K_{Ai}}{T_{Ai}} \tag{A.25}$$

$$\frac{\partial f_{5i}}{\partial V_{REFi}} = \frac{aK_{Ai}}{T_{Ai}} \tag{A.26}$$

$$i = 1, ..., m$$

For function f_{6i} from (4.38):

$$\begin{aligned} f_{6i} &= \dot{X}_{E1i} \\ &= -\frac{1}{T_{Ri}} X_{E1i} + \frac{1}{T_{Ri}} V_{Ti} \qquad i = 1, ..., m \end{aligned}$$

The partial derivatives are:

$$\frac{\partial f_{6i}}{\partial E'_{qj}} = \frac{1}{T_{Ri}} \frac{\partial V_{Ti}}{\partial E'_{qj}} \tag{A.27}$$

$$\frac{\partial f_{6i}}{\partial E'_{dj}} = \frac{1}{T_{Ri}} \frac{\partial V_{Ti}}{\partial E'_{dj}} \tag{A.28}$$

$$\frac{\partial f_{6i}}{\partial \delta_{k1}} = \frac{1}{T_{Ri}} \frac{\partial V_{Ti}}{\partial \delta_{k1}} \tag{A.29}$$

$$\frac{\partial f_{6i}}{\partial X_{E1i}} = -\frac{1}{T_{Ri}} \tag{A.30}$$

$$\frac{\partial f_{6i}}{\partial V_{n+1}} = \frac{1}{T_{Ri}} \frac{\partial V_{Ti}}{\partial V_{n+1}} \tag{A.31}$$

$$\frac{\partial f_{6i}}{\partial \theta_{n+1}} = \frac{1}{T_{Ri}} \frac{\partial V_{Ti}}{\partial \theta_{n+1}} \tag{A.32}$$

$$i,\ j = 1, ..., m \qquad k = 2, ..., n$$

For function f_{7i} from (4.39):

$$\begin{aligned} f_{7i} &= \dot{X}_{E2i} \\ &= -\frac{1}{T_{Bi}} X_{E2i} + \frac{1-a}{T_{Bi}} (V_{REFi} - X_{E1i}) \qquad i = 1, ..., m \end{aligned}$$

The partial derivatives are:

$$\frac{\partial f_{7i}}{\partial X_{E1i}} = \frac{a-1}{T_{Bi}} \tag{A.33}$$

$$\frac{\partial f_{7i}}{\partial X_{E2i}} = -\frac{1}{T_{Bi}} \tag{A.34}$$

$$\frac{\partial f_{7i}}{\partial V_{REFi}} = \frac{1-a}{T_{Bi}} \tag{A.35}$$

$$i = 1, ..., m$$

For function f_8 from (4.40):

$$\begin{aligned} f_8 &= \dot{X}_{S1} \\ &= -\frac{1}{T_3} X_{S1} + \frac{(1-a_1)K}{T_3}(V_{n+1} - V_{REF,SVC}) \end{aligned}$$

The partial derivatives are:

$$\frac{\partial f_8}{\partial X_{S1}} = -\frac{1}{T_3} \tag{A.36}$$

$$\frac{\partial f_8}{\partial V_{n+1}} = \frac{(1-a_1)K}{T_3} \tag{A.37}$$

$$\frac{\partial f_8}{\partial V_{REF,SVC}} = \frac{(a_1-1)K}{T_3} \tag{A.38}$$

For function f_9 from (4.41):

$$\begin{aligned} f_9 &= \dot{X}_{S2} \\ &= \frac{1-a_2}{T_4} X_{S1} - \frac{1}{T_4} X_{S2} + \frac{(1-a_2)a_1K}{T_4}(V_{n+1} - V_{REF,SVC}) \end{aligned}$$

The partial derivatives are:

$$\frac{\partial f_9}{\partial X_{S1}} = \frac{1-a_2}{T_4} \tag{A.39}$$

$$\frac{\partial f_9}{\partial X_{S2}} = -\frac{1}{T_4} \tag{A.40}$$

$$\frac{\partial f_9}{\partial V_{n+1}} = \frac{(1-a_2)a_1K}{T_4} \tag{A.41}$$

$$\frac{\partial f_9}{\partial V_{REF,SVC}} = \frac{(a_2-1)a_1K}{T_4} \tag{A.42}$$

For function f_{10} from (4.42):

$$\begin{aligned} f_{10} &= \dot{B}_{SVC} \\ &= \frac{a_2}{T_5}X_{S1} + \frac{1}{T_5}(X_{S2} - B_{SVC}) + \frac{a_1 a_2 K}{T_5}(V_{n+1} - V_{REF,SVC}) \end{aligned}$$

The partial derivatives are:

$$\frac{\partial f_{10}}{\partial X_{S1}} = \frac{a_2}{T_5} \tag{A.43}$$

$$\frac{\partial f_{10}}{\partial X_{S2}} = \frac{1}{T_5} \tag{A.44}$$

$$\frac{\partial f_{10}}{\partial B_{SVC}} = -\frac{1}{T_5} \tag{A.45}$$

$$\frac{\partial f_{10}}{\partial V_{n+1}} = \frac{a_1 a_2 K}{T_5} \tag{A.46}$$

$$\frac{\partial f_{10}}{\partial V_{REF,SVC}} = -\frac{a_1 a_2 K}{T_5} \tag{A.47}$$

Some derivatives on the right sides of (A.3) — (A.47) are still unknown. From (4.17) and (4.18), we have

$$I_{qi} = \sum_{j=1}^{m}[F_{G+B}(\delta_{ij})E'_{qj} - F_{B-G}(\delta_{ij})E'_{dj}] + \sum_{k=m+1}^{n} F_{G+B}(\delta_{ik})E_k + F_{G+B}(\delta_{i,n+1})V_{n+1}$$

$$I_{di} = \sum_{j=1}^{m}[F_{B-G}(\delta_{ij})E'_{qj} + F_{G+B}(\delta_{ij})E'_{dj}] + \sum_{k=m+1}^{n} F_{B-G}(\delta_{ik})E_k + F_{B-G}(\delta_{i,n+1})V_{n+1}$$

$$I_k = \sum_{j=1}^{m}[F_{G+B}(\delta_{kj})E'_{qj} - F_{B-G}(\delta_{kj})E'_{dj}] + \sum_{l=m+1}^{n} F_{G+B}(\delta_{kl})E_l + F_{G+B}(\delta_{k,n+1})V_{n+1}$$

$$i = 1, 2, ..., m \qquad k, l = m+1, ..., n$$

Therefore

$$\frac{\partial I_{qi}}{\partial E'_{qj}} = F_{G+B}(\delta_{ij}) \qquad i = 1, ..., n \quad j = 1, ..., m \tag{A.48}$$

$$\frac{\partial I_{qi}}{\partial E'_{dj}} = -F_{B-G}(\delta_{ij}) \qquad i = 1, ..., n \quad j = 1, ..., m \tag{A.49}$$

$$\frac{\partial I_{qi}}{\partial \delta_{k1}} = \sum_{j=1}^{n} \frac{\partial \delta_{ij}}{\partial \delta_{k1}}[F_{B-G}(\delta_{ij})E'_{qj} + F_{G+B}(\delta_{ij})E'_{dj}]$$

$$i, j = 1, ..., n \qquad k = 2, ..., n \tag{A.50}$$

$$\frac{\partial I_{qi}}{\partial V_{n+1}} = F_{G+B}(\delta_{i,n+1}) \qquad i=1,...,n \tag{A.51}$$

$$\frac{\partial I_{qi}}{\partial \theta_{n+1}} = -F_{B-G}(\delta_{i,n+1})V_{n+1} \qquad i=1,...,n \tag{A.52}$$

$$\frac{\partial I_{di}}{\partial E'_{qj}} = F_{B-G}(\delta_{ij}) \qquad i,j=1,...,m \tag{A.53}$$

$$\frac{\partial I_{di}}{\partial E'_{dj}} = F_{G+B}(\delta_{ij}) \qquad i,j=1,...,m \tag{A.54}$$

$$\frac{\partial I_{di}}{\partial \delta_{k1}} = \sum_{j=1}^{n} \frac{\partial \delta_{ij}}{\partial \delta_{k1}}[-F_{G+B}(\delta_{ij})E'_{qj} + F_{B-G}(\delta_{ij})E'_{dj}]$$
$$i,j=1,...,m \qquad k=2,...,n \tag{A.55}$$

$$\frac{\partial I_{di}}{\partial V_{n+1}} = F_{B-G}(\delta_{i,n+1}) \qquad i=1,...,m \tag{A.56}$$

$$\frac{\partial I_{di}}{\partial \theta_{n+1}} = F_{G+B}(\delta_{i,n+1})V_{n+1} \qquad i=1,...,m \tag{A.57}$$

where

$$\frac{\partial \delta_{ij}}{\partial \delta_{k1}} = \begin{cases} 1 & \text{for } i=k, i\neq j \\ -1 & \text{for } j=k, j\neq i \\ 0 & \text{otherwise} \end{cases} \tag{A.58}$$

For the exciter input voltage V_T:

$$\begin{aligned} V_T^2 &= V_{Tq}^2 + V_{Td}^2 \\ &= (E'_q + x'_d I_d)^2 + (E'_d - x'_q I_q)^2 \end{aligned} \tag{A.59}$$

Therefore,

$$\frac{\partial V_{Ti}}{\partial E'_{qj}} = \frac{1}{V_{Ti}}[V_{qi}(\frac{\partial E'_{qi}}{\partial E'_{qj}} + x'_{di}\frac{\partial I_{di}}{\partial E'_{qj}}) - V_{di}x'_{qi}\frac{\partial I_{qi}}{\partial E'_{qj}}] \tag{A.60}$$

$$\frac{\partial V_{Ti}}{\partial E'_{dj}} = \frac{1}{V_{Ti}}[V_{di}(\frac{\partial E'_{di}}{\partial E'_{dj}} - x'_{qi}\frac{\partial I_{qi}}{\partial E'_{dj}}) + V_{qi}x'_{qi}\frac{\partial I_{di}}{\partial E'_{dj}}] \tag{A.61}$$

$$\frac{\partial V_{Ti}}{\partial \delta_{k1}} = \frac{1}{V_{Ti}}(V_{qi}x'_{di}\frac{\partial I_{di}}{\partial \delta_{k1}} - V_{di}x'_{qi}\frac{\partial I_{qi}}{\partial \delta_{k1}}) \tag{A.62}$$

$$\frac{\partial V_{Ti}}{\partial V_{n+1}} = \frac{V_{qi}}{V_{Ti}}\frac{\partial I_{di}}{\partial V_{n+1}}x'_{di} - \frac{V_{di}}{V_{Ti}}\frac{\partial I_{qi}}{\partial V_{n+1}}x'_{qi} \tag{A.63}$$

$$\frac{\partial V_{Ti}}{\partial \theta_{n+1}} = \frac{V_{qi}}{V_{Ti}}\frac{\partial I_{di}}{\partial \theta_{n+1}}x'_{di} - \frac{V_{di}}{V_{Ti}}\frac{\partial I_{qi}}{\partial \theta_{n+1}}x'_{qi} \tag{A.64}$$
$$i,j=1,...,m$$

Substituting (A.48)—(A.64) into (A.3) — (A.47), we can write the linearized equation of (A.1) as follows:

$$
\begin{bmatrix} \Delta\dot{E}'_{qj} \\ \Delta\dot{E}'_{dj} \\ \Delta\dot{\omega}_i \\ \Delta\dot{\delta}_{k1} \\ \Delta\dot{E}_{FDi} \\ \Delta\dot{X}_{E1i} \\ \Delta\dot{X}_{E2i} \\ \Delta\dot{X}_{S1} \\ \Delta\dot{X}_{S2} \\ \Delta\dot{B}_{SVC} \end{bmatrix} =
\begin{bmatrix}
\frac{\partial f_{1i}}{\partial V_{n+1}} & \frac{\partial f_{1i}}{\partial \theta_{n+1}} \\
\frac{\partial f_{2i}}{\partial V_{n+1}} & \frac{\partial f_{2i}}{\partial \theta_{n+1}} \\
\frac{\partial f_{3i}}{\partial V_{n+1}} & \frac{\partial f_{3i}}{\partial \theta_{n+1}} \\
0 & 0 \\
0 & 0 \\
\frac{\partial f_{6i}}{\partial V_{n+1}} & \frac{\partial f_{6i}}{\partial \theta_{n+1}} \\
0 & 0 \\
\frac{\partial f_8}{\partial V_{n+1}} & 0 \\
\frac{\partial f_9}{\partial V_{n+1}} & 0 \\
\frac{\partial f_{10}}{\partial V_{n+1}} & 0
\end{bmatrix}
\begin{bmatrix} \Delta V_{n+1} \\ \Delta\theta_{n+1} \end{bmatrix} +
\begin{bmatrix}
0 & 0 \\
0 & 0 \\
0 & 0 \\
0 & 0 \\
\frac{\partial f_{5i}}{\partial V_{REFi}} & 0 \\
0 & 0 \\
\frac{\partial f_{7i}}{\partial V_{REFi}} & 0 \\
0 & \frac{\partial f_8}{\partial V_{REF,SVC}} \\
0 & \frac{\partial f_9}{\partial V_{REF,SVC}} \\
0 & \frac{\partial f_{10}}{\partial V_{REF,SVC}}
\end{bmatrix}
\begin{bmatrix} \Delta V_{REFi} \\ \Delta V_{REF,SVC} \end{bmatrix}
$$

$$
+
\begin{bmatrix}
\frac{\partial f_{1i}}{\partial E'_{qj}} & \frac{\partial f_{1i}}{\partial E'_{dj}} & 0 & \frac{\partial f_{1i}}{\partial \delta_{k1}} & \frac{\partial f_{1i}}{\partial E_{FDi}} & 0 & 0 & 0 & 0 & 0 \\
\frac{\partial f_{2i}}{\partial E'_{qj}} & \frac{\partial f_{2i}}{\partial E'_{dj}} & 0 & \frac{\partial f_{2i}}{\partial \delta_{k1}} & 0 & 0 & 0 & 0 & 0 & 0 \\
\frac{\partial f_{3i}}{\partial E'_{qj}} & \frac{\partial f_{3i}}{\partial E'_{dj}} & \frac{\partial f_{3i}}{\partial \omega_i} & \frac{\partial f_{3i}}{\partial \delta_{k1}} & 0 & 0 & 0 & 0 & 0 & 0 \\
0 & 0 & \frac{\partial f_{4i}}{\partial \omega_i} & 0 & 0 & 0 & 0 & 0 & 0 & 0 \\
0 & 0 & 0 & 0 & \frac{\partial f_{5i}}{\partial E_{FDi}} & \frac{\partial f_{5i}}{\partial X_{E1i}} & \frac{\partial f_{5i}}{\partial X_{E2i}} & 0 & 0 & 0 \\
\frac{\partial f_{6i}}{\partial E'_{qj}} & \frac{\partial f_{6i}}{\partial E'_{dj}} & 0 & \frac{\partial f_{6i}}{\partial \delta_{k1}} & 0 & \frac{\partial f_{6i}}{\partial X_{E1i}} & 0 & 0 & 0 & 0 \\
0 & 0 & 0 & 0 & 0 & \frac{\partial f_{7i}}{\partial X_{E1i}} & \frac{\partial f_{7i}}{\partial X_{E2i}} & 0 & 0 & 0 \\
0 & 0 & 0 & 0 & 0 & 0 & 0 & \frac{\partial f_8}{\partial X_{S1}} & 0 & 0 \\
0 & 0 & 0 & 0 & 0 & 0 & 0 & \frac{\partial f_9}{\partial X_{S1}} & \frac{\partial f_9}{\partial X_{S2}} & 0 \\
0 & 0 & 0 & 0 & 0 & 0 & 0 & \frac{\partial f_{10}}{\partial X_{S1}} & \frac{\partial f_{10}}{\partial X_{S2}} & \frac{\partial f_{10}}{\partial B_{SVC}}
\end{bmatrix}
\begin{bmatrix} \Delta E'_{qj} \\ \Delta E'_{dj} \\ \Delta\omega_i \\ \Delta\delta_{k1} \\ \Delta E_{FDi} \\ \Delta X_{E1i} \\ \Delta X_{E2i} \\ \Delta X_{S1} \\ \Delta X_{S2} \\ \Delta B_{SVC} \end{bmatrix}
$$

The above equation corresponds to (4.43).

For the algebraic equations (4.30) and (4.31):

$$
\begin{aligned}
g_1 &= 0 \\
&= \sum_{i=1}^{m} [F_{G+B}(\delta_{n+1,i}) E'_{qi} - F_{B-G}(\delta_{n+1,i}) E'_{di}]
\end{aligned}
$$

$$+ \sum_{i=m+1}^{n} [F_{G+B}(\delta_{n+1,i})E_i] + G_{n+1,n+1}V_{n+1} \tag{A.65}$$

$$\begin{aligned} g_2 &= 0 \\ &= \sum_{i=1}^{m}[F_{G+B}(\delta_{n+1,i})E'_{di} + F_{B-G}(\delta_{n+1,i})E'_{qi}] \\ &\quad + \sum_{i=m+1}^{n} [F_{B-G}(\delta_{n+1,i})E_i] + (B_{n+1,n+1} - B_{SVC})V_{n+1} \end{aligned} \tag{A.66}$$

We have the partial derivatives of g_1 and g_2 with respect to state variables (X) and non-state variables (Y) as follows:

$$\frac{\partial g_1}{\partial E'_{qi}} = F_{G+B}(\delta_{n+1}, i) \qquad i = 1, ..., m \tag{A.67}$$

$$\frac{\partial g_1}{\partial E'_{di}} = -F_{B-G}(\delta_{n+1}, i) \qquad i = 1, ..., m \tag{A.68}$$

$$\begin{aligned} \frac{\partial g_1}{\partial \delta_{k1}} &= \sum_{i=1}^{m} \frac{\partial \delta_{n+1,i}}{\partial \delta_{k,1}}[F_{B-G}(\delta_{n+1,i})E'_{qi} + F_{G+B}(\delta_{n+1,i})E'_{di}] \\ &\quad + \sum_{i=m+1}^{n} \frac{\partial \delta_{n+1,i}}{\partial \delta_{k,1}}[F_{B-G}(\delta_{n+1,i})E_i] \qquad k = 2, ..., n \end{aligned} \tag{A.69}$$

$$\frac{\partial g_1}{\partial V_{n+1}} = G_{n+1,n+1} \tag{A.70}$$

$$\begin{aligned} \frac{\partial g_1}{\partial \theta_{n+1}} &= \sum_{i=1}^{m}[F_{B-G}(\delta_{n+1,i})E'_{qi} + F_{G+B}(\delta_{n+1,i})E'_{di}] \\ &\quad + \sum_{i=m+1}^{n} [F_{B-G}(\delta_{n+1,i})E_i] \end{aligned} \tag{A.71}$$

where

$$\frac{\partial \delta_{n+1,i}}{\partial \delta_{k1}} = \begin{cases} -1 & i = k, k = 2, ..., n \\ 0 & \text{otherwise} \end{cases} \tag{A.72}$$

And

$$\frac{\partial g_2}{\partial E'_{qi}} = F_{B-G}(\delta_{n+1}, i) \qquad i = 1, ..., m \tag{A.73}$$

$$\frac{\partial g_2}{\partial E'_{di}} = F_{G+B}(\delta_{n+1}, i) \qquad i = 1, ..., m \tag{A.74}$$

$$\begin{aligned} \frac{\partial g_2}{\partial \delta_{k1}} &= \sum_{i=1}^{m} \frac{\partial \delta_{n+1,i}}{\partial \delta_{k1}}[F_{B-G}(\delta_{n+1,i})E'_{di} - F_{G+B}(\delta_{n+1,i})E'_{qi}] \\ &\quad - \sum_{i=m+1}^{n} \frac{\partial \delta_{n+1,i}}{\partial \delta_{k1}}[F_{G+B}(\delta_{n+1,i})E_i] \qquad k = 2, ..., n \end{aligned} \tag{A.75}$$

$$\frac{\partial g_2}{\partial B_{SVC}} = -V_{n+1} \tag{A.76}$$

$$\frac{\partial g_2}{\partial V_{n+1}} = B_{n+1,n+1} - B_{SVC} \tag{A.77}$$

$$\frac{\partial g_2}{\partial \theta_{n+1}} = \sum_{i=1}^{m}[F_{B-G}(\delta_{n+1,i})E'_{di} - F_{G+B}(\delta_{n+1,i})E'_{qi}] - \sum_{i=m+1}^{n}[F_{G+B}(\delta_{n+1,i})E_i] \tag{A.78}$$

Therefore, the matrices of the partial derivatives $\frac{\partial g}{\partial X}$ and $\frac{\partial g}{\partial Y}$ in (4.45) are obtained. Hence the A and B matrices in (4.48) and (4.49) can be calculated directly.

APPENDIX B PARTIAL DERIVATIVES OF CURRENTS AT LOAD BUSES

Here we derive the partial derivatives used in (6.20)—(6.23).

For (6.20), we have

$$\frac{\partial f_1}{\partial E'_{qi}} = G_{n+2,i}\cos\delta_i - B_{n+2,i}\sin\delta_i \tag{B.1}$$

$$\frac{\partial f_1}{\partial E'_{di}} = -G_{n+2,i}\sin\delta_i - B_{n+2,i}\cos\delta_i \tag{B.2}$$

$$\frac{\partial f_1}{\partial \delta_{k1}} = E'_{qk}\frac{\partial f_1}{\partial E'_{dk}} - E'_{dk}\frac{\partial f_1}{\partial E'_{qk}} \qquad k = 2,3,...,m \tag{B.3}$$

$$\frac{\partial f_1}{\partial \delta_{k1}} = E_k(-G_{n+2,k}\sin\delta_k - B_{n+2,k}\cos\delta_k) \qquad k = m+1,...,n \tag{B.4}$$

$$\frac{\partial f_1}{\partial V_{n+1}} = G_{n+2,n+1}\cos\theta_{n+1} - B_{n+2,n+1}\sin\theta_{n+1} \tag{B.5}$$

$$\frac{\partial f_1}{\partial \theta_{n+1}} = V_{n+1}(-G_{n+2,n+1}\sin\theta_{n+1} - B_{n+2,n+1}\cos\theta_{n+1}) \tag{B.6}$$

$$\frac{\partial f_1}{\partial V_{n+2}} = G_{n+2,n+2}\cos\theta_{n+2} - B_{n+2,n+2}\sin\theta_{n+2} \tag{B.7}$$

$$\frac{\partial f_1}{\partial \theta_{n+2}} = V_{n+2}(-G_{n+2,n+2}\sin\theta_{n+2} - B_{n+2,n+2}\cos\theta_{n+2}) \tag{B.8}$$

$$\frac{\partial f_1}{\partial V_{n+3}} = G_{n+2,n+3}\cos\theta_{n+3} - B_{n+2,n+3}\sin\theta_{n+3} \tag{B.9}$$

$$\frac{\partial f_1}{\partial \theta_{n+3}} = V_{n+3}(-G_{n+2,n+3}\sin\theta_{n+3} - B_{n+2,n+3}\cos\theta_{n+3}) \tag{B.10}$$

For (6.21), we have

$$\frac{\partial f_2}{\partial E'_{qi}} = G_{n+2,i}\sin\delta_i + B_{n+2,i}\cos\delta_i = -\frac{\partial f_1}{\partial E'_{di}} \tag{B.11}$$

$$\frac{\partial f_2}{\partial E'_{di}} = G_{n+2,i}\cos\delta_i - B_{n+2,i}\sin\delta_i = \frac{\partial f_1}{\partial E'_{qi}} \tag{B.12}$$

$$\frac{\partial f_2}{\partial \delta_{k1}} = E'_{qk}\frac{\partial f_2}{\partial E'_{dk}} - E'_{dk}\frac{\partial f_2}{\partial E'_{qk}} \qquad k = 2, 3, ..., m \tag{B.13}$$

$$\frac{\partial f_2}{\partial \delta_{k1}} = E_k(G_{n+2,k}\cos\delta_k - B_{n+2,k}\sin\delta_k) \qquad k = m+1, ..., n \tag{B.14}$$

$$\frac{\partial f_2}{\partial V_{n+1}} = -\frac{1}{V_{n+1}}\frac{\partial f_1}{\partial \theta_{n+1}} \tag{B.15}$$

$$\frac{\partial f_2}{\partial \theta_{n+1}} = V_{n+1}\frac{\partial f_1}{\partial V_{n+1}} \tag{B.16}$$

$$\frac{\partial f_2}{\partial V_{n+2}} = -\frac{1}{V_{n+2}}\frac{\partial f_1}{\partial \theta_{n+2}} \tag{B.17}$$

$$\frac{\partial f_2}{\partial \theta_{n+2}} = V_{n+2}\frac{\partial f_1}{\partial V_{n+2}} \tag{B.18}$$

$$\frac{\partial f_2}{\partial V_{n+3}} = -\frac{1}{V_{n+3}}\frac{\partial f_1}{\partial \theta_{n+3}} \tag{B.19}$$

$$\frac{\partial f_2}{\partial \theta_{n+3}} = V_{n+3}\frac{\partial f_1}{\partial V_{n+3}} \tag{B.20}$$

For (6.22), we have

$$\frac{\partial f_3}{\partial E'_{qi}} = G_{n+3,i}\cos\delta_i - B_{n+3,i}\sin\delta_i \tag{B.21}$$

$$\frac{\partial f_3}{\partial E'_{di}} = -G_{n+3,i}\sin\delta_i - B_{n+3,i}\cos\delta_i \tag{B.22}$$

$$\frac{\partial f_3}{\partial \delta_{k1}} = E'_{qk}\frac{\partial f_3}{\partial E'_{dk}} - E'_{dk}\frac{\partial f_3}{\partial E'_{qk}} \qquad k = 2, 3, ..., m \tag{B.23}$$

$$\frac{\partial f_3}{\partial \delta_{k1}} = E_k(-G_{n+3,k}\sin\delta_k - B_{n+3,k}\cos\delta_k) \qquad k = m+1, ..., n \tag{B.24}$$

$$\frac{\partial f_3}{\partial V_{n+1}} = G_{n+3,n+1}\cos\theta_{n+1} - B_{n+3,n+1}\sin\theta_{n+1} \tag{B.25}$$

$$\frac{\partial f_3}{\partial \theta_{n+1}} = V_{n+1}(-G_{n+3,n+1}\sin\theta_{n+1} - B_{n+3,n+1}\cos\theta_{n+1}) \tag{B.26}$$

$$\frac{\partial f_3}{\partial V_{n+2}} = G_{n+3,n+2}\cos\theta_{n+2} - B_{n+3,n+2}\sin\theta_{n+2} \tag{B.27}$$

$$\frac{\partial f_3}{\partial \theta_{n+2}} = V_{n+2}(-G_{n+3,n+2}\sin\theta_{n+2} - B_{n+3,n+2}\cos\theta_{n+2}) \tag{B.28}$$

$$\frac{\partial f_3}{\partial V_{n+3}} = G_{n+3,n+3}\cos\theta_{n+3} - B_{n+3,n+3}\sin\theta_{n+3} \tag{B.29}$$

$$\frac{\partial f_3}{\partial \theta_{n+3}} = V_{n+3}(-G_{n+3,n+3}\sin\theta_{n+3} - B_{n+3,n+3}\cos\theta_{n+3}) \tag{B.30}$$

Finally for (6.23), we have

$$\frac{\partial f_4}{\partial E'_{qi}} = -\frac{\partial f_3}{\partial E'_{di}} \tag{B.31}$$

$$\frac{\partial f_4}{\partial E'_{di}} = \frac{\partial f_3}{\partial E'_{qi}} \tag{B.32}$$

$$\frac{\partial f_4}{\partial \delta_{k1}} = E'_{qk}\frac{\partial f_4}{\partial E'_{dk}} - E'_{dk}\frac{\partial f_4}{\partial E'_{qk}} \qquad k = 2, 3, ..., m \tag{B.33}$$

$$\frac{\partial f_4}{\partial \delta_{k1}} = E_k(G_{n+3,k}\cos\delta_k - B_{n+3,k}\sin\delta_k) \qquad k = m+1, ..., n \tag{B.34}$$

$$\frac{\partial f_4}{\partial V_{n+1}} = -\frac{1}{V_{n+1}}\frac{\partial f_3}{\partial \theta_{n+1}} \tag{B.35}$$

$$\frac{\partial f_4}{\partial \theta_{n+1}} = V_{n+1}\frac{\partial f_3}{\partial V_{n+1}} \tag{B.36}$$

$$\frac{\partial f_4}{\partial V_{n+2}} = -\frac{1}{V_{n+2}}\frac{\partial f_3}{\partial \theta_{n+2}} \tag{B.37}$$

$$\frac{\partial f_4}{\partial \theta_{n+2}} = V_{n+2}\frac{\partial f_3}{\partial V_{n+2}} \tag{B.38}$$

$$\frac{\partial f_4}{\partial V_{n+3}} = -\frac{1}{V_{n+3}}\frac{\partial f_3}{\partial \theta_{n+3}} \tag{B.39}$$

$$\frac{\partial f_4}{\partial \theta_{n+3}} = V_{n+3}\frac{\partial f_3}{\partial V_{n+3}} \tag{B.40}$$

BIBLIOGRAPHY

[1] C.W. Taylor, "Improving grid behavior," *IEEE Spectrum,* vol. 36, no. 6, 1999, pp. 40-45.

[2] M. Klien, G. J. Rogers, and P. Kundur, "A fundamental study of interarea oscillations in power systems," *IEEE Trans. on Power Systems,* vol. 6, no. 3, August 1991, pp. 914-921.

[3] E.V. Larsen, J.J. Sanchez-Gasca, and J.H. Chow, "Concepts for design of FACTS controllers to damp power swings," *IEEE Trans. on Power Systems,* vol. 10, vo. 2, May 1995, pp. 948-955.

[4] Canadian Electrical Association, *Investigation of Low Frequency Inter-area Oscillation Problems in Large Interconnected Power Systems*, Report of Research Project 294T622, 1993.

[5] E.V. Larsen, and D.A. Swann, "Applying power system stabilizers part I: general concepts," *IEEE Trans. on PAS,* vol. PAS-100, No. 6, June 1981, pp. 3017-3024.

[6] E.V. Larsen, and D.A. Swann, "Applying power system stabilizers part II: performance objectives and turning concepts," *IEEE Trans. on PAS,* vol. PAS-100, No. 6, June 1981, pp. 3025-3033.

[7] P. Kundur, M. Klien, G. J. Rogers, and M. Zwyno, "Applications of power system stabilizers for enhancement of overall system stability," *IEEE Trans. on Power Systems,* vol. 4, No. 2, May 1989, pp. 614-622.

[8] D.R. Ostojic, "Stabilization of multimodal electromechanical oscillations by coordinated application of power system stabilizers," *IEEE Trans. on Power Systems,* vol. 6, No. 4, November 1991, pp. 1439-1445.

[9] H.E. Schweickardt, G. Romegialli, and K. Reichert, "Closed loop control of static VAR sources on EHV transmission lines," in *Proc. of IEEE PES Winter Meeting,* 1978, Paper A78, pp. 135-136.

[10] L. Gyugyi, "Fundamentals of thyristor-controlled static var compensators in electric power system applications," in *IEEE Tutorial Course: Application of SVS for System Dynamic Performance,* 87 TH0187-5-PWR, 1987, pp. 8-27.

[11] P.K. Kundur, *Power System Stability and Control.* New York: McGraw-Hill,Inc., 1993.

[12] K.R. Padiyar and R.K. Varma, "Damping torque analysis of static var system controllers," *IEEE Trans. on Power Systems,* vol. 6, no. 2, May 1991, pp. 458-465.

[13] J.R. Smith, D.A. Pierre, D.A. Rudberg, and A.P. Johnson, "An enhanced LQ adaptive var unit controller for power system damping," *IEEE Trans. on Power Systems,* vol. 4, no. 2, May 1989, pp. 443-451.

[14] J.R. Smith, D.A. Pierre, I. Sadighi, M.H. Nehrir, and J.F. Hauer, "A supplementary adaptive var unit controller for power system damping," *IEEE Trans. on Power Systems,* vol. 4, no. 3, August 1989, pp. 1017-1023.

[15] C.W. Taylor, "Dynamic reactive support in a complex ac/dc power system: applications on the western north American interconnection/Pacific intertie," in *IEEE Tutorial Course: Application of SVS for System Dynamic Performance,* 87 TH0187-5-PWR, 1987, pp. 72-78.

[16] J.F. Hauer, "Reactive power control as a means for enhanced interarea damping in the western U.S. power system — a frequency-domain perspective considering robustness needs" in *IEEE Tutorial Course: Application of SVS for System Dynamic Performance,* 87 TH0187-5-PWR, 1987, pp. 79-92.

[17] E.V. Larsen and J.H. Chow, "SVC control design concepts for system dynamic performance," in *IEEE Tutorial Course: Application of SVS for System Dynamic Performance,* 87 TH0187-5-PWR, 1987, pp. 36-53.

[18] J.F. Hauer, "Robust damping controls for large power systems", *IEEE Control Systems Magazine,* vol. 9, no. 1, Jan. 1989,pp. 12-18.

[19] T. Smed, and G. Anderson, "Utilizing HVDC to damp power oscillations", *IEEE Trans. on Power Delivery,* vol. 8, no. 2, April 1993, pp. 620-627.

[20] N. Yang, Q. Liu, and J.D. McCalley, "TCSC controller design for damping interarea oscillations", *IEEE Trans. on Power Systems*, vol. 13, no. 4, November 1998, pp. 1304-1310.

[21] G.N. Taranto, J.K. Shiau, J.H. Chow, and H.A. Othman, "Robust decentralised design for multiple FACTS damping controllers", *IEE Proceedings on Generatioins, Transmission, and Distributions*, vol. 144, no. 1, January 1997, pp. 61-67.

[22] E. Khutoryansky, and M.A. Pai, "Parametric Robust Stability of Power Systems Using Generalized Kharitonov's Theorem," *Proceedings of the 36th*

IEEE Conference on Decision and Control, San Diego, California, 1997, pp. 3097-3099.

[23] M.A. Pai, C.D. Vournas, A.N. Michel, and H. Ye, "Application of interval matrices in power system stabilizer Design," *International Journal of Electric Power and Energy Systems,* vol. 17, no. 3, 1997, pp. 197-184.

[24] M.H. Khammash, V. Vittal, and C.D. Pawloski, "Analysis of control performance for stability robustness of power systems," *IEEE Trans. on Power Systems,* vol. 9, no. 4, November 1994, pp. 1861-1867.

[25] S. Venkataraman, M.H. Khammash, and V. Vittal, "Analysis and Synthesis of HVDC Controls for Stability of Power Systems," *IEEE Trans. on Power Systems,* vol. 10, no. 4, November 1995, pp. 1933-1939.

[26] S. Chen, and O.P. Malik, "H_∞ Optimization Based Power System Stabilizer Design," *IEE Proceedings, Part C,* vol. 142, no. 2, March 1995, pp. 179-184.

[27] S. Chen, and O.P. Malik, "Power System Stabilizer Design Using H_∞ Synthesis," *IEEE Trans. on Energy Conversion,* vol. 10, no. 1, March 1995, pp. 175-181.

[28] R. Asgharian, and S.A. Tavakoli, "Systematic Approach to Performance Weights Selection in Design of Robust H_∞ PSS Using Genetic Algorithms," *IEEE Trans. on Energy Conversion,* vol. 11, no. 1, March 1996, pp. 111-117.

[29] M. Klien, L.X. Le, G. J. Rogers, and S. Farrokhpay, "H_∞ Damping Controller Design in Large Power Systems," *IEEE Trans. on Power Systems,* vol. 10, no. 1, Feburary 1995, pp158-166.

[30] S.S. Ahmed, L. Chen, and A. Petroianu, "Design of Suboptimal H_∞ Excitation Controllers," *IEEE Trans. on Power Systems,* vol. 11, no. 1, Feburary 1996, pp312-318.

[31] Q. Zhao and J. Jiang, "Robust SVC controller design for improving power system damping," *IEEE Trans. on Power Systems,* vol. 10, no. 4, November 1995, pp. 1927-1932.

[32] G.E. Boukharim, G.N. Taranto, J.H.Chow, and H.A. Othman, "A Parameter Space Approach to Power System Uncertainty Modeling," *Proceedings of the 28th North American Power Symposium,* M.I.T., November 1996, pp. 63-70.

[33] M.H. Khammash, and J.B. Pearson, "Performance Robustness of Discrete-Time Systems with Structured uncertainty," *IEEE Trans. on Automatic Control,* vol. AC-36, No. 4, 1991, pp398-342.

[34] M.H. Khammash, and J.B. Pearson, "Analysis and Design for Robust Performance with Structured uncertainty," *Systems and Control Letters,* No. 20, 1993, pp179-187.

[35] M.H. Khammash, "Necessary and Sufficient Conditions for the Robustness of Time-Varying Systems with Applications to Sampled-Data Systems," *IEEE Trans. on Automatic Control,* to be published.

[36] M. Djukanovic, M.H. Khammash, and V. Vittal, "Structured Singular Value Theory Based Stability Robustness of power systems: Part I-Robust Analysis and Part II-Controller Synthesis," in *Proceeding of the 36th IEEE Conference on Control and Decision*, vol. 3, 1997, pp. 2702 -2707.

[37] M. Djukanovic, M.H. Khammash, and V. Vittal, "Application of the Structured Singular Value Theory for Robust Stability and Control Synthesis in

Multimachine Power Systems, Part I: Framework Development and Part II: Numerical Simulation and Results," *IEEE Trans. on Power Systems,* vol. 13, no. 4, November 1998, pp. 1311-1316.

[38] M. Djukanovic, M.H. Khammash, and V. Vittal, "Sequential synthesis of structured singular value based decentralized controllers in power systems," *IEEE Trans. on Power Systems,* Vol. 14, no. 2, May 1999, pp. 635-641.

[39] V. Vittal, M. Khammash, and M. Djukanovic, *Robust Analysis and Design of Control in Power Systems*, EPRI Research Report TR-111922, December 1998.

[40] J. Doyle, "Analysis of feedback systems with structured uncertainty," *IEE Proceedings, Part D,* vol. 129, November 1982, pp. 242-250.

[41] M.G. Sanofov, "Stability margins of diagonally perturbed multivariable feedback systems," *IEE Proceedings, Part D,* vol. 129, November 1982, pp. 251-256.

[42] P.M. Young, and J.C. Doyle, "Computation of μ with real and complex uncertainties," in *Proceedings of the 29th Conferences on Decision and Control,* Honolulu, Hawaii, December 1990.

[43] S. Skogestad, and I. Postlethwaite, *Multivariable Feedback Control Analysis and Design.* Chichester:John Wiley & Sons, 1998.

[44] P.M. Young, "*Robustness with Parametric and Dynamic Uncertainty,*" Ph.D. Dissertation, California Institute of Technology, 1993.

[45] A.K. Packard, and J.C. Doyle, "The complex structured singular value," *Automatica,* vol. 29, 1993, pp. 71-109.

[46] G.J. Balas, J.C. Doyle, K. Glover, A. Packard, and R. Smith, *μ-Analysis and Synthesis Toolbox User's Guide.* Natick, Mass.:Mathwork, 1993.

[47] J.C. Doyle, "Structured uncertainty in control system design," in *Proceedings of the 24^{th} Conference on Decision and Control*, 1985, pp. 260-265.

[48] J.C. Doyle, and A. Packard, "Uncertain multivariable systems from a state space perspective," in *Proceedings of the American Control Comference,* 1987, pp. 2147-2152.

[49] P.M. Anderson and A.A. Fouad, *Power System Control and Stability.* IEEE Press, 1994.

[50] C.D. Pawloski, *Robust Design and Performance of Controls in Power Systems*, M.S. thesis, Iowa State University, 1993.

[51] P. Kundur, G.J. Rogers, and D.Y. Wong, *Extended Transient-midterm Stability Program Package: Version 2.0, User's Manuals*, EPRI EL-6648, December 1989.

[52] IEEE Committee Report, "Excitation System Models for Power System Stability Studies," *IEEE Trans. on Power Apparatus and Systems,* vol. PAS-100, pp. 494-509, Feburary 1981.

[53] P. Kundur, G.J. Rogers, D.Y. Wong, S. Arabi, and L. Wang, *Small Signal Stability Analysis Program Package: Version 3.1, User's Manuals*, EPRI TR-101850-V2R1. Palo Alto, California, May 1994.

[54] P. Kundur, G.K. Morison, Voltage Stability Analysis Program: Version 2.2, Application Guide, EPRI, November 1993.

[55] G. Jang, *Nonlinear Control Design for Stressed Power Systems Using Normal Forms of Vector Fields*, Ph.D. dissertation, Iowa State University, 1997.

[56] V. Vittal, "Transient Stability Test Systems for Direct Stability Methods" *IEEE Trans. on PAS,* vol. 7, No. 1, Feburary 1992, pp. 37-42,

[57] V. Vittal, M.H. Khammash, and X. Yu, *Robust Analysis and Controller Design of Static Var Compensators in Power Systems*, Research Report, Iowa State University. January 2000.